VON KARMAN CENTER

ASTRIONICS DIVISION

SPATIAL FILTER SYNTHESIS ANALYSIS
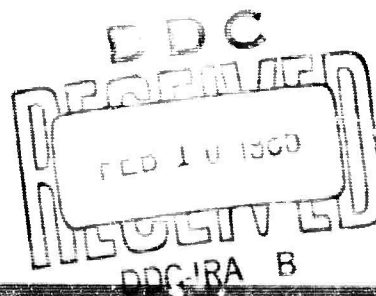
A FINAL REPORT TO THE

DIRECTOR, ADVANCED RESEARCH PROJECTS AGENCY
THE PENTAGON, WASHINGTON 25, D.C.

CONTRACT Onr-4556(00)
ARPA ORDER NO. 369

REPORT NO. 2985 / 29 JANUARY 1965 / COPY NO. 17

AEROJET
GENERAL TIRE
GENERAL

AEROJET-GENERAL CORPORATION

AEROJET
GENERAL TIRE
GENERAL

SPATIAL FILTER SYNTHESIS ANALYSIS

a final report to the

DIRECTOR, ADVANCED RESEARCH PROJECTS AGENCY
THE PENTAGON, WASHINGTON 25, D.C.

Contract NOnr-4556(00)
ARPA Order No. 369

Report No. 2985   29 January 1965

AEROJET-GENERAL CORPORATION

FOREWORD

This research effort is part of Project DEFENDER, under the joint sponsorship of the Advanced Research Projects Agency, Department of Defense, and the Office of Naval Research.
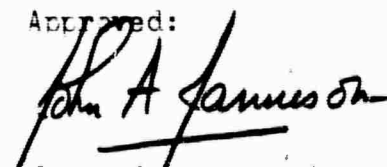
Authors:

      Khalil Seyrafi, PhD (EE)
      G. A. Davison, MS (EE)
      J. L. Gaston, MS (EE)

ABSTRACT

This report discusses the design and synthesis of low-pass and band-pass one-dimensional and two-dimensional spatial filters using arrays or matrices of detectors. The synthesis was performed for alternate assumptions of negligible and significant detector gaps. The detector width and the detector weighting functions are the two optimized parameters.

A frequency analyzer, using a narrow-band one-dimensional filter, was designed and simulated. Tests indicated performance as expected.

Approved:

J. A. Jamieson, Manager
Research and Development
Astrionics Division

CONTENTS

CONTENTS (cont.)

CONTENTS (cont.)

CONTENTS (cont.)

SYMBOLS

A_i	weighting coefficient of ith detector
i	indexing variable on X axis
W	width of detector plus gap
j	$\sqrt{-1}$
m	spatial frequency in cycles/unit length
$F_i(m)$	transfer function of ith detector
$F^*(m)$	transfer function of detector array
n	number of detectors on either side of the origin
$F_{PB}(m)$	ideal pass band transfer function
$F_{SB}(m)$	ideal stop band transfer function
m_c	cut-off frequency
Δ	filter error
E	mean square error
K	limit of optimized spatial frequency domain
W_g	gap between detectors
g	ratio of gap width to detector width
η	number of loops in an ideal filter function
$f(x)$	space function
$N'(x)$	detector density
μ	density constant
x_T	upper limit in space domain
N_{Total}	total number of detectors right of the origin

SYMBOLS (cont.)

f_{max}	value of the spatial function at a maximum
f_{min}	value of the spatial function at a minimum
m_1	spatial frequency axis corresponding to x direction
m_2	spatial frequency axis corresponding to y direction
m_{c_1}	cut-off frequency on m_p axis
m_{c_2}	cut-off frequency on m_2 axis
k	indexing variable on y axis
A_{ik}	weighting coefficient of i, k detector
W_1	width of detector in x direction
W_2	width of detector in y direction
$\phi\ (m_1,\ m_2)$	envelope function in two dimensions
$\psi\ (m_1,\ m_2)$	edge function in two dimensions
m_{1Z}	location of filter approximation zeros on m_1 axis
m_{2Z}	location of filter approximation zeros on m_2 axis
α_1	all integers
α_2	all integers
θ	angle of scan measured from x axis
ρ	radial frequency coordinate
n	an integer
n	a real number
ω	spatial frequency in radians per unit length
$F_a\ (m)$	approximating spatial frequency function

SYMBOLS (cont.)

$F_e(m)$ — difference between $F(m)$ and $Fa(m)$, that is, $F(m) - Fa(m)$

ϵ — integral of squared error

a — detector weighting

b — detector shortening coordinate

$Si(x)$ — the sine integral of x

a_{mn} — detector weighting in a two-dimensional array

A_{mn} — the area of the mnth detector

ω_x, ω_y — two-dimensional spatial frequency variables in radians per unit length

J_o, J_1 — Bessel functions of the first kind

ω_c — cutoff frequency of a circularly symmetric ideal low-pass spatial filter

r_n — detector radius

α_1 — $= \dfrac{a_1}{\omega_o^2}$, a substitute variable

α_n — $= \dfrac{a_n}{\omega_o^2}$, a substitute variable

z_n — $= r_n \omega_c$, a substitute variable

r_{-2} — reduced detector radius

z_{-2} — $= r_{-2} \omega_c$, a substitute variable

ℓ_1 — approximation limit on $f(x)$

$f_2(x)$ — filter framing function

$G_1(m)$ — one-dimensional spatial frequency spectrum

$g_2(x)$ — scene framing function

ℓ_2 — limits of scene framing function

D — positive constant

γ — log $(\text{transmissivity})^{-1}/\log(\text{exposure})$

I.   INTRODUCTION

A.   GENERAL

Recently, the detector mosaic concept has become the basis of many new optical processes. In long wavelength reconnaissance systems, terminal guidance, and pattern detection in particular, image dissection has been found a prerequisite. These systems contain a relatively large numb r of input detectors for parallel processing and recognition of the object with high resolution and high value of signal to noise.

A spatial filter, as defined by this study, also uses a detector mosaic as the input. Its function in space is analogous to classical time filtering in that it scans space and selectively passes spatial frequencies.

A spatial filter, in effect, performs a convolution in space. Its space function, or transient response, analogous to the system function in time filtering, is constructed by weighting each detector in the array. The weighted detector signals are summed. The output signal of the summing network at a fixed position of the detector array corresponds to one point of the convolution integral. As the array is scanned over a scene, a new scene is generated whose spatial frequency spectrum is the product of the filter transfer function (the Fourier transform of the space function) and the original scene's spatial frequency spectrum.

Spatial filters can be one-dimensional, in which case, the detectors are rectangular and the scan motion is parallel to the short dimension. Spatial filters can be two-dimensional in which case, the detector dimensions are then determined by the symmetry of the filter transfer function. For example, if the transfer function is circularly symmetric in the frequency domain, the detectors also will be circularly symmetric in the form of annuli. A two-dimensional

filter can take any form so long as it has quadrantal symmetry with respect to both frequencies' axes; that is, positive and negative frequency must be filtered identically.

The spatial filter has certain fundamental limitations. For example, a high-pass transfer function cannot be generated because it would require detectors of infinitesimal size. But its relative simplicity and the ease with which its operation can be generalized (by employing adjustable weights, for example) support arguments for investigation of the spatial filter as a potentially valuable technique in electro-optical processing.

Previous work (Appendix A) has reported an approximation method for the design and synthesis of a one-dimensional low-pass and a band-pass spatial filter. The method consisted of approximating the transient response of the filter with a linear, finite-width array of rectangular detectors. The analysis included a parametric evaluation of approximation accuracy as a function of detector size and number.

The continued study was visualized as aiming toward a synthesis procedure which could be useful for design in any specific problem. To demonstrate the value of the technique, the classical problems of low pass and band-pass filters with infinite attenuation at the cutoff frequencies were treated as examples. The effects of various parameters in approximation of these functions were then evaluated. It is believed that practical problems do not present such tight specifications. Therefore the approximation in a real case would be performed with greater accuracy.

In a general sense, detector size, gaps between detectors, and detector geometry are parametrically as significant in spatial filter design, as the detector weights. As a starting point in the general analysis, one can assume that minimization of detector number is important and that close approximation to some ideal filter response is desired. Emphasis on various aspects of the response function results from a choice of approximation criteria. One might choose, for example, to optimize for least-mean-square-error over a region of interest, or to optimize for least-mean-absolute-error. Or, as in time filtering, maximally flat criteria might be chosen. To a limited degree, one can estimate

simply the errors resulting from certain approximation methods. Many minimum-error optimizations, however, can be accomplished only through iterative computations best implemented with a high-speed digital computer.

Aside from its value in spatial filtering, a detector array has the advantage in image forming of mechanical simplicity over a single scanned detector. By combining this stationary image-forming capability with the spatial filter concept, recognizable patterns are obtained without mechanical scanning. A frequency analyzer which embodies this combination was, therefore, proposed and simulated.

Thus, the purpose of the study herein reported was to determine in greater detail the properties and parametric potential of the spatial filter. Because the spatial filter employs a detector array (either one- or two-dimensional) of variable size, and because the fabrication problems of detector arrays and processing electronics will determine the feasibility of various applications, establishing the parametric sensitivity of the concept is a matter of practical importance.

The initial sections of the report develop the analytical theory for several logical approximations in both one- and two-dimensions. Particular emphasis is placed on the least-mean-square error (LMSE) approximation because of the relative ease in computing the optimization. Several analyses develop the theoretical problems of special geometries. In these cases, the actual computation of filter approximations was considered unjustified at this time and the analytical results are summarized in order that the study of these cases may be continued later if desired.

The later sections summarize the numerical and experimental work and compare the various filter approximations. The practical implications of the experimental results are also developed.

B.   SUMMARY OF PROGRAM GOALS

The program started on 1 July 1964 and was organized into the following tasks:

1.   Optimization of detector size

2.   Extension to two-dimensional synthesis

3.   Background discrimination and target detection

4.   Frequency analyzer

5.   Multicolor correlation synthesis.

A mid-term presentation was made to Mr. P. Nutting of ARPA on 26 October 1964 to report the results of the contract and to concur on the direction of the remainder of the effort. Mr. Nutting suggested that more emphasis be placed in the detector optimization, considering detector gaps as another parameter and de-emphasize the color correlation and target detection.* The program was scheduled accordingly. Figure 1 shows the schedule and performance of each phase.

1.   The first phase entailed the evaluation of an optimization scheme which could be used for detector width and weighting function.

2.   The second phase was an extension of the synthesis procedure to two-dimensional detector arrays. A least-mean-square-error criteria was developed.

3.   The third phase consisted of a synthesis procedure for practical detector arrays including detector gaps. The procedure developed in the first and second phase was implemented in this phase.

4.   The fourth phase consisted of a numerical solution of the above three phases to evaluate the effect of detector parameters on the filter response.

5.   The fifth phase consisted of developing a theory design and fabricating a frequency analyzer for experimental verification of the spatial filter theory.

_____

* The importance of gaps should be observed in practical design. In a one-dimensional or two-dimensional mosaic array, fabrication and interconnection requirements necessitate some gaps between detectors. Therefore a practical synthesis technique should recognize their existence. In addition, considerations of economy often prescribe a maximum number of detectors for a particular application. It is not clear that a uniform, closely packed arrangement will achieve the most precise synthesis. Variable sizes, non-uniform distributions and provision of gaps may be preferable. An optimization analysis should investigate gap width as a parameter. The numerical solution discussed in this report shows that gaps can be introduced to advantage.

C.   SUMMARY OF PROGRAM RESULTS

In summarizing the results of the spatial filter study we conclude:

1.   Minimization of least-mean-square error is a successful method of approximating spatial filter functions. For many approximations the conventional technique coincides with this approach.

2.   Detector gaps with regular spacing tend to degrade the filter performance, but in certain cases (Section IV) with a limited number of detectors, variable gaps can improve the overall filter response.

3.   Two-dimensional square-response filters can be approximated with a cross detector array.

4.   When a square-response filter is approximated with a square detector array, the approximation in the stop band improves on axes between the x and y axes, but the pass-band ripple is worse.

5.   Narrow-band spatial filters can be satisfactorily simulated with transparencies and the operation of a non-scanning frequency analyzer has been demonstrated.

6.   One additional approximation method, detector density distribution proportional to space function slope, has been explored analytically.

7.   The space domain least-mean-square-error (LMSE) method produces accurate approximations with a minimum of computation.

These results, along with the specific parametric data are significant in any future filter design.

II. SYNTHESIS OF ONE-DIMENSIONAL SPATIAL FILTER

A. LEAST-MEAN-SQUARE-ERROR APPROXIMATION

1. Low-Pass Filter

For a linear array of detectors, the overall detector transfer function is the summation of the individual detector transfer functions. In a uniform-size-detector array, the transfer function of the ith detector having a weight A_i and centered at the point, $\left(i - \frac{1}{2}\right) W$ (where W is the detector width) would be

$$F_i(m) = A_i \; \frac{\sin \pi m W}{\pi m} \; \exp \left[\left(-\frac{2i-1}{2} \right) W j \, (2 \pi m) \right] \tag{II-1}$$

The transform of the array is therefore

$$F^*(m) = \sum_{i=-n+1}^{+n} A_i \; \frac{\sin \pi m W}{\pi m} \; \exp \left[\left(-\frac{2i-1}{2} \right) W j \, (2 \pi m) \right] \tag{II-2}$$

Because of the symmetry of the transform with respect to positive and negative frequency, Equation (II-2) can be written as

$$F^*(m) = 2 \; \frac{\sin \pi m W}{\pi m} \; \sum_{i=1}^{n} A_i \; \cos \left[(2i-1) \pi m W \right] \tag{II-3}$$

An ideal low-pass filter has the following pass-band and stop-band characteristics

$$F_{PB}(m) = 1 \qquad 0 < |m| < |m_c| \tag{II-4}$$

$$F_{SB}(m) = 0 \qquad |m| > |m_c| \tag{II-5}$$

where m_c is the cutoff frequency of the filter.

The error, Δ, in the pass-band is

$$\Delta = F^* - F_{PB} \qquad\qquad 0 < |m| < |m_c| \qquad\qquad \text{(II-6)}$$

and in the stop-band it is

$$\Delta = F^* - F_{SB} \qquad\qquad |m| > |m_c| \qquad\qquad \text{(II-7)}$$

The mean square error, E, over a region, $-K < m < K$, is then

$$E = \frac{1}{2K} \int_{-K}^{K} \Delta^2 \, dm \qquad\qquad \text{(II-8)}$$

Equation (II-8) takes the following form

$$E = \frac{1}{2K} \left\{ \int_{-m_c}^{m_c} \left[1 - \frac{\sin\pi mW}{\pi m} \sum_{i=1}^{n} A_i \cos (2i-1)\pi mW \right]^2 dm \right.$$

$$\left. + 2 \int_{m_c}^{K} \left[\frac{\sin\pi mW}{\pi m} \sum_{i=1}^{n} A_i \cos (2i-1)\pi mW \right]^2 dm \right\} \qquad \text{(II-9)}$$

To have the LMSE we require

$$\frac{\partial E}{\partial A_1} = 0$$

$$\frac{\partial E}{\partial A_2} = 0$$

$$\cdot$$
$$\cdot$$
$$\cdot$$

$$\frac{\partial E}{\partial A_n} = 0 \qquad\qquad\qquad \text{(II-10)}$$

These conditions produce a set of simultaneous algebraic equations in A_1, $A_2 \cdots A_n$ which can be solved for these parameters.

Equation (II-9) can be expanded as follows

$$E = \frac{1}{K} \int_0^{m_c} \left\{ 1 + \left(\frac{\sin \pi m W}{\pi m} \right)^2 \left[\sum_{i=1}^n A_i \cos (2i-1)\pi m W \right]^2 \right.$$

$$\left. -2 \frac{\sin \pi m W}{\pi m} \sum_{i=1}^n A_i \cos (2i-1)\pi m W \right\} dm$$

$$+ \frac{1}{K} \int_{m_c}^K \left(\frac{\sin \pi m W}{\pi m} \right)^2 \left[\sum_{i=1}^n A_i \cos (2i-1)\pi m W \right]^2 dm \qquad (II-11)$$

As the set of partial derivatives, (II-10), is independent of the order of integration in (II-11), the set of Equation (II-10) can then be written as

$$\frac{\partial E}{\partial A_i} = \frac{1}{K} \int_0^{m_c} \left\{ \left(\frac{\sin \pi m W}{\pi m} \right)^2 2 \left[\sum_{i=1}^n A_i \cos (2i-1)\pi m W \right] \cos (2i-1)\pi m W \right.$$

$$\left. -2 \frac{\sin}{\pi m} \quad \cos (2i-1)\pi m W \right\} dm$$

$$+ \frac{1}{K} \int_{m_c}^K \left(\frac{\sin \pi m W}{\pi m} \right)^2 2 \left[\sum_{i=1}^n A_i \cos (2i-1)\pi m W \right] \cos (2i-1)\pi m W \, dm \qquad (II-12)$$

After simplification, this can be written

$$\frac{\partial E}{\partial A_i} = \frac{1}{K} \int_0^K 2 \left(\frac{\sin \pi m W}{\pi m}\right)^2 \left[\sum_{i=1}^n A_i \cos (2i-1)\pi m W\right] \cos (2i-1)\pi m W \, dm$$

$$- \frac{2}{K} \int_0^{m_c} \frac{\sin \pi m W}{\pi m} \cos (2i-1)\pi m W \, dm = 0 \qquad (II\text{-}13)$$

The set of Equations (II-13) can not easily be solved analytically. A numerical solution is clearly indicated.

If the limit of integration, K, is allowed to become very large, the numerical manipulation can become quite complex. For practical purposes, however, it is possible to assign an upper bound to K, above which the response is not of any interest. This might be due, for example, to lack of information in that portion of the frequency spectrum.

A program was written for the IBM 7094 computer for the cases of $n = 2$, 4, 6, 8, and 10, and $K = 4 \, m_c$. The results of the numerical solution are discussed in Section V.

2.   Band-Pass Filter

Equation (II-2) applies also to the band-pass case. The coefficients, A_i, however, are chosen such that the transform satisfies the following equations instead of (II-4) and (II-5)

$$F (m) = F_{PB} (m) = 1 \qquad \left|m_c - \frac{\Delta m}{2}\right| < |m| < \left|m_c + \frac{\Delta m}{2}\right|$$

$$F (m) = F_{SB} (m) = 0 \qquad \begin{cases} |m| < \left|m_c - \frac{\Delta m}{2}\right| \\ |m| > \left|m_c + \frac{\Delta m}{2}\right| \end{cases} \qquad (II\text{-}14)$$

where m_c is the center frequency of the band-pass filter and Δm is the band-width. Applying LMSE criteria, Equation (II-9) can be rewritten

$$E = \frac{1}{K_{max} - K_{min}} \left\{ \int_{K_{min}}^{m_c - \frac{\Delta m}{2}} \left(\frac{\sin \pi mW}{\pi m}\right)^2 \left[\sum_{i=1}^{n} A_i \cos (2i-1)\pi mW\right]^2 dm \right.$$

$$+ \int_{m_c - \frac{\Delta m}{2}}^{m_c + \frac{\Delta m}{2}} \left[1 - \frac{\sin \pi mW}{\pi m} \sum_{i=1}^{W} A_i \cos (2i-1)\pi mW\right]^2 dm$$

$$\left. + \int_{m_c + \frac{\Delta m}{2}}^{K_{max}} \left(\frac{\sin \pi mW}{\pi m}\right)^2 \left[\sum_{i=1}^{n} A_i \cos (2i-1)\pi mW\right]^2 dm \right\} \qquad (II-15)$$

Equation (II-15) can be expanded as follows

$$E = \frac{1}{K_{max} - K_{min}} \int_{K_{min}}^{K_{max}} \left(\frac{\sin \pi mW}{\pi m}\right)^2 \left[\sum_{i=1}^{n} A_i \cos (2i-1)\pi mW\right]^2 dm \qquad (II-16)$$

$$+ \frac{1}{K_{max} - K_{min}} \int_{m_c - \frac{\Delta m}{2}}^{m_c + \frac{\Delta m}{2}} \left\{1 - 2 \frac{\sin \pi mW}{\pi m} \left[\sum_{i=1}^{n} A_i \cos (2i-1)\pi mW\right]\right\} dm$$

For LMSE, the set of Equations, (II-10), must be satisfied. Differentiating the integral, we can write

$$\frac{\partial E}{\partial A_i} = \frac{1}{K_{max} - K_{min}} \int_{K_{min}}^{K_{max}} 2 \left(\frac{\sin \pi mW}{\pi m}\right)^2 \left[\sum_{i=1}^{n} A_i \cos (2i-1)\pi mW\right] \cos (2i-1)\pi mW \, dm$$

$$- \frac{2}{K_{max} - K_{min}} \int_{m_c - \frac{\Delta m}{2}}^{m_c + \frac{\Delta m}{2}} \left(\frac{\sin \pi mW}{\pi m}\right) \cos (2i-1)\pi mW \, dm \qquad (II-17)$$

Equation (II-17) can not be solved analytically. A numerical solution can be obtained after assigning values for K_{max} and K_{min}.

3.   Low-Pass One-Dimensional Spatial Filter Approximation
Including Detector Gaps

For the detector in the original one-dimensional analysis having
width, W, we substitute a new detector of width, $W_d < W$, and a gap, Wg. (See
Figure 2)

$$Wg = g \, W_d \quad \text{and} \quad g < 1$$

therefore   (II-18)

$$W_d = \frac{W}{1+g}$$

The first detector, as in the earlier analysis, is still centered at $\frac{W}{2}$, the

second at $3 \frac{W}{2}$, etc.

For an approximation over η loops and using 2n detectors

$$\frac{\eta}{2 \, m_c} = nW = n \, (1+g) \, W_d \qquad (II-19)$$

Equation (II-3) can now be written

$$F \ (m) = 2 \ \frac{\sin \pi m W_d}{\pi m} \ \sum_{i=1}^{n} A_i \cos (2i-1)\pi mW \qquad (II-20)$$

$$= 2 \ \frac{\sin \left(\pi m \frac{W}{1+g} \right)}{\pi m} \ \sum_{i=1}^{n} A_i \cos (2i-1)\pi mW$$

for η loops $W = \dfrac{\eta}{2 \, m_c \, n}$ and

$$F \ (m) = 2 \ \frac{\sin \pi m \dfrac{\eta}{n \, m_c \, (1+g)}}{\pi m} \ \sum_{i=1}^{n} A_i \cos \left[(2i-1) \, \pi m \, \frac{\eta}{2 \, n \, m_c} \right] \qquad (II-21)$$

Us. Equation (II-13) for optimization on the basis of LMSE, we have

$$\frac{\partial E}{\partial A_i} = \frac{1}{K} \int_0^K 2 \left[\frac{\sin\left(\pi m \frac{\eta}{n\, m_c\,(1+g)}\right)}{\pi m} \right]^2 \left[\sum_{i=1}^n A_i \cos(2i-1)\pi m \frac{\eta}{2\,n\,m_c} \right]$$

$$(II-22)$$

$$\cos\left[(2i-1)\pi m \frac{\eta}{2\,n\,m_c}\right] dm - \frac{2}{K} \int_0^{m_c} \frac{\sin \pi m \frac{\eta}{n\,m_c\,(1+g)}}{\pi m} \cos\left[(2i-1)\pi m \frac{\eta}{2\,n\,m_c}\right] dm = 0$$

The set of Equations (II-22) determines the coefficients, A_i. A numerical solution to these equations has been made on the 7094 computer. The results are discussed in Section V.

B. SLOPE CRITERIA FOR DETECTOR DENSITY

In addition to the conventional and LMSE methods for obtaining detector weights, another parameter, detector density, can be incorporated in the optimization procedure. One such technique would be to have the detector density proportional to the slope of the ideal space function, that is, the detectors would be concentrated where the function changes most rapidly.

$$f(x) = \frac{\sin 2\pi m_c x}{\pi x} \tag{II-23}$$

and the slope

$$\frac{d\,f(x)}{d\,x} = \frac{1}{\pi} \frac{2\pi m_c x \cos 2\pi m_c x - \sin 2 - m_c x}{x^2} \tag{II-24}$$

The detector density as a function of x is given by

$$N'(x) = \mu \left| \frac{d\,f(x)}{d\,x} \right| \tag{II-25}$$

where μ is a density constant determined by the total number of available detectors and the truncation point.   In the limit as the truncation point and the number of detectors becomes large,

$$\lim_{x_T \longrightarrow \infty} \int_0^{x_T} N'(x)\ d\ x = N_{Total} = \int_0^\infty \mu\ \left| \frac{d\ f(x)}{d\ x} \right|\ d\ x \qquad (II\text{-}26)$$

Therefore

$$N_{Total} = \mu\ \left| -\frac{\sin 2\pi m_c x}{\pi x} \right|_0^{x_1} + \frac{\sin 2\pi m_c x}{\pi x} \bigg|_{x_1}^{x_2} - \frac{\sin 2\pi m_c x}{\pi x} \bigg|_{x_2}^{x_3} + \dots \right|$$

$$(II\text{-}27)$$

where x_1, x_3, x_5, etc., are the abscissas of the $\dfrac{\sin 2\pi m_c x}{\pi x}$ minima, and

x_2, x_4, x_6, etc., are the abscissas of the $\dfrac{\sin 2\pi m_c x}{\pi x}$ maxima.

Therefore

$$N_{Total} = \mu\ \left[1 + 2 \sum \left(f_{max} - f_{min} \right) \right] \qquad (II\text{-}28)$$

For a given number of detectors, N_{Total},

$$\mu = \frac{N_{Total}}{1 + 2 \sum \left(f_{max} - f_{min} \right)} \qquad (II\text{-}29)$$

The increasing series, $\sum \left(f_{max} - f_{min} \right)$, does not converge because for large x_n it becomes

$$\frac{4\ m_c}{\pi}\ \sum_n\ \frac{1}{2\ n+1}$$

which clearly diverges. Therefore, in a practical application, some finite range for x must be chosen and $\sum \left(f_{max} - f_{min} \right)$ must be evaluated in that region.

III. TWO-DIMENSIONAL SPATIAL FILTER SYNTHESIS

A. CONVENTIONAL APPROXIMATION TECHNIQUE

Assume that the weights for a two-dimensional mosaic of detectors are to be chosen such that the array has a low-pass characteristic from $-m_{c_1}$ to $+m_{c_1}$ in the m_1 direction, and from $-m_{c_2}$ to $+m_{c_2}$ in the m_2 direction, as shown in Figure 3 i.e.,

$$F(m_1, m_2) = F_{PB}(m_1, m_2) = 1 \quad \begin{cases} 0 < |m_1| < |m_{c_1}| \\ \\ 0 < |m_2| < |m_{c_2}| \end{cases} \tag{III-1}$$

$$F(m_1, m_2) = F_{SB}(m_1, m_2) = 0 \quad \begin{cases} |m_1| > |m_{c_1}| \\ \\ |m_2| > |m_{c_2}| \end{cases} \tag{III-2}$$

The synthesis procedure here is analogous to that of the one-dimensional filter. The inverse transform of this ideal filter characteristic can be written as

$$f(x,y) = \frac{1}{\pi^2} \frac{\sin 2\pi m_{c_1} x}{x} \frac{\sin 2\pi m_{c_2} y}{y} \tag{III-3}$$

$$f(x,y) = 4 m_{c_1} m_{c_2} \frac{\sin 2\pi m_{c_1} x}{2\pi m_{c_1} x} \frac{\sin 2\pi m_{c_2} y}{2\pi m_{c_2} y} \tag{III-4}$$

The two-dimensional space function $f(x,y)$ is shown in Figure 3.

For a mosaic of detectors, the approximation can be carried on for 2 loops, 3 loops, etc., independently in either the x or y directions. A weight value for each detector can be obtained by either the conventional method of assigning to the detector the value of $f(x,y)$ at the detector's center or by applying the LMSE technique.

The value of $f(x,y)$ at the center of a detector located in the ith row and the kth column is

$$A_{ik} = f(x,y)_{x_i y_k} = 4 \; \frac{\sin 2 \pi m_{c_1} x_i}{2 \pi x_i} \; \frac{\sin 2 \pi m_{c_2} y_k}{2 \pi y_k} \qquad \text{(III-5)}$$

$$= 4 \; \frac{\sin 2 \pi (2i-1)\frac{W_1}{2} m_{c_1}}{2 \pi (2i-1) \frac{W_1}{2}} \; \frac{\sin 2 \pi m_{c_2} (2k-1) \frac{W_2}{2}}{2 \pi (2k-1) \frac{W_2}{2}}$$

The transform of a rectangular matrix truncated after n elements in the x direction and p elements in the y direction would therefore be

$$F^* (m_1, \; m_2) = \frac{4}{\pi^2} \; \frac{\sin \pi m_1 W_1}{\pi m_1 W_1} \; \frac{\sin \pi m_2 W_2}{\pi m_2 W_2}$$

$$\qquad \text{(III-6)}$$

$$x \sum_{i=1}^{n} \sum_{k=1}^{p} \frac{\sin(2i-1)\pi W_1 m_{c_1}}{(2i-1)} \; \frac{\sin(2k-1)\pi W_2 m_{c_2}}{(2k-1)} \cos(2i-1)W_1 \pi m_1 \cos(2k-1)W_2 \pi m_2$$

Equation (III-6) can also be written as

$$F^* (m_1, \; m_2) = \frac{4}{\pi^2} \; \frac{\sin \pi m_1 W_1}{\pi m_1 W_1} \; \frac{\sin \pi m_2 W_2}{\pi m_2 W_2} \sum_{i=1}^{n} \sum_{k=1}^{p} \left[\sin(2i-1)\pi W_1 (m_{c_1} + m_1) \right.$$

$$\qquad \text{(III-7)}$$

$$\left. + \sin(2i-1)\pi W_1 (m_{c_1} - m_1) \right] \left[\sin(2k-1)\pi W_2 (m_{c_2} + m_2) + \sin(2k-1)\pi W_2 (m_{c_2} - m_2) \right]$$

As in the case of the one-dimensional filter, $F^* (m_1, \; m_2)$ can be separated into two factors

$$\phi (m_1, \; m_2) = \frac{\sin \pi m_1 W_1}{\pi m_1 W_1} \; \frac{\sin \pi m_2 W_2}{\pi m_2 W_2} \qquad \text{(III-8)}$$

Page III-2

and

$$\Psi(m_1, m_2) = \sum_{i=1}^{n} \sum_{k=1}^{p} \frac{\sin\left[(2i-1)\, W_1\, \pi\, m_{c_1}\right] \cos\left[(2i-1)\, W_1\, \pi\, m_1\right]}{2i-1}$$
$$x \quad \frac{\sin\left[(2k-1)\, W_2\, \pi\, m_{c_2}\right] \cos(2k-1)\, W_2\, \pi\, m_2}{2k-1}$$

$(III-9)$

The function $\phi(m_1, m_2)$ and $\Psi(m_1, m_2)$ are called the envelope function and edge function, respectively.

Scanning the two-dimensional filter in the x space direction corresponds to filtering with the one-dimensional response function on the m_1 axis; i.e., $m_2 = 0$. The envelope function $\phi(m_1, m_2)$ for scanning in the x direction therefore takes the form of $\dfrac{\sin \pi\, m_1\, W_1}{\pi\, m_1\, W_1}$, the same as in the one-dimensional case.

The zeros of this function occur when

$$m_{1_Z} W_1 = \alpha_1 \quad \text{or at} \quad m_{1_Z} = \frac{\alpha_1}{W_1}$$

$(III-10)$

where α_1 is an integer.

Scanning the detector array in the y space direction corresponds to filtering with the one-dimensional response function on the m_2 axis, i.e., $m_1 = 0$. For this case, the envelope function reduces to

$$\frac{\sin \pi\, m_2\, W_2}{\pi\, m_2\, W_2}$$

whose zeros occur at

$$m_{2_Z} = \frac{\alpha_2}{W_2}$$

$(III-11)$

where α_2 is an integer.

Scanning at some arbitrary angle, Θ, with respect to the x axis in the space domain corresponds to filtering with the one-dimensional response function on the radial line making an angle Θ with the m_1 axis. For this line

$$m_1 = \rho \cos \Theta$$

$$m_2 = \rho \sin \Theta$$

(III-12)

where ρ is the radial distance from the origin in the frequency plane. Applying (III-11) in Equation (III-7) we find

$$\phi (\rho,\Theta) = \frac{\sin (\pi W_1 \rho \cos \Theta)}{\pi W_1 \rho \cos \Theta} \quad \frac{\sin (\pi W_2 \rho \sin \Theta)}{\pi W_2 \rho \sin \Theta}$$

(III-13)

Zeros of the envelope function along the radial axis defined by Θ are therefore

$$\rho_Z = \frac{\alpha_1}{W_1 \cos \Theta} = \beta$$

(III-14)

$$\rho_Z = \frac{\alpha_2}{W_2 \sin \Theta} = \gamma$$

For low values of Θ, i.e., $\Theta < \tan^{-1} \frac{W_1}{W_2}$, the zeros of $\sin (\pi W_1 \rho \cos \Theta)$ occur more frequently than the zeros of $\sin (\pi W_2 \rho \sin \Theta)$. Figure 4a shows these two terms separately.

As the value of Θ increases, the zeros of ϕ_2 move closer to the origin and the zeros of ϕ_1 move away from the origin. For values of Θ approaching $\tan^{-1} \frac{W_1}{W_2}$ the negative loops of $\phi_1 \phi_2$ become increasingly smaller in amplitude and extent. In the limit when $W_1 \rho \cos \Theta = W_2 \rho \sin \Theta$ the negative loops in $\phi = \phi_1 \phi_2$ disappear completely. A more quickly attenuating curve as shown in Figure 4b results, where

$$\phi = \left[\frac{\sin (\pi W_1 \rho \cos \Theta)}{\pi W_1 \rho \cos \Theta} \right]^2$$

(III-15)

Page III-4

Returning to the edge function, $\Psi(m_1, m_2)$, on the m_1 axis, $m_2 = 0$, and the function is a summation of cosine terms whose zeros are $(2i-1) W_1 m_{1_Z} = (2\alpha-1)$ where α is an integer. $\Psi(m_1, m_2 = 0)$ has a maxima at $m_1 = \frac{\alpha}{W_1}$ for even values of α, and minima at $\frac{\alpha}{W_1}$ for odd values of α. The function, $F(m_1, m_2 = 0)$, has therefore, maxima and minima on either side of each $\frac{\alpha}{W_1}$ which is a zero of $\Psi(m_1, m_2)$. A similar result exists for the m_2 axis and $\frac{\alpha}{W_2}$.

For axes at an arbitrary Θ, however, the edge function is a summation of mixed terms such as

$$\cos\left[(2i-1) W_1 \pi \rho \cos \Theta\right] \cos\left[(2k-1) W_2 \pi \rho \sin \Theta\right]$$

For small values of Θ where

$$(2i-1) W_1 \cos \Theta >> (2k-1) W_2 \sin \Theta$$

the zeros of

$$\cos\left[(2i-1) W_1 \pi \rho \cos \Theta\right]$$

appear more often than the zeros of

$$\cos\left[(2k-1) W_2 \pi \rho \sin \Theta\right]$$

As Θ increases, the zeros of

$$\cos\left[(2i-1) W_1 \pi \rho \cos \Theta\right]$$

move to the left and those of

$$\cos\left[(2k-1) W_2 \pi \rho \sin \Theta\right]$$

move to the right. When

$$(2i-1) W_1 \cos \Theta = (2k-1) W_2 \sin \Theta$$

the product degenerates to a cosine squared function.

B.   LMSE APPROXIMATION IN FREQUENCY DOMAIN

In the LMSE criteria, the weighting function of a detector located in the ith and j^{th} column would be a value A_{ij} which has to be found by the approximating procedure. In this case, formula (III-6) takes the form

$$F\ (m_1,\ m_2) = \frac{4}{\pi^2}\ \frac{Sin\ \pi\ m_1\ W_1}{m_1}\ \frac{Sin\ \pi\ m_2\ W_2}{m_2}\ \sum_{i=1}^{n}\ \sum_{k=1}^{P}\ A_{ik}\ Cos\Big[(2i-1)\ \pi\ m_1\ W_1\Big]$$

(III-16)

$$x\ Cos\Big[(2k-1)\ \pi\ m_2\ W_2\Big]$$

An ideal low-pass filter in the two-dimensional case has the characteristics

$$F_{PB}\ (m_1,\ m_2) = 1 \qquad \begin{cases} 0 < \big|\ m_1\ \big| < \big|\ m_{c_1}\big| \\[2ex] 0 < \big|m_2\big| < \big|m_{c_2}\big| \end{cases}$$

(III-17)

and

$$F_{SB}\ (m_1,\ m_2) = 0 \qquad \begin{cases} \big|m_1\big| > \big|m_{c_1}\big| \\[2ex] \big|m_2\big| > \big|m_{c_2}\big| \end{cases}$$

(III-18)

where m_{c_1} and m_{c_2} are the cutoff frequencies of the filter in m_1 and m_2 directions, respectively.

The error in the pass-band and stop-band is similar to that described by Equations (II-6) and (II-7). The total error, therefore, in this case would be

$$E = \frac{1}{4\ K_1\ K_2}\ \int_0^{K_1}\int_0^{K_2} \Delta^2\ d\ m_1\ d\ m_2 \ \Bigg|_{\substack{K_1 \to \infty \\ K_2 \to \infty}}$$

(III-19)

$$E = \frac{1}{4 K_1 K_2} \int_0^{m_{c_1}} \int_0^{m_{c_2}} \left\{ 1 - \frac{4}{\pi^2} \frac{\sin \pi m_1 W_1}{m_1} \frac{\sin \pi m_2 W_2}{m_2} \sum_{i=1}^{n} \sum_{k=1}^{p} \right.$$

$$\left. \cdot A_{ik} \cos \left[(2i-1) \pi m_1 W_1 \right] \cos \left[(2k-1) \pi m_2 W_2 \right] \right\} dm_1 \, dm_2 + \frac{1}{4 K_1 K_2} \int_{m_{c_1}}^{K_1} \int_{m_{c_2}}^{K_2}$$

$$\cdot \left\{ \frac{4}{\pi^2} \frac{\sin \pi m_1 W_1}{m_1} \frac{\sin \pi m_2 W_2}{m_2} \sum_{i=1}^{n} \sum_{k=1}^{p} A_{ik} \cos \left[(2i-1) \pi m_1 W_1 \right] \right.$$

$$\left. \cdot \cos \left[(2k-1) \pi m_2 W_2 \right] \right\}^2 dm_1 \, dm_2 \tag{III-20}$$

To have the LMSE criteria satisfied, we require

$$\frac{\partial E}{\partial A_{11}} = 0$$

$$\frac{\partial E}{\partial A_{12}} = 0 \tag{III-21}$$

$$\cdot$$
$$\cdot$$
$$\cdot$$

$$\frac{\partial E}{\partial A_{np}} = 0$$

These conditions produce a set of np simultaneous algebraic equations in A_{11}, A_{12}, ... A_{np} which can be solved for these parameters. The solution of these equations, however, can not be easily obtained analytically. Expanding these equations similar to the expansion of formula (II-11) through (II-13) for the one dimensional case would be adaptable to a computer input. A numerical solution for cases of 8×8, 10×10 and 20×20 square matrix is obtained. The results of these solutions are discussed in Section V.

C.   LOW BAND-PASS TWO-DIMENSIONAL SPATIAL FILTER APPROXIMATION
INCLUDING DETECTOR GAPS

For the two-dimensional case including detector gap, Equation (III-6)
becomes

$$F^*(m_1, m_2) = \frac{\text{Sin } \pi m_1 W_{d_1}}{\pi m_1 W_{d_1}} \frac{\text{Sin } \pi m_2 W_{d_2}}{m_2 W_{d_2}} \sum_{i=1}^{n} \sum_{k=1}^{p} A_{ik} \text{Cos}\left[\frac{(2i-1)}{2} 2 \pi m_1 W_1\right]$$

$$\cdot \text{Cos}\left[\frac{(2k-1)}{2} 2 \pi m_2 W_2\right]$$

where

(III-20) $W_1 = (1+g_1) W_{d_1}$

and

$W_2 = (1+g_2) W_{d_2}$

W_{d_1} and W_{d_2} are the width of the detectors in the x and y directions,
respectively.   Detector gaps in the x direction and y direction are $g_1 W_{d_1}$, and

(III-21) $g_2 W_{d_2}$, respectively.   An optimum approximation to the filter function can be
obtained by the same procedure of LMSE discussed in the previous section.   The
parameters, g_1 and g_2, must be chosen for the approximation.   In a more elaborate
procedure, one may optimize not only on the basis of LMSE for the weighting
function, but also for g_1 and g_2.

IV. SPATIAL FREQUENCY FILTER DESIGN BY MINIMIZING INTEGRAL SQUARE ERROR IN THE DETECTOR PLATE

A. INTRODUCTION

In the spatial filter design methods described in the preceding sections, detector weighting coefficients were chosen so as to minimize the integral, over a prescribed finite region, of the square of the difference between the desired and approximate frequency domain functions. In the method presented here, detector weighting coefficients are chosen so as to minimize the integral, over the detector length (area in the two-dimensional case), of the square of the difference between the desired and approximate space domain functions. But, by Parseval's theorem for Fourier transforms, the latter method simultaneously minimizes the integral, over the infinite region, of the square of the difference between the desired and approximate frequency domain functions.

As mentioned in Section II, the minimization of error in the spatial frequency domain was over a limited finite region because extending the region would have led to computional difficulties on the IBM 7094. The method presented here overcomes this difficulty in that it minimizes error over the infinite spatial frequency region.

Perhaps the main advantage of the method of detector plane fitting, as shown in detail below, is that detector weighting coefficients, for all of the cases treated in the preceding sections, can be found by using tabulated functions, thereby eliminating the digital computations.

Furthermore, as shown in Sections IV,D and IV,F, detector plane fitting offers a simple way of finding, with the aid of a digital computer, optimum non-uniform detector widths as well as weighting coefficients.

To see how Parseval's theorem applies here, let

$$F(m) = F_a(m) + F_e(m) \tag{IV-1}$$

where $F(m)$ represents the desired spatial frequency characteristics, $F_a(m)$ the approximation, and $F_e(m)$ the error. Also, let $f(x)$, $f_a(x)$ and $f_e(x)$ be the

2985

IV Spatial Frequency Filter Design, A (cont.)   Report No. 2985

corresponding inverse Fourier transforms. Then let the integral of $F_e^2(m)$ over
$0 \leq m \leq \infty$ defines the approximation error ϵ:

$$\epsilon = \int_0^\infty F_e^2(m) \, dm \tag{IV-2}$$

Now since $f(x)$ is real and thus has a real Fourier transform, Parseval's theorem
can be written as

$$\int_0^\infty f_e^2(x) \, dx = \int_0^\infty F_e^2(m) \, dm = \epsilon \tag{IV-3}$$

This equation shows that if a design procedure minimizes $\int_0^\infty f_e^2(x) \, dx$ by fitting
in the detector plane, it also simultaneously minimizes the spatial frequency
approximation error.

In the above equations m represents the spatial frequency variable in
cycles per unit length. But in the remainder of this section $\omega = 2\pi m$ in radians
per unit length is used for the spatial frequency variable. Although this change
simplifies notation here by eliminating factors of 2π in many places, it requires
that one be careful in relating the equations of this section to those appearing
elsewhere in the report. Parseval's theorem can be written in this way because
$f(x)$ is an even function and thus has a real Fourier transform. From Equation
(IV-2) we see that if the design process matches $f_a(x)$ to $f(x)$ by minimizing

$$\int_0^\infty \left[f(x) - f_a(x) \right]^2 dx \tag{IV-4}$$

then the spatial frequency error over $0 \leq m \leq \infty$ is simultaneously minimized.

Of major significance here, fitting $f_a(x)$ to $f(x)$ does not require
solving a set of simultaneous equations to obtain detector weighting coefficients.
In contrast, the present computer optimization solves a set of n simultaneous

equations for an array of n detectors; and, for example, in the case of $n = 100$ in a two-dimensional array, solving the equations is not an easy task even for the IBM 7094.

B.   QUALITY OF APPROXIMATION

Because the computer optimization minimizes error over only $0 \leq \omega \leq n\omega c$ whereas the detector plane fitting described here minimizes error over $0 \leq \omega \leq \infty$, one would expect a smaller error over $0 \leq \omega \leq n\omega c$ to result from the computer optimization. But the detector plane fitting described in Sections IV,D and IV,F leads to detectors of variable width, whereas the computer optimizations performed thus far have used detectors of equal widths. It will not be too surprising, then, to find that, as a result of the latter factor, a filter designed by detector plane fitting may have less error than by frequency domain fitting. Furthermore, with equal width detectors, the fact that the error criteria of the two methods become more alike as $n\ \omega_c$ increases shows that, for sufficiently large $n\ \omega_c$, the resulting approximations will differ negligibly.

Although they will not be used elsewhere in this report, we now formulate expressions of approximation errors for future use in comparing computer optimization with detector plane fitting. Thus, let $F_{a1}(\omega)$ represent the approximation to $F(\omega)$ that results from frequency domain fitting over $0 \leq \omega \leq \infty$; let $F_{a2}(\omega)$ represent the approximation to $F(\omega)$ that results from detector plane fitting. For an ideal low-pass filter, let $F(\omega) = 1$ over $0 \leq \omega \leq \omega_c$, and $F(\omega) = 0$ elsewhere.

Then $F_{a1}(\omega)$ minimizes

$$\epsilon_1 = \int_0^{\omega_c} \left[1 - F_{a1}(\omega)\right]^2 d\omega + \int_{\omega_c}^{n\omega_c} F_{a1}^2(\omega)\ d\omega, \qquad \text{(IV-5)}$$

and $F_{a2}(\omega)$ minimizes

$$\epsilon_2 = \int_0^{\omega_c} \left[1 - F_a^2(\omega)\right]^2 d\omega + \int_{\omega_c}^{\infty} F_{a2}^2(\omega)\ d\omega. \qquad \text{(IV-6)}$$

Let ϵ_3 represent the error with $F_{a2}(\omega)$ over $0 \leq \omega \leq n\omega_c$:

$$\epsilon_3 = \int_0^{\omega_c} \left[1 - F_{a2}(\omega)\right]^2 d\omega + \int_{\omega_c}^{n\omega_c} F_{a2}^2(\omega)\ d\omega. \qquad \text{(IV-7)}$$

Combining integrands, gives

$$\epsilon_3 - \epsilon_1 = \int_0^{\omega_c} (F_{a2}^2 - F_{a1}^2)\, d\omega + 2 \int_0^{\omega_c} (F_{a1} - F_{a2})\, d\omega \qquad (IV-8)$$

The ratio $\dfrac{\epsilon_3 - \epsilon_1}{\epsilon_1}$ thus offers a measure for comparing detector plane fitting with frequency plane fitting on the basis of integral square error in frequency plane approximation.

C.   OPTIMIZATION OF WEIGHTING COEFFICIENTS IN A ONE-DIMENSIONAL ARRAY OF CONTIGUOUS DETECTORS

The ideal low-pass spatial frequency function again serves as an example. The method suggested in Section IV,A and used in this and the following sections, applies to arbitrary filter functions; the details should be easier to follow for the low-pass case because of its simplicity and prior treatment by other methods elsewhere in this report.

Thus, consider Figure 6, in which four detectors, each of length $\dfrac{\pi}{2}$, lie in the interval $0 \leq x \leq 2\pi$ (by symmetry, we need consider only the half-plane $x \geq 0$). As suggested in Section IV,A, for each detector the integral, taken over the length of the detector, of the square of the difference between its amplitude and $\dfrac{1}{\pi} \dfrac{\sin x}{x}$ is minimized with respect to detector amplitude.

For example, in the second interval

$$\epsilon_2 = \int_{\pi/2}^{\pi} \left(\frac{1}{\pi} \frac{\sin x}{x} - a_2 \right)^2 dx \qquad (IV-9)$$

is minimized by letting a_2 equal the value found in solving $\dfrac{\partial \epsilon_2}{\partial a_2} = 0$. Carrying out the minimization,

$$\frac{\partial \epsilon_2}{\partial a_2} = \int_{\pi/2}^{\pi} \frac{\partial}{\partial a_2} \left(\frac{1}{\pi^2} \frac{\sin^2 x}{x^2} - \frac{2a_2}{\pi} \frac{\sin x}{x} + a_2^2 \right) dx \qquad (IV-10)$$

Then, solving $\dfrac{\partial \epsilon_2}{\partial a_2} = 0$ gives

$$a_2 = \frac{2}{\pi^2} \int_{\pi/2}^{\pi} \frac{\sin x}{x}\, dx = \frac{2}{\pi^2} \left[Si(\pi) - Si\left(\frac{\pi}{2}\right) \right] \qquad (IV-11)$$

where $Si(x)$ represents the sine integral of x.

For the other detectors,

$$a_1 = \frac{2}{\pi^2} \left[Si \left(\frac{\pi}{2}\right) - 0 \right]$$

$$a_3 = \frac{2}{\pi^2} \left[Si \left(\frac{3\pi}{2}\right) - Si \left(\pi\right) \right] \qquad \text{(IV-12)}$$

$$a_4 = \frac{2}{\pi^2} \left[Si \left(2\pi\right) - Si \left(\frac{3\pi}{2}\right) \right]$$

D. OPTIMIZATION OF WEIGHTING COEFFICIENTS AND DETECTOR WIDTHS FOR A ONE-DIMENSIONAL ARRAY OF UNEQUALLY SPACED DETECTORS

Consider the expanded sketch in Figure 7 of the interval $\frac{\pi}{2} \leq x \leq \pi$ where the diagonally striped areas represent the integration areas of the error integral. Assume for the moment that a_2 has been determined as above. Now consider what happens to the error integral when the second detector, which originally extended from $\frac{\pi}{2}$ to π, is replaced by one that extends from $\frac{\pi}{2}$ to b_2, thereby forming a gap from b_2 to π.

As a result of this shortening, the entire striped area no longer represents the integration area of the error integral; to the right of $x = b_2$, the dotted area replaces the striped area. Since the added dotted area exceeds the deleted striped area, the total error decreases.

This discussion shows roughly how shortening a detector can reduce total error; Equations (IV-17) and (IV-18) shows the interdependence between b_2 and a_2. That is, the procedure in the previous section for optimizing a_2 no longer applies if b_2 is to be optimized also.

Further consideration of this shortening process, as applied to the example of four detectors, brings out some additional points. First of all, shortening the detector that belongs to the interval $0 \leq x \leq \frac{\pi}{2}$ will not reduce the error. This follows from noticing that the absolute value of the difference between $\frac{\sin x}{x}$ and a_1 is less than $\frac{\sin x}{x}$ itself throughout the interval. Secondly, in the interval $\pi \leq x \leq \frac{3\pi}{2}$ the left end of the detector gets cut off, rather than the right end.

The procedure given here applies to any $f(x)$; the low-pass filter provided only a convenient example. Design for an arbitrary $f(x)$ can start by marking approximating rectangles on a sketch of the exact function prior to making the optimizing calculations. This helps to organize the work and to avoid unnecessary calculations in regions where optima do not exist.

The calculation of the optimum values of a_2 and b_2 in the above example proceeds by first writing the error as

$$\epsilon_2 (a_2, b_2) = \int_{\pi/2}^{b_2} \left(\frac{1}{\pi} \frac{\sin x}{x} - a_2 \right)^2 dx + \int_{b_2}^{\pi} \frac{1}{\pi^2} \left(\frac{\sin x}{x} \right)^2 dx \qquad (IV\text{-}13)$$

Then setting $\dfrac{\partial \epsilon_2}{\partial a_2} = 0$ and $\dfrac{\partial \epsilon_2}{\partial b_2} = 0$ gives

$$\frac{\partial \epsilon_2}{\partial a_2} = - \int_{\pi/2}^{b_2} \frac{2}{\pi} \frac{\sin x}{x} dx + 2a_2 \int_{\pi/2}^{b_2} dx = 0 \qquad (IV\text{-}14)$$

from which

$$a_2 = \frac{1}{\pi} \frac{\int_{\pi/2}^{b_2} \frac{\sin x}{x} dx}{b_2 - \frac{\pi}{2}} = \frac{1}{\pi} \frac{Si(b_2) - Si(\frac{\pi}{2})}{b_2 - \frac{\pi}{2}} ; \qquad (IV\text{-}15)$$

and

$$\frac{\partial \epsilon_2}{\partial b_2} = \left(\frac{1}{\pi} \frac{\sin b_2}{b_2} - a_2 \right)^2 - \left(\frac{1}{\pi} \frac{\sin b_2}{b_2} \right)^2 = 0, \qquad (IV\text{-}16$$

from which

$$\frac{1}{\pi} \frac{\sin b_2}{b_2} = \frac{a_2}{2} \qquad (IV\text{-}17)$$

Substituting (IV-17) into (IV-15) gives

$$Si\,(b_2) - Si\,\left(\frac{\pi}{2}\right) = \left| 2 - \frac{\pi}{b_2}\; \sin b_2 \right. \tag{IV-18}$$

This equation is readily solved with an IBM 7094 program. For rough calculations a trial and error procedure is also feasible; substituting the value of a_2 that was found for continguous detectors in the previous section into $\frac{1}{\pi}\,\frac{\sin b_2}{b_2} = \frac{a_2}{2}$ and then finding b_2 in tables of $\frac{\sin x}{x}$ furnishes an initial trial value.

E.   OPTIMIZATION OF WEIGHTING COEFFICIENTS IN A SQUARE TWO-DIMENSIONAL DETECTOR ARRAY

The two-dimensional ideal low-pass filter will be used as an example of the optimization method. Let $F(\omega_x,\,\omega_y) = $ 1 for $|\omega_x| \le 1$, $\omega_y \le 1$

         0 elsewhere.

Taking the Fourier inverse transform gives

$$f(x,y) = \frac{1}{\pi^2}\,\frac{\sin x}{x}\;\frac{\sin y}{y} \tag{IV-19}$$

for the exact detector function. Assuming that the detector locations and areas have been prescribed, the error for each detector can be written as

$$\varepsilon_{mn} = \int_{A_{mn}} \left(\frac{1}{\pi^2}\,\frac{\sin x}{x}\,\frac{\sin y}{y} - a_{mn} \right)^2 dx\,dy \tag{IV-20}$$

where A_{mn} represents the area of the mnth detector.

Minimizing ε_{mn} by setting $\dfrac{\partial \varepsilon_{mn}}{\partial a_{mn}} = 0$ gives

$$\frac{\partial \varepsilon_{mn}}{\partial a_{mn}} = \int_{A_{mn}} \int - \frac{2}{\pi^2}\,\frac{\sin x}{x}\,\frac{\sin y}{y}\,dx\,dy + 2\,a_{mn}\,A_{mn} \tag{IV-21}$$

Hence

$$a_{mn} = \frac{1}{\pi^2 A_{mn}} \underset{A_{mn}}{\int} \frac{\sin x}{x} \frac{\sin y}{y} \, dx \, dy \qquad (IV\text{-}22)$$

Finally, by separating the double integral,

$$a_{mn} = \frac{1}{\pi^2 A_{mn}} \left[Si\,(x_m) - Si\,(x_{m-1}) \quad Si(y_n) - Si\,(y_{n-1}) \right] \qquad (IV\text{-}23)$$

where x_m, x_{m-1}, y_n, and y_{n-1} denote the boundaries of the mnth detector.

F.   OPTIMIZATION OF ANNULAR WIDTHS AND WEIGHTING COEFFICIENTS IN A TWO-DIMENSIONAL CIRCULARLY SYMMETRIC SPATIAL FREQUENCY FILTER

The analysis in this section uses the zeroth order Fourier-Bessel transform (known also as a zeroth order Hankel transform). For detector weighting functions that are independent of polar angle, the pertinent transforms become

$$f(r) = \int_0^\infty \omega F(\omega) \, J_0 \,(r\omega) \, d\omega \qquad (IV\text{-}24)$$

and

$$F(\omega) = \int_0^\infty r \, f\,(r) \, J_0 \,(r\omega) \, dr \qquad (IV\text{-}25)$$

Here we apply the method of detector plane fitting to the problem of approximating a circularly symmetric ideal low-pass spatial filter by a set of annular detectors.

Hence,

$$F(\omega) = 1 \quad \text{for} \quad \omega \leq \omega_c$$

and

$$F(\omega) = 0 \quad \text{for} \quad \omega > \omega_c$$

Taking the inverse transform,

$$f(r) = \int_0^{\omega_c} \omega \, J_0(r\omega) \, d\omega = \frac{1}{r} \left[\omega \, J_1(r\omega) \right]_0^{\omega_c} = \frac{\omega_c}{r} J_1(r\omega_c) \qquad (\text{IV-26})$$

Since $f(r)$ appears here almost in the form of the function that describes Fraunhoffer diffraction at a circular aperture, [1] we may take advantage of this similarity by forming

$$\frac{f(r)}{\omega_c^2} = \frac{J_1(r\omega_c)}{r\omega_c}$$

and modifying a circular aperture diffraction pattern to plot $\dfrac{f(r)}{\omega_c^2}$ vs $r\omega_c$ as in Figure 8.

1. Weighting Coefficient Optimization

We first consider the optimization of weighting coefficients only, and assume that the detector radii have already been chosen. Figure 8 shows the detector configuration and the desired spatial function.

Let ϵ_1 represent the error over the area of the innermost detector, and a_1 the weighting coefficient. Then

$$\epsilon_1 = 2\pi \int_0^{r_1} \left[f(r) - a_1 \right]^2 r \, dr \qquad (\text{IV-27})$$

To simplify notation, let $z = r\omega_c$, $z_1 = r_1\omega_c$, and $\alpha_1 = \dfrac{a_1}{\omega_c^2}$, so that by substituting (IV-26) into (IV-27)

$$\epsilon_1 = 2\pi \, \omega_c^2 \int_0^{z_1} \left(\frac{J_1(z)}{z} - \alpha_1 \right)^2 z \, dz \qquad (\text{IV-28})$$

Setting $\dfrac{\partial \epsilon_1}{\partial \alpha_1} = 0$ gives

$$\frac{\partial \epsilon_1}{\partial \alpha_1} = 2\pi \, \omega_c^2 \left\{ -2 \int_0^{z_1} J_1(z) \, dz + 2\alpha_1 \int_0^{z_1} z \, dz \right\} = 0 \qquad (\text{IV-29})$$

---

[1] M. Born and E. Wolf, _Principles of Optics_, Pergamon Press Ltd., 1959, pp. 394-396.

Hence,

$$\alpha_1 = \frac{\int_0^{z_1} J_1(z)dz}{z_1^2/2} = -\frac{\left[J_0(z_1) - J_0(0)\right]}{z_1^2/2} \tag{IV-30}$$

Similarly, for a detector extending from r_n to r_{n-1},

$$\alpha_n = \frac{J_0(z_{n-1}) - J_0(z_n)}{z_n^2 - z_{n-1}^2/2} \tag{IV-31}$$

where $\alpha_n = \dfrac{a_n}{\omega_c^2}$ and $z_n = r_n \omega_c$

2. Simultaneous Optimization of Weighting Coefficient and Radius

The procedure here follows that shown in Section IV,D for one-dimensional detectors. Using the preceding example of four annular detectors, we shall show how to find the optimum radius along with the optimum weighting coefficient.

From Figure 8, we expect that reducing the outside radius of the second detector should reduce its error in approximating $\dfrac{J_1(r\omega_c)}{r\omega_c}$ over the interval $r_1 \leq r \leq r_2$. Letting r_{-2} denote the reduced radius, and using the notation on Equation (IV-28), gives

$$\epsilon_2 = 2\pi\,\omega_c^2 \int_{z_1}^{z_{-2}} \left(\frac{J_1(z)}{z} - \alpha_2\right)^2 z\,dz + 2\pi\,\omega_c^2 \int_{z_{-2}}^{z_2} \left(\frac{J_1(z)}{z}\right)^2 z\,dz \tag{IV-32}$$

As in Section IV,D, the solution follows from setting $\dfrac{\partial\epsilon_2}{\partial\alpha_2} = 0$ and $\dfrac{\partial\epsilon_2}{\partial z_{-2}} = 0$

Thus,

$$\frac{\partial\epsilon_2}{\partial\alpha_2} = 2\pi\,\omega_c^2 \left\{-2\int_{z_1}^{z_{-2}} J_1(z)\,dz + \partial\alpha_2 \int_{z_1}^{z_{-2}} z\,dz\right\} = 0 \tag{IV-33}$$

whence

$$\alpha_2 = 2 \; \frac{\left[J_o(z_1) - J_o(z_{-2}) \right]}{z_{-2}^2 - z_1^2}; \qquad (\text{IV-34})$$

and

$$\frac{\partial \epsilon_2}{\partial z_{-2}} = 2\pi \, \omega_c^{\;2} \left\{ \left(\frac{J_1(z_{-2})}{z_{-2}} - \alpha_2 \right)^2 z_{-2} - \left(\frac{J_1(z_{-2})}{z_{-2}} \right)^2 z_{-2} \right\} \qquad (\text{IV-35})$$

$$= \frac{2\pi \, \omega_c^{\;2}}{z_{-2}} \left\{ \left(J_1(z_{-2}) - \alpha_2 \, z_{-2} \right)^2 - J_1^{\;2}(z_{-2}) \right\} = 0 \qquad (\text{IV-36})$$

whence

$$\alpha_2 = \frac{2 \, J_1(z_{-2})}{z_{-2}} \qquad (\text{IV-37}$$

Equating (IV-34 and (IV-37) gives

$$\frac{J_1(z_{-2})}{z_{-2}} = \frac{J_o(z_1) - J_o(z_{-2})}{z_{-2}^2 - z_1^2} \qquad (\text{IV-38})$$

This transcendental equation in z_{-2} should be easy to solve with the IBM 7094.

V. NUMERICAL SOLUTION

A. INTRODUCTION

To evaluate the effect of finite size detectors and the effect of detector number, or truncation, in the design of the previously described low-pass, band-pass, one-dimensional and two-dimensional filter, numerical solutions were taken from an IBM 7094 and a hybrid computer (HYDAC 2400). To normalizations were performed to obtain a generalized result. First, the detector width was normalized by m_c, the cutoff frequency, so that

$$m_c W = \frac{1}{2\alpha} \qquad (V-1)$$

where α is an integer. This normalization guarantees an integral number of detectors in every loop of the envelope function.

Second, the truncation point in the space domain was normalized by the cutoff frequency m_c i.e.,

$$2x_T m_c = \eta \qquad (V-2)$$

where x_T is the abcissa of the truncation point in space domain and η is an integer which corresponds to the number of loops to be approximated in the envelope function.

The LMSE criteria was first applied to an array without detector gaps in order to compare these results with those of the conventional approach as described in Appendix A. After demonstrating the value of LMSE, this method alone was used for approximation of linear arrays including detector gaps. The reason was that the conventional approach could not compensate for the contribution of the gap between the detectors.

For practical reasons, LMSE criteria may not be over an infinite frequency range. The limit frequency band chosen for the evaluation of the error depends on the constraints of the signal-and-noise spectrum in the stop-band. In following numerical solutions, the approximation has been optimized up to four octaves above the cutoff frequency. Approximation for a different frequency band can be performed in the same manner.

B. ONE-DIMENSIONAL FILTER

Figure 9 is a numerical solution for a low-pass filter truncated after two loops of the envelope function, $\eta = 2$, and employing four detectors. The approximation was performed by both the conventional method and the LMSE method with zero detector gap. As shown in the figure, there is a negligible effect on both the pass-band and stop-band response. Furthermore, the weighting function obtained by these two independent methods were identical out to three decimal places.

C. TWO-DIMENSIONAL FILTER

Numerical solutions for a two-dimensional square response spatial filter using square arrays of 8 x 8, 10 x 10, and 20 x 20 detectors were also obtained. To generalize the solution, the frequency spectrum was normalized by m_{c_1} and m_{c_2} as in the case of one-dimensional synthesis. The frequency of an 8 x 8 detector matrix along the x axis and y axis is identical with the one-dimensional low-pass filter (Figure 10). As Θ, the scanning angle with respect to the X axis, increases, the amplitude of the harmonic maxima and minima in the stop-band decrease as illustrated in Figure 11. The same phenomena were observed for the cases of 10 x 10 and 20 x 20 detectors. This confirms the theoretical discussion of Section III,B. The band pass ripple increases for an angle Θ between 0 and 90°, reaches a maximum at $\Theta = 45^\circ$. The reason for this increased ripple in the band-pass may be that the optimization criteria which was applied for $\Theta = 0^\circ$ and $\Theta = 90^\circ$ only, thus allowing larger ripple for $0^\circ < \Theta < 90^\circ$.

The two-dimensional approximation was performed by:

1. Conventional method of assigning the value of the inverse transform of the cube at the center of each detector to that detector; and,

2. LMSE to minimize error out to $4\ m_c$.

The weighting functions for each case were similar. Differences between the weighting functions obtained by the two methods, occurred in the 3rd and higher decimals. The weighting functions were, of course, symmetrical with respect to both the x axis and y axis. Table 1 gives the value of these functions.

A point of interest is that the values $A_{i,j}$ for high i and j, become extremely small. The value of $A_{3,3}$ for 8 x 8 detectors is about 0.03 while A_{11} is 0.81. The values of $A_{i,j}$ for i > 3 and j > 3 are all less than 0.01. This indicates that the effect of detectors located beyond the 3rd row and 3rd column becomes negligible. Therefore, one can use a reduced matrix of detectors in the form of a cross with each arm of the cross containing four rows of detectors.

Figure 12 shows a two-dimensional spatial filter response which is obtained by approximating two loops of the $\dfrac{\sin 2\pi\, m_{c_1} x}{\pi\, m_{c_1}}\, \dfrac{\sin 2\pi\, m_{c_2} y}{\pi\, m_{c_2}}$ function with a 20 x 20 detector array. A comparison between this curve and the curve obtained by a matrix of 8 x 8 detectors indicates no difference in the band-pass response. The curve indicates, however, a better approximation in the stop-band in the region $m_c < m < 4m_c$ than in the case of 8 x 8 detectors. This may be due to the motion of the harmonic maxima and minima being farther from the cutoff frequency.

Attention is directed to the large ripple in the stop-band just behond $4\, m_c$. Had the approximation been carried on for a wider band than $4m_c$, this ripple would obviously have been attenuated at a cost of an increase in the ripple in either band-pass or stop-band before $4\, m_c$.

This iscussion can be extrapolated to the cases of circular symmetry, low-pass and band-pass filters. A series of circular ring detectors centered at the origin and weighted by $\dfrac{J_1(r)}{r}$ may be used. Since the first-order Bessel's function is itself damped with increasing r, $\dfrac{J_1(r)}{r}$ decreases more rapidly than $\dfrac{\sin x}{x}$. Thus, the effect of detectors located far from the origin is less important, which allows earlier truncation in the approximation procedure. The numerical solution for this case would be similar to that of the one-dimensional case and, therefore, was not performed at this time.

D.   NUMERICAL SOLUTION INCLUDING DETECTOR GAP

Figures 13 and 14 show the approximation of the low-pass filter by using an array of (tectors with varying detector gaps. As described in the

theoretical discussion, the detectors are centered at the same point as in the case of no gap. The width of the detector is decreased to allow a variable gap. The phase function of these detectors, therefore, is unchanged. The frequency spectrum contributed by each detector, however, is smaller in amplitude and more slowly damped than the wider detectors. It is, therefore, necessary to modify the weighting function to approximate the same overall spatial filter response. Due to this general, lower amplitude, the weighting function of each detector must be increased to approximate a band-pass characteristic. Increasing the weighting function also increases the ripple in the stop-band compared to that obtained with the wide detectors. These results were confirmed numerically. Figure 13 shows the effect of detector gap or the band-stop ripple. From this figure, it is seen, that for an eight-detector approximation, the band-pass characteristic is similar to that with no detector gap. Ripple, however, is developed in the stop-band region of 4-5 m_c, 8 m_c and 10 m_c. If less ripple is required in the stop-band, the weighting function of the detector must be reduced accordingly. This, of course, results in larger ripple in the pass-band. The slope of the curve around the cutoff frequency is much slower because of the narrow detectors. Figure 14 shows a numerical solution of a three-loop approximation for various detector gaps. The figure illustrates closely that as the detector gap is increased, although the ripple in the stop-band stays fairly constant, the approximation in the pass band becomes worse.

A comparison between figures indicates a sharper slope in the cutoff frequency of a three-loop approximation, similar to the case of no detector gap. The case with detector gaps is less accurate than in case of no gaps. A better approximation in either band-pass or stop-band can be accomplished by weighting the corresponding error in the LMSE computation more heavily.

VI.   FREQUENCY ANALYZER

A.   INTRODUCTION

Pattern identification is one example of a promising application of the spatial filter phenomena. In this case, a criteria for categorizing patterns on the basis of their spatial characteristics must be chosen. One of the simplest is two-dimensional power spectra.

There are a number of methods that might be used to determine two-dimensional power spectra. Such spectra are obtained conventionally by scanning a slit across a scene and analyzing the resulting time-function with a variable narrow-band filter, i.e., a wave analyzer; or, the autocorrelation function is computed.

An alternate procedure, analogous to the wave analyzer, would require scanning a succession of narrow-band spatial filters across the scene and determine the power in each bandwidth. Since for this discussion spatial filters are weighted detector arrays, a simpler modification would use a single array and variable weights. Further economic argument modifies the system to that illustrated in Figure 15. In this case, the need for scanning the array with each change of weighting function, is eliminated. Instead, the equivalent of scanning the array is accomplished by causing the weighting function to travel across the array. This weighting function scan can be achieved practically by using a tapped delay line. A large number of equivalent scans, therefore, can be made in a short time.

However, as will be shown, the methods of scanning the array and scanning the weights are not exactly equivalent, because both the array and the weighting function are truncated or framed. Framing introduces a distortion into the measured spectra.

B.   DESCRIPTION OF SCANNED WEIGHT FREQUENCY ANALYZER

Given a one-dimensional weighting function, $f(x)$, for a narrow-band spatial filter, having a center frequency, m_c, and bandwidth, Δm

$$f(x) = \frac{2}{\pi x} \sin(\pi \Delta m x) \cos(2\pi m_c x) \qquad \text{(VI-1)}$$

We initially neglect the effect of a finite density of detectors; that is, we assume that $f(x)$ is approximated perfectly over some region $-\ell_1 < x < \ell_1$. Whenever $|x| > \ell_1$, the truncated $f(x) = 0$

The effective filter, $F^*(m)$, is the transform of the truncated $f(x)$, i.e.,

$$F^*(m) = \int_{-\ell_1}^{+\ell_1} \frac{2}{\pi x} \sin(\pi \Delta m x) \cos(2\pi m_c x) e^{-2\pi m x} dx \qquad (VI-2)$$

$$= F_1(m) * F_2(m)$$

where

$$F_1(m) = 1 \quad \text{for} \quad \left| m_c - \frac{\Delta m}{2} \right| < |m| < \left| m_c + \frac{\Delta m}{2} \right|$$

$$= 0 \quad \text{for} \quad |m| < m_c - \frac{\Delta m}{2}$$

$$|m| > m_c + \frac{\Delta m}{2}$$

and

$$F_2(m) = \frac{\sin 2\pi m \ell_1}{\pi m}$$

In examining Equation (VI-2), we note that the convolution of $F_1(m)$ and $F_2(m)$ degrades the edges of the ideal filter function and produces ripples in both the pass-band and stop-band. In the limit as ℓ_1 becomes very large, $F_2(m)$ becomes an impulse and the convolution returns the ideal filter function.

For a practical situation with a finite detector density, $F_1(m)$ will not be perfect, but will exhibit the periodic maxima and minima demonstrated in Appendix A.

In addition to the distortion of the filter characteristic by truncation, or framing, the scene's apparent spectral content is distorted because of a second frame imposed by a finite focal plane. Assume a scene having a one-dimensional spectral distribution, $G_1(m)$. If the scene is framed by a function, $G_2(x)$, where

$$G_2(x) = 1 \quad \text{for } \ell_2 < x < \ell_2$$

$$= 0 \quad \text{for } \ell_2 < |x|$$

then the apparent frequency spectrum, $G^*(m)$, the the convolution of $G_1(m)$ and $G_2(m)$. That is

.

$$G^*(m) = G_1(m)^* G_2(m) \qquad\qquad (\text{VI-3})$$

where

$$G_2(m) = \int_{-\ell_2}^{\ell_2} e^{-j2\pi mx} \, dx$$

$$= \frac{1}{\pi m} \sin 2\text{-}m\ell_2$$

The true frequency spectrum of the scene is spread by $G_2(m)$. Clearly $G_2(m)$ sets a limit on both the resolution of spectral measurement and on the lowest spatial frequency measurable. In other words, if a scene contains two impulse functions in its spectral distribution these cannot be resolved if they are separated by a frequency less than $\frac{1}{\ell_2}$, because the frame blurs the two impulse functions in the apparent spectral distribution. Furthermore, frequencies less than $\frac{1}{\ell_2}$ cannot be resolved because they cannot be separated from the impulse always present in dc (the average level of a scene must be positive).

The frequency spectrum of the signal at the output of the narrow-band filter is the product of $F^*(m)$, the effective filter function, and $G^*(m)$, the scene's apparent frequency spectrum.

Notice that for the case where the scene is scanned across the array, the weighting function is framed, but the scene is not. Spectral resolution, therefore, is limited solely by the truncated weighting function and finite detector density. When the weights are scanned and the scene is fixed on the detectors there is the additional limitation of a framed scene.

In the following simulation experiment, the variable transmissivity of
a photographic film weighted the intensity distribution of a scene. Mathematically,
since such weighting can only be positive, this is equivalent to adding a positive
constant to the weighting function. Comparing with Equation (VI-2)

$$F_{film}^{*}(\,m) = \int_{-\ell_1}^{+\ell_2} \left[\frac{2}{\pi x} \sin\,(\pi \triangle mx)\,\cos\,2\pi m_c x + D \right] e^{-j\,2\pi mx}\,dx$$

$$(VI\text{-}4)$$

$$= F^*(\,m) + \frac{D}{\pi m}\,\sin\,2\pi m \ell_1$$

The constant, D, must be larger than $2\triangle$ m to keep $f_{film}(x)$ positive. The
new term, $\frac{D}{\pi m}\,\sin\,2\pi m\ell_1$, is centered at m = 0, and it distorts the filter's low
frequency characteristic.

C.   SIMULATION EXPERIMENT

The experiment simulating the frequency analyzer is illustrated by
Figure 16. As mentioned above, photographic film replaced the scanned weighting
function. The 35-mm film was driven by a slow-moving transport across the image
plane of a camera. A photomultiplier behind the film collected the light from the
weighted scene. This signal was plotted by a pen-recorder.

One problem in the simulation was construction of a film transmissivity
proportional to the desired one-dimensional narrow-band characteristic. Figure 17
illustrates the procedure used; note how the desired function is plotted in the
form of a silhouette. By using a cylindrical lens, each vertical line image
appearing at the film plane of the view camera has an intensity proportional to
the total illumination of the corresponding line at the silhouette. The vertical
cylindrical lens, in other words, images every point on a vertical line in object
space to every point in a vertical line in image space.

A negative constructed in this fashion is shown in Figure 18. This
negative was then used to construct a positive transparency on 35-mm film. In
processing both the negative and positive it was necessary to develop to a γ = 1
to maintain linearity.

The figures illustrating the film processing show that the filter chosen extended only to the first minimum of the envelope, that is, to where

$$\pi \Delta m \ell_1 = \pi \qquad \text{and} \qquad \ell_1 = \frac{1}{\Delta m}$$

Also Δm was chosen such that

$$\frac{\Delta m}{m_c} = 0.1$$

and

$$D \approx 2\Delta m$$

Referring to Equations (VI-2) and VI-4)

$$F_2(m) = \frac{1}{\pi m} \sin 20\pi \frac{m}{m_c} \tag{VI-8}$$

and

$$F_{film}^*(m) = F^*(m) + \frac{0.2m_c}{\pi m} \sin 20\pi \frac{m}{m_c} \tag{VI-9}$$

The term, $\dfrac{0.2m_c}{\pi m} \sin 20\pi \dfrac{m}{m_c}$, is negligibly small.   Therefore

$$F_{film}^*(m) \approx F^*(m) \tag{VI-10}$$

Also, since $\ell_2 = \ell_1$ (because both are the length of a 35-mm frame),

$$G_2(m) = \frac{1}{\pi m} \sin 20\pi \frac{m}{m_c} \tag{VI-11}$$

Three "picket fence" scenes with frequencies m_c, $\dfrac{m_c}{2}$, and $\dfrac{m_c}{3}$, and the resultant signals when scanned with the film band-pass filter are shown in Figures 19, 20, and 21. The effect of framing the scenes i.e., $G_2(m)$ is seen in the

gradual increase and decrease of the trace at the beginning and end of the scan. Theoretically a picket fence of frequency, $\frac{m_c}{2}$, contains no energy in its second harmonic, m_c. However, the cumulative errors in the spectral measurement produce a small signal at m_c in Figure 20.

A picket fence of frequency, $\frac{m_c}{3}$, should contain a signal at m_c with an amplitude one third that of the fundamental. Figures 19 and 21 illustrate the 3:1 amplitude ratio of the m_c components.

The high frequency "hash" at the edges of the traces are presumed due to the effect of transparent tape attaching opaque backing at the edges of the filter function.

In the film simulation, the following suggestions may be considered for future work:

1.   As noted earlier, by exposing the film with too much contrast the film is driven beyond the linear region. A reduction in contrast would make a measurable improvement in the filter function.

2.   A more exact simulation could be made by imitating the finite detector density with steps in the silhouette function.

3.   By splicing together various strips of film, it should be possible to enlarge the length of the filter function, i.e., increase ℓ_1. This also should make it possible to reduce extraneous effects such as the very high frequency noise.

4.   A complete set of bandpass filters and test patterns might be constructed to explore completely the potential of the frequency analyzer principle.

It is also possible to use two separate films in a beam splitter, with one beam for positive weights and one for negative weights. The outputs of the two are subtracted to get an exact equivalent weighting function, thus eliminating the d-c term in the original function.
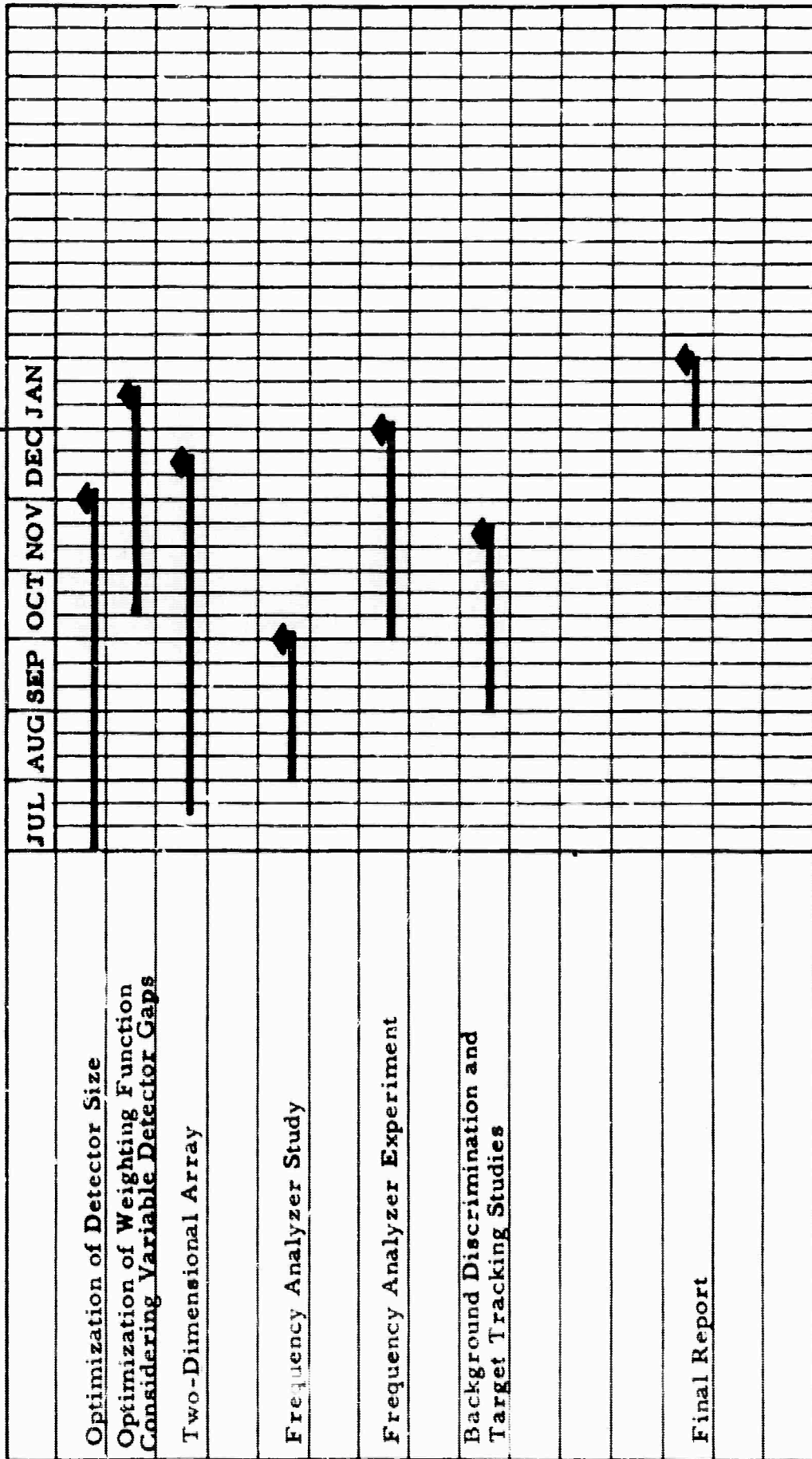
VII. ADAPTIVE WEIGHTING

As described in the report, there are numerous parameters which affect the performance of a spatial filter including detector width, number of detectors, detector gaps, detector density function, and optical system transfer function. As the analysis of these parameters combined is cumbersome, this study was directed toward evaluating the effect of each parameter independently in the overall filter response. An optimum design for a specific filter function should enjoy the flexibility of varying these parameters simultaneously.

The design of a practical detector array may become more complex, however, if the non-uniformities of detector response and telescope transfer function as well as detector width and gap tolerances are to be considered functions of the f cal plane dimensions. These difficulties and attendant problems can be avoided or minimized by applying the adaptive learning technique in the design of these filters. This scheme would entail placing an array of detectors in the focal plane of a telescope. Each detector signal would be fed to a variable weighting element which would be adjusted by the signal of a comparator network. The comparator would sense the difference between the actual output of the detector array and a described output for a prescribed input function. The weighing element would be adjusted repeatedly until the difference becomes zero. At this time, the weighting function values would be fixed. A sequential and iterative process thus could be employed to realize a filter with prescribed frequency response characteristics.

Future work should include the feasibility evaluation of adaptive learning techniques for realization of the spatial filters.
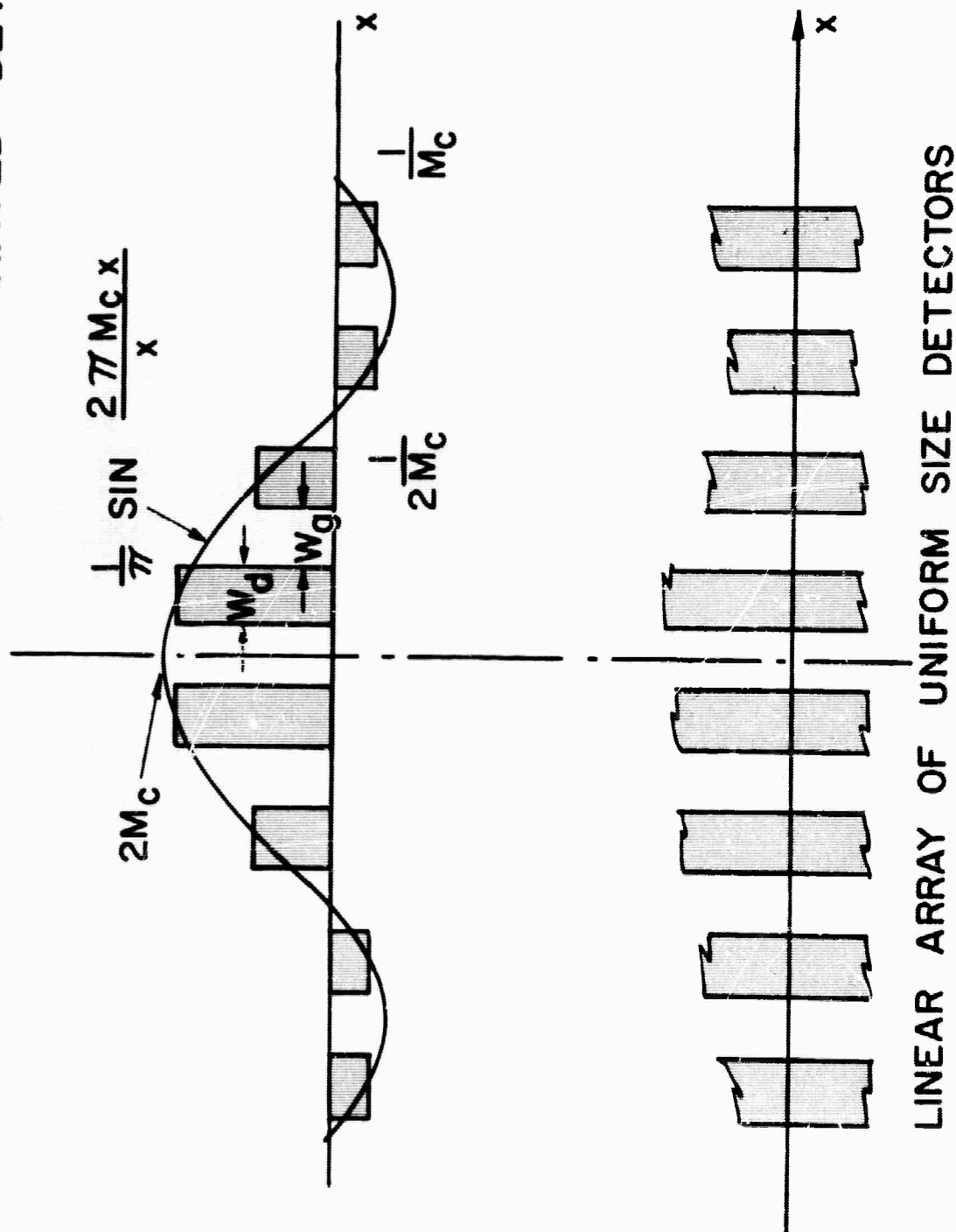
1964   1965

	JUL	AUG	SEP	OCT	NOV	DEC	JAN

Optimization of Detector Size

Optimization of Weighting Function
Considering Variable Detector Gaps

Two-Dimensional Array

Frequency Analyzer Study

Frequency Analyzer Experiment

Background Discrimination and
Target Tracking Studies

Final Report

MILESTONE CHART

A3814:65-83

AEROJET GENERAL

ASTRIONICS DIVISION

APPROXIMATION OF THE TRANSIENT RESPONSE OF A 1-DIMENSIONAL LOW-PASS FILTER WITH SEPARATED DETECTORS

$$\frac{1}{\pi} \text{SIN} \frac{2\pi M_c x}{x}$$

$2M_c$

W_d

W_g

$\frac{1}{2M_c}$

$\frac{1}{M_c}$

x

LINEAR ARRAY OF UNIFORM SIZE DETECTORS

x

Figure 2

INVERSE TRANSFORM OF A TWO-DIMENSIONAL LOW-PASS FILTER
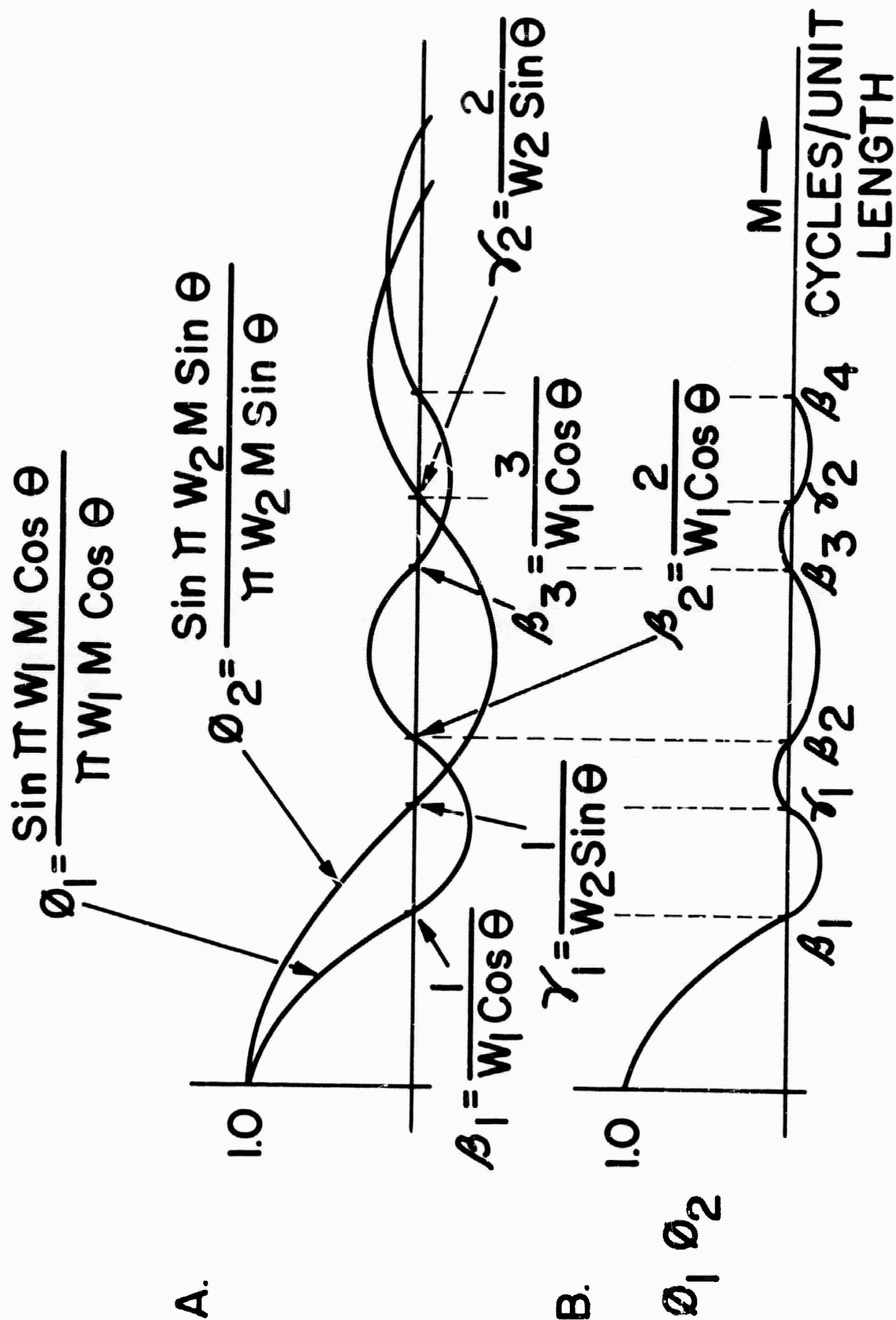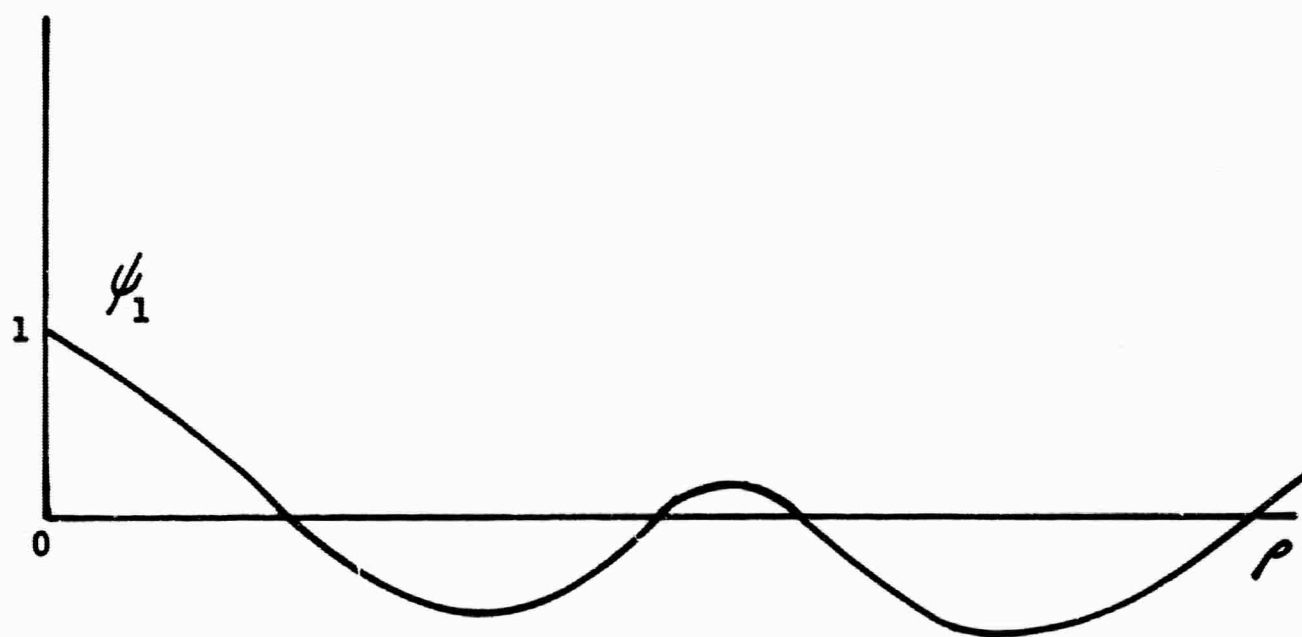
TWO-DIMENSIONAL IDEAL LOW-PASS FILTER
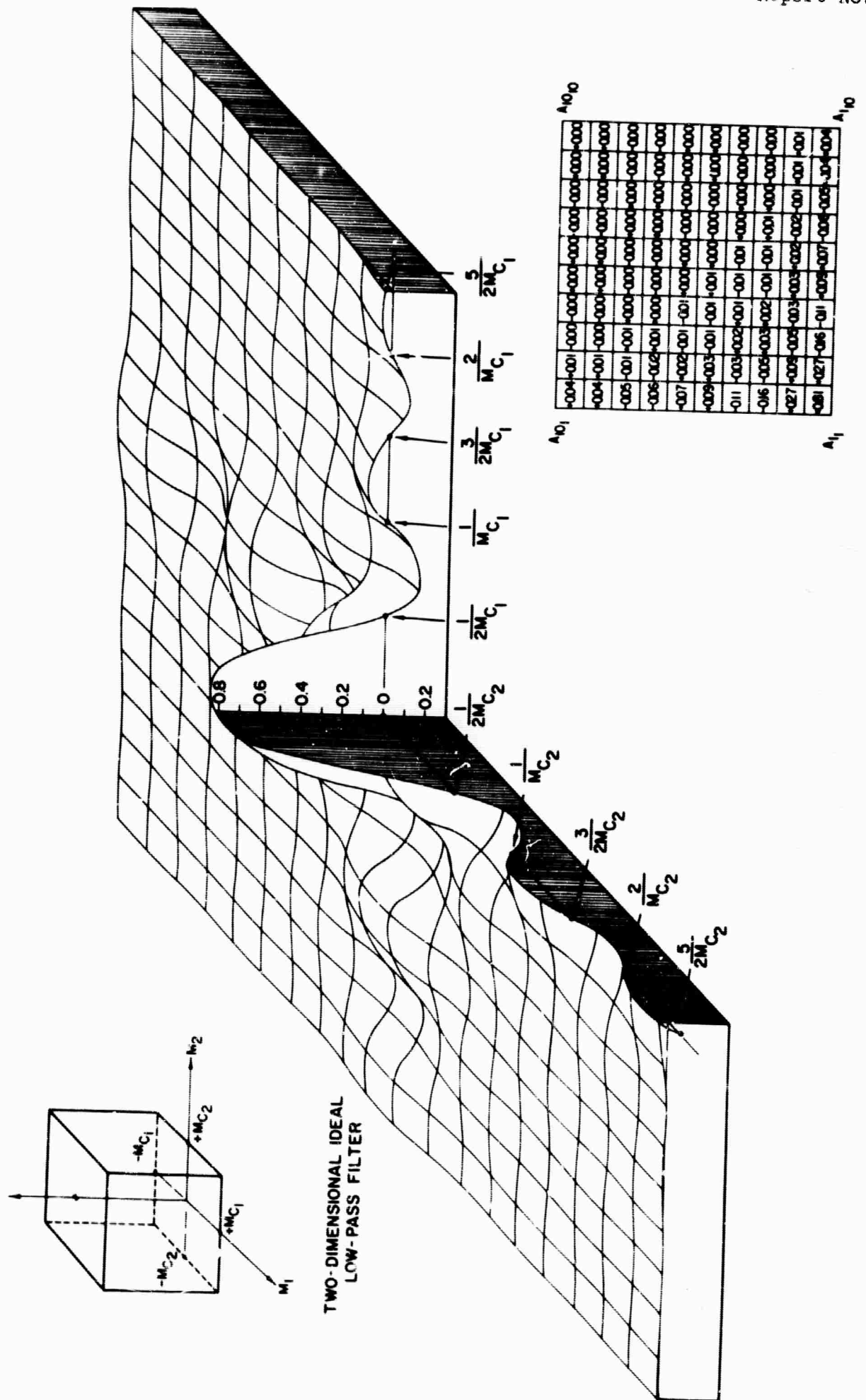
Figure 3

ENVELOPE FUNCTION OF A DETECTOR IN A TWO-DIMENSIONAL SPATIAL FILTER

A.

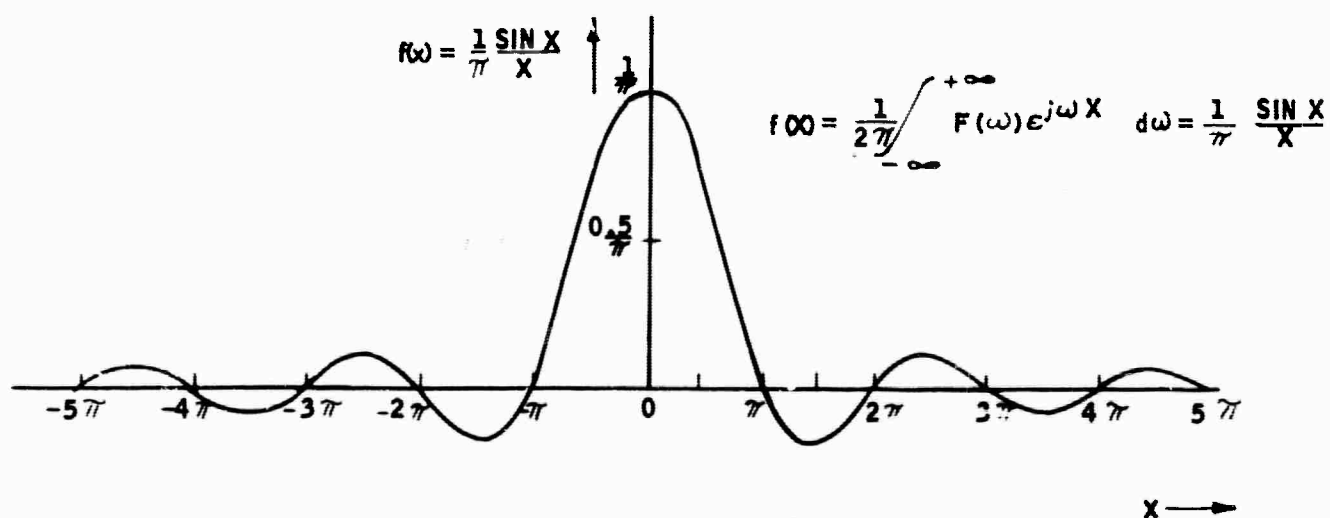$$\emptyset_1 = \frac{\mathrm{Sin}\,\pi\,W_1\,M\,\mathrm{Cos}\,\Theta}{\pi\,W_1\,M\,\mathrm{Cos}\,\Theta}$$

$$\emptyset_2 = \frac{\mathrm{Sin}\,\pi\,W_2\,M\,\mathrm{Sin}\,\Theta}{\pi\,W_2\,M\,\mathrm{Sin}\,\Theta}$$

$$\gamma_2 = \frac{2}{W_2\,\mathrm{Sin}\,\Theta}$$

$$\beta_3 = \frac{3}{W_1\,\mathrm{Cos}\,\Theta}$$

$$\beta_2 = \frac{2}{W_1\,\mathrm{Cos}\,\Theta}$$

$$\gamma_1 = \frac{1}{W_2\,\mathrm{Sin}\,\Theta}$$

$$\beta_1 = \frac{1}{W_1\,\mathrm{Cos}\,\Theta}$$

1.0

$$M \longrightarrow$$

$$\beta_1 \quad \gamma_1 \quad \beta_2 \quad \beta_3 \quad \gamma_2 \quad \beta_4 \quad \text{CYCLES/UNIT LENGTH}$$

B.

1.0

$$\emptyset_1 \quad \emptyset_2$$

Figure 4

$$\cos\left[(2i-1)\,W_1\,\pi\rho\cos\theta\right]$$

$$\cos\left[(2k-1)\,W_2\,\pi\rho\sin\theta\right]$$
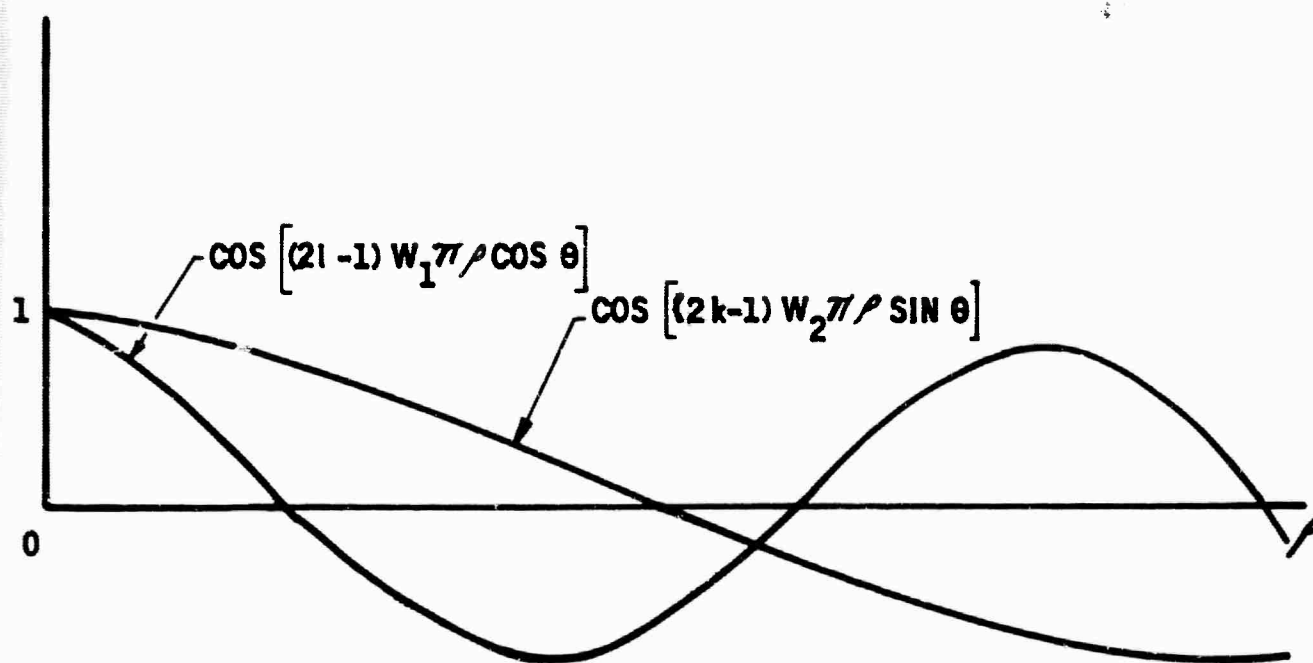
ψ_1, A COMPONENT OF THE EDGE FUNCTION $\psi\,(\rho,\theta)$

AEROJET GENERAL

ASTRIONICS DIVISION

A3814:65-90

Figure 5

$\omega = 2\pi m$ (RADIANS PER UNIT LENGTH) WHERE

m = SPATIAL FREQUENCY (CYCLES PER UNIT LENGTH)

$F(\omega)$

1

1   0   1

$\omega \longrightarrow$

IDEAL LOW-PASS SPATIAL FREQUENCY FUNCTION

$f(x) = \frac{1}{\pi} \frac{SIN\ X}{X}$

$\frac{1}{\pi}$

$f(x) = \frac{1}{2\pi} \int_{-\infty}^{+\infty} F(\omega)\epsilon^{j\omega X}\ d\omega = \frac{1}{\pi} \frac{SIN\ X}{X}$

$\frac{0.5}{\pi}$

$-5\pi \quad -4\pi \quad -3\pi \quad -2\pi \quad -\pi \quad 0 \quad \pi \quad 2\pi \quad 3\pi \quad 4\pi \quad 5\pi$

$X \longrightarrow$
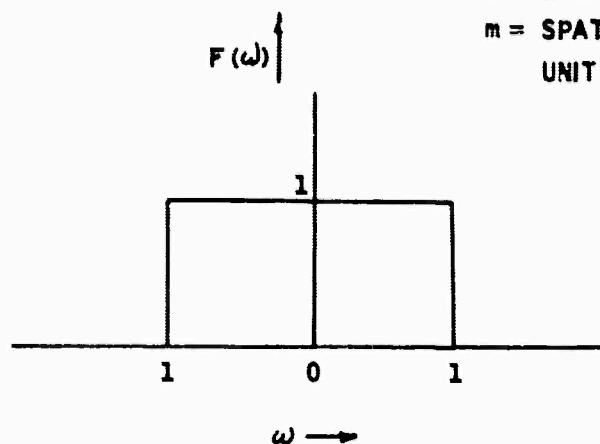
DETECTOR DISTRIBUTION

D_1	D_2	D_3	D_4

$0 \quad \frac{\pi}{2} \quad \pi \quad \frac{3\pi}{2} \quad 2\pi$

IDEAL LOW-PASS SPATIAL FREQUENCY FILTER AND A DETECTOR DISTRIBUTION

B3814:65-67

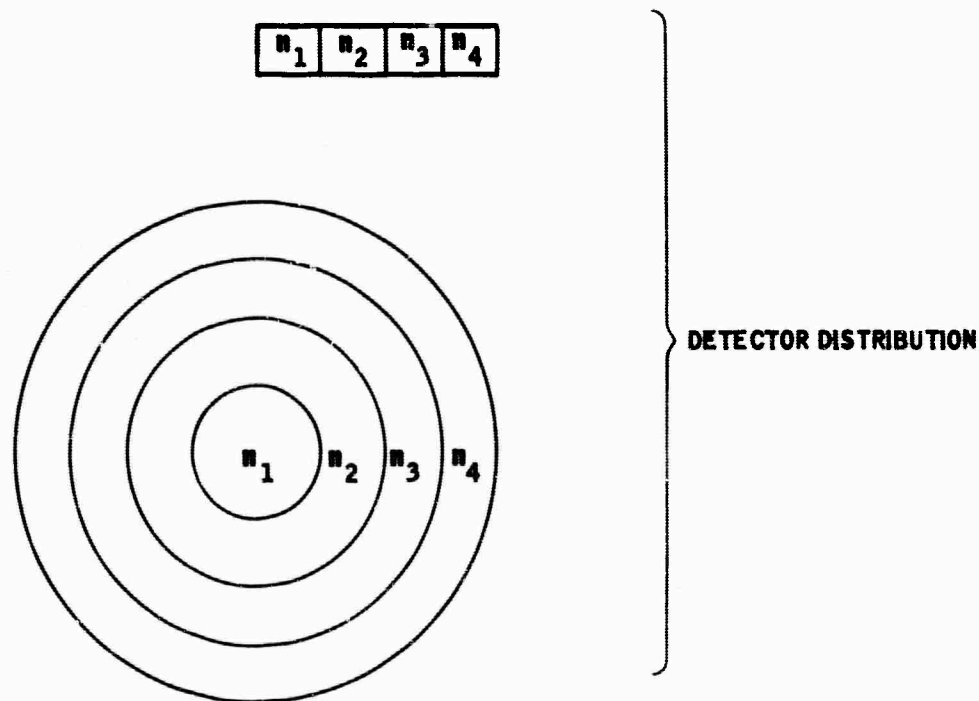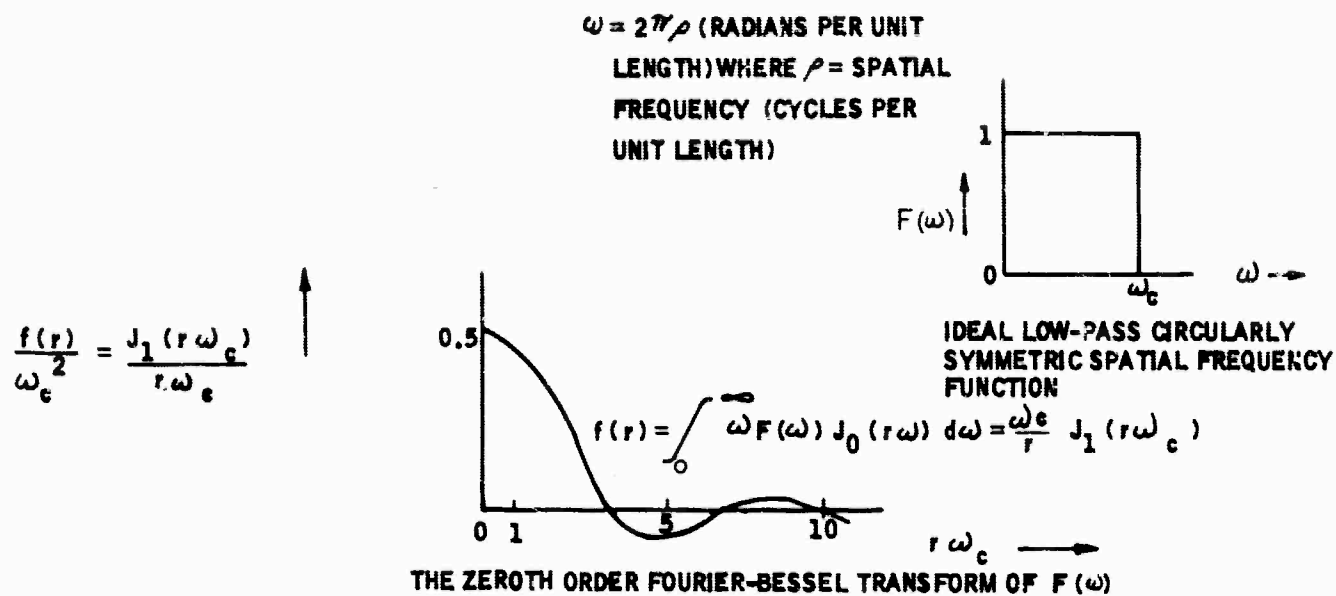Figure 6

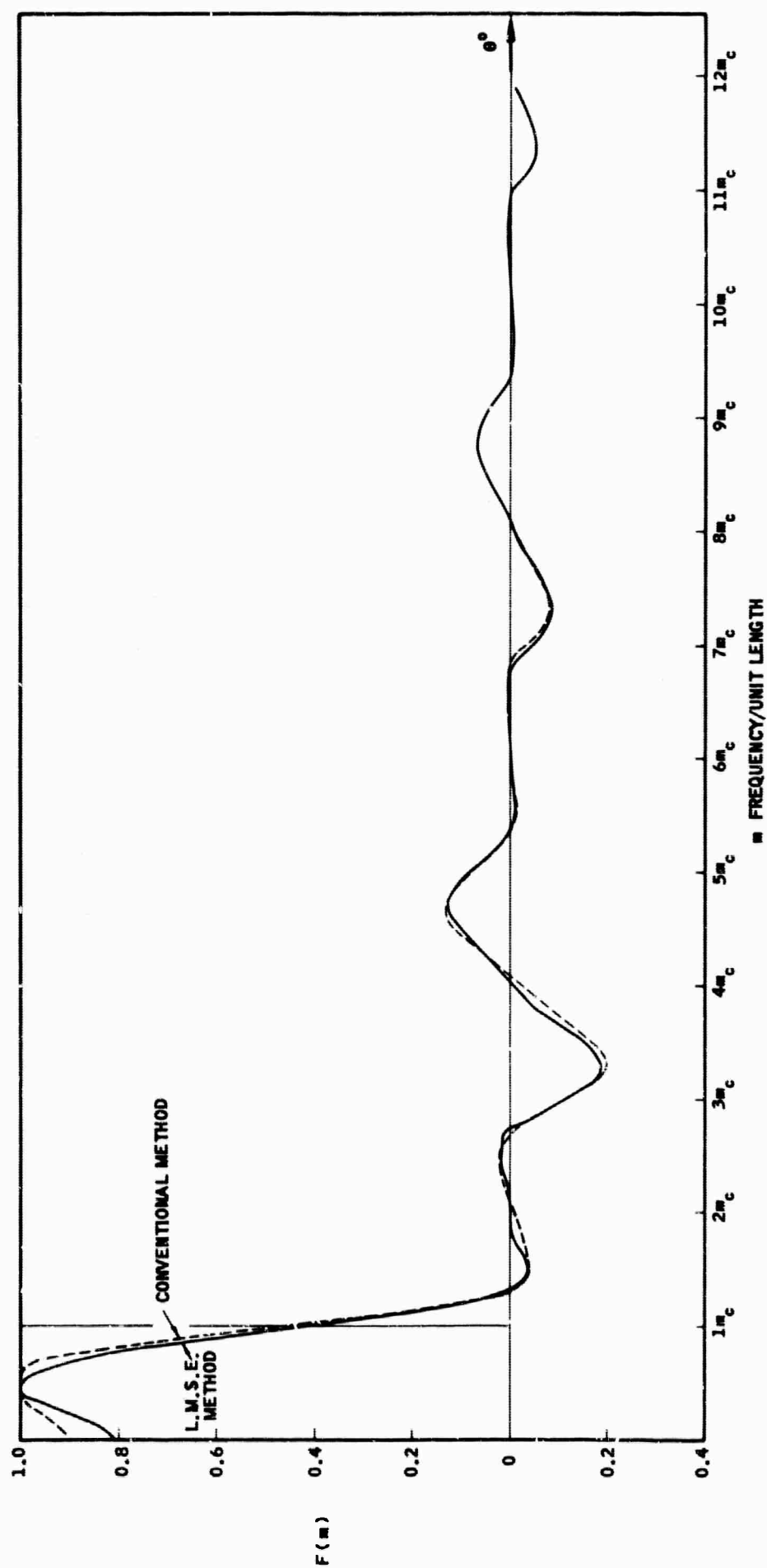$$f(x) = \frac{1}{\pi} \frac{\sin x}{x}$$

$$a_2 = \frac{0.306}{\pi}$$
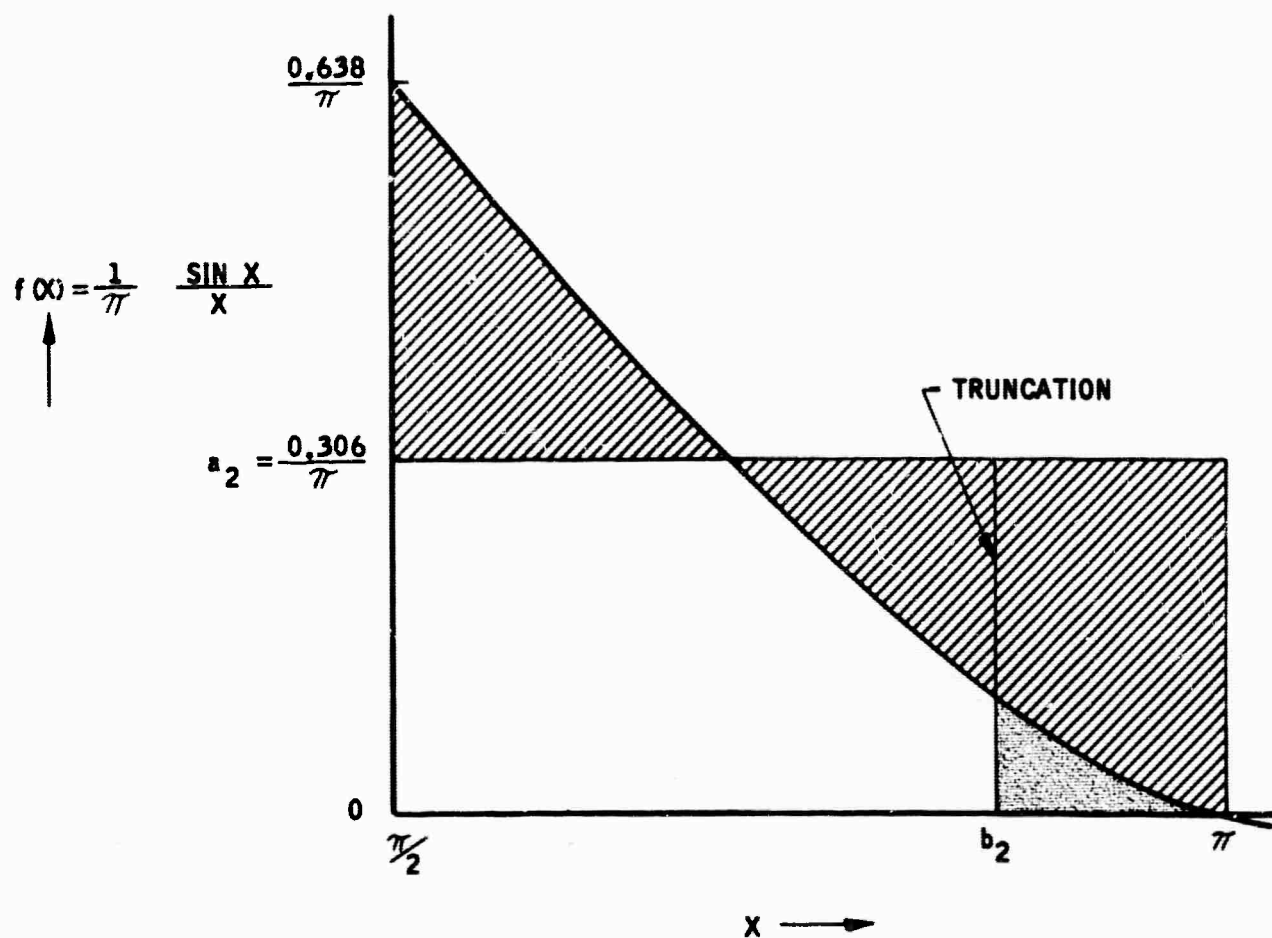
AFTER TRUNCATION AT b_2, THE SMALLER DOTTED AREA REPLACES THE LARGER STRIPED AREA ABOVE IT IN THE CALCULATION OF THE ERROR INTEGRAL.

ILLUSTRATION OF ERROR INTEGRAL REDUCTION
## BY TRUNCATION OF A DETECTOR

Figure 7

$\omega = 2\pi\rho$ (RADIANS PER UNIT LENGTH) WHERE ρ = SPATIAL FREQUENCY (CYCLES PER UNIT LENGTH)

$$\frac{f(r)}{\omega_c^2} = \frac{J_1(r\omega_c)}{r\omega_c}$$

$$f(r) = \int_0^\infty \omega F(\omega) J_0(r\omega)\, d\omega = \frac{\omega_c}{r} J_1(r\omega_c)$$

IDEAL LOW-PASS CIRCULARLY SYMMETRIC SPATIAL FREQUENCY FUNCTION

THE ZEROTH ORDER FOURIER-BESSEL TRANSFORM OF F(ω)

DETECTOR DISTRIBUTION

THE CIRCULARLY SYMMETRIC IDEAL LOW-PASS SPATIAL FREQUENCY FILTER

AEROJET GENERAL

ASTRIONICS DIVISION

53814:65-66

Figure 8

A COMPARISON BETWEEN FREQUENCY RESPONSES OF A ONE-DIMENSIONAL
FILTER OBTAINED BY CONVENTIONAL AND L.M.S.E. METHODS $X_T m_c$ · 1
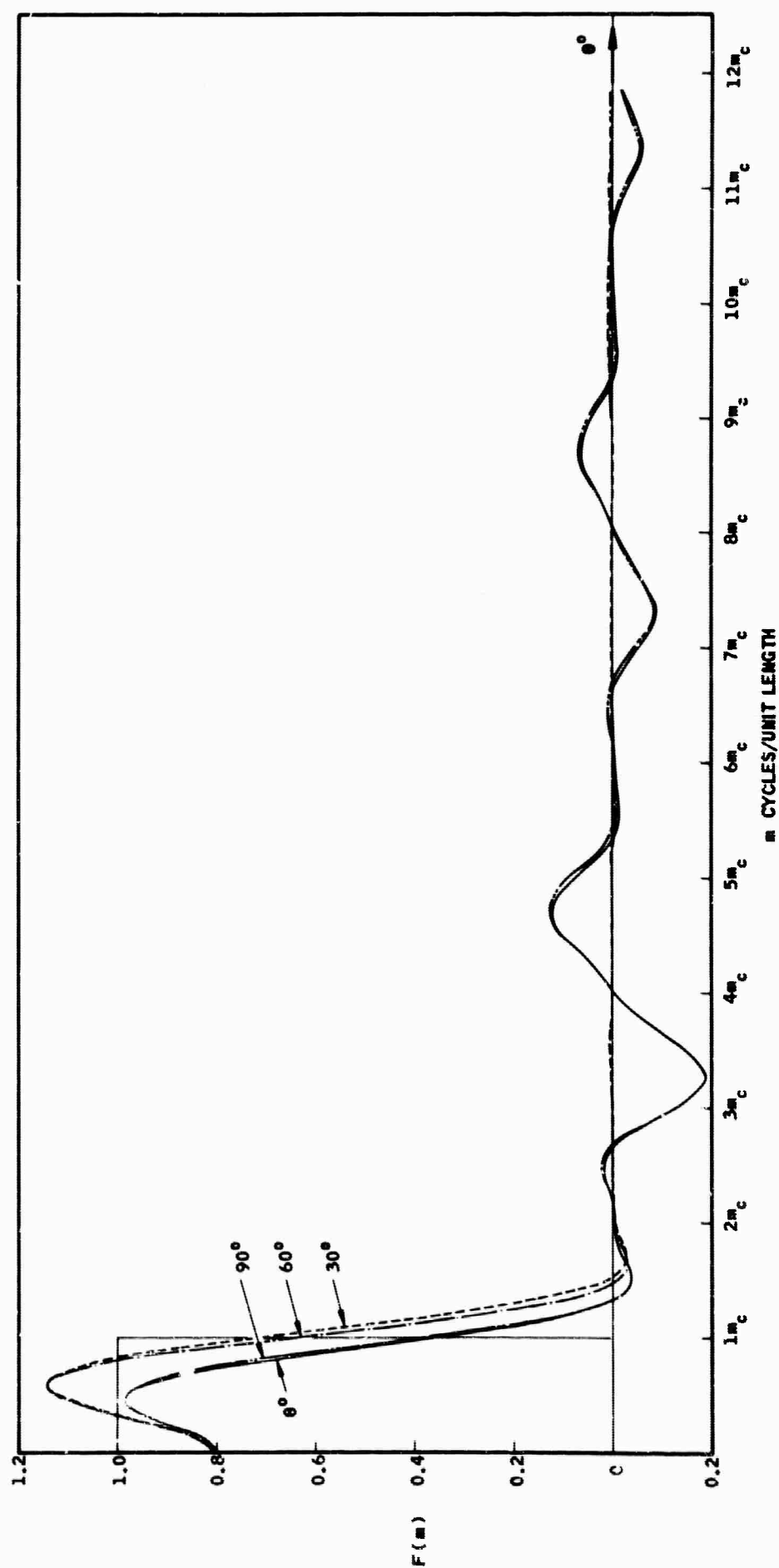
B3814:65-64

Figure 9

FREQUENCY RESPONSE OF AN 8x8 TWO-DIMENSIONAL SPATIAL FILTER
FOR 0°, 30°, 60°, AND 90° SCANNING ANGLE $X_T m_{c_i} = Y_T m_{c_2} = 1$

B3814:65-65

Figure 10
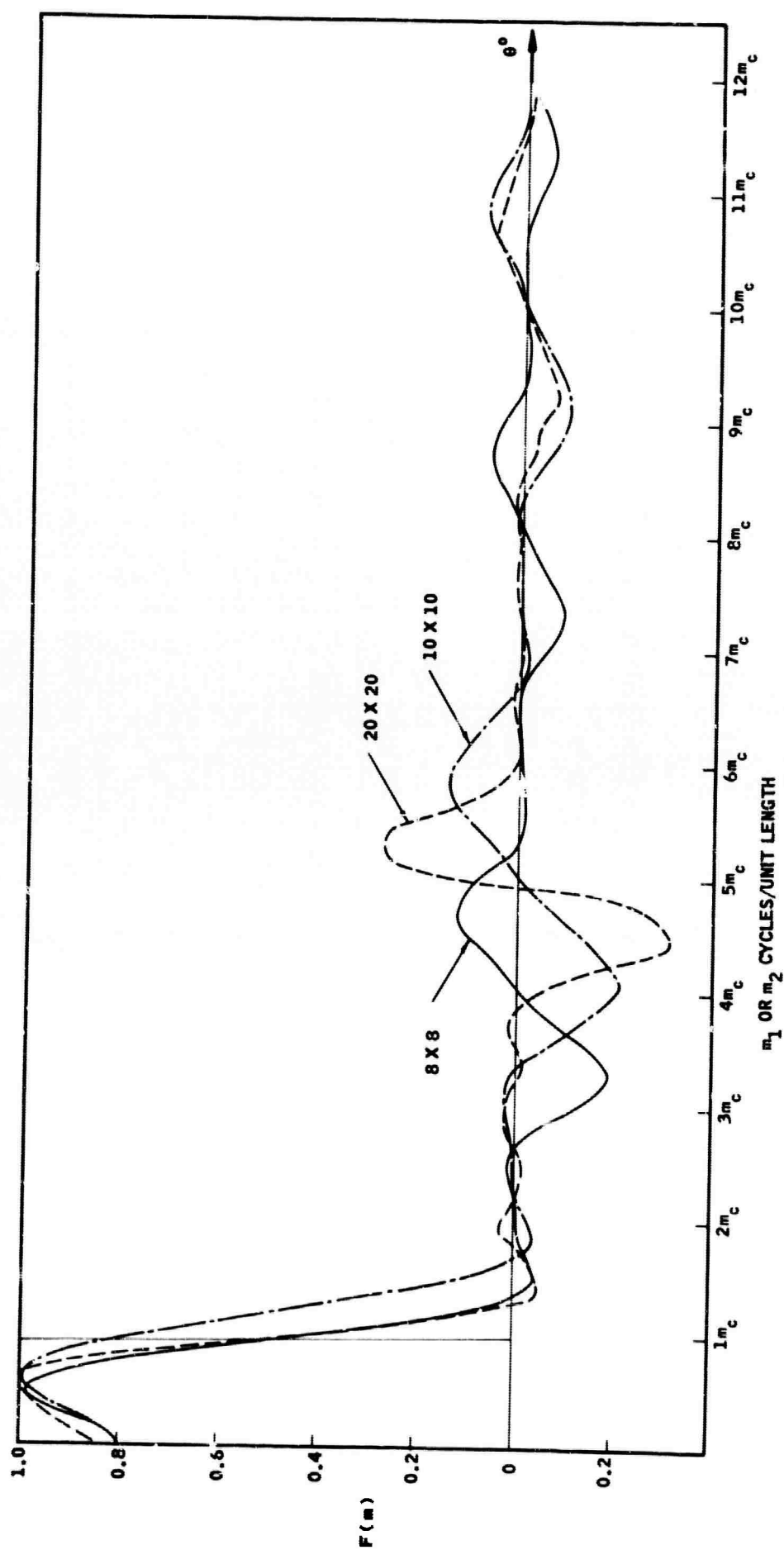
B3814:65-63

THE RESPONSE OF A TWO-DIMENSIONAL SPATIAL FILTER ON m_1 OR m_2 AXES USING 8x8, 10x10, AND 20x20 DETECTOR ARRAY $X_T m_{c_1} \cdot Y_T m_{c_2} - 1$

Figure 11

SPATIAL FREQ. RESPONSE OF ONE-DIMENSIONAL DETECTOR ARRAYS, $\eta = 2$
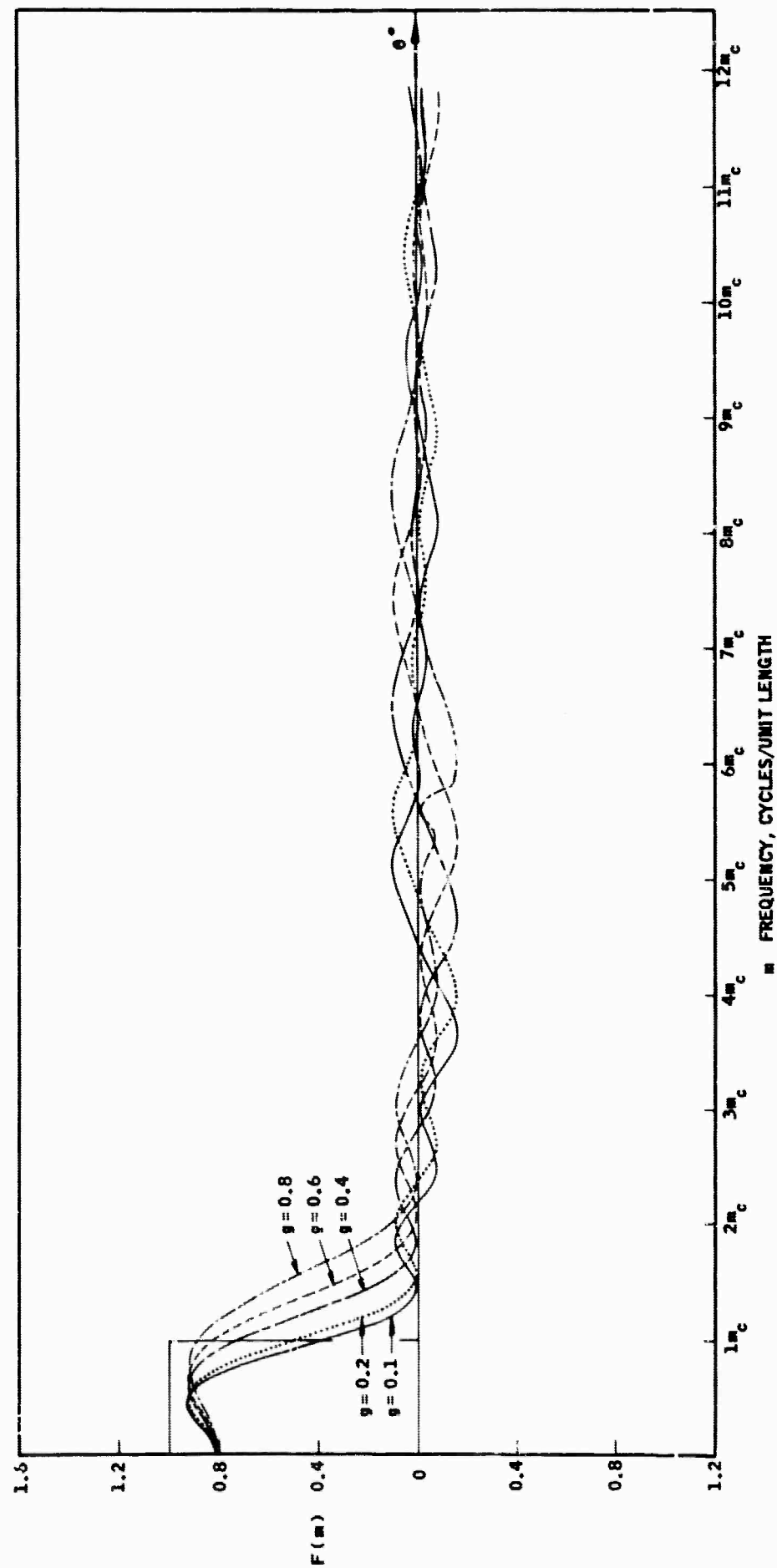(FITTED TO RECTANGULAR FREQ. CHARACTERISTIC)
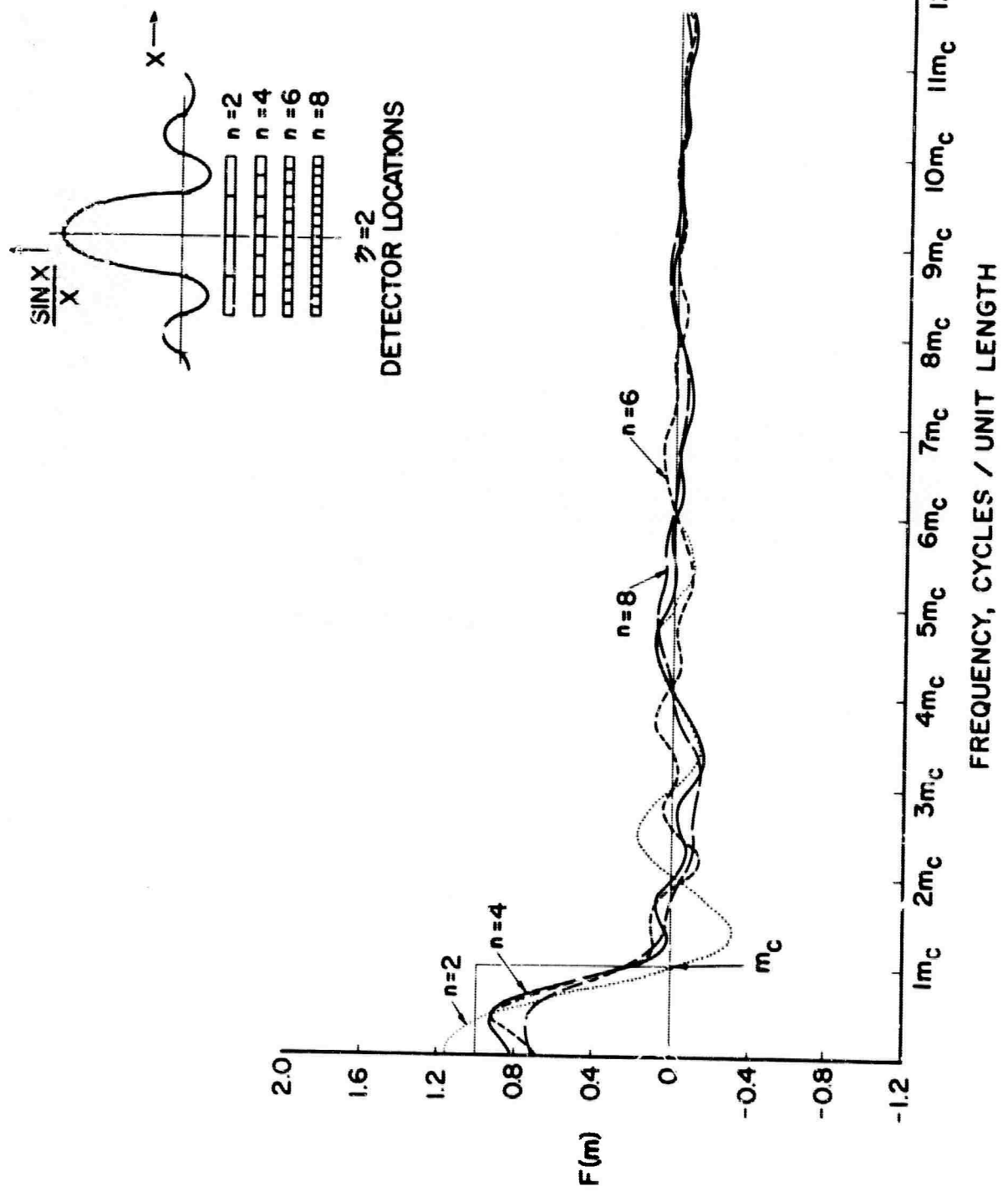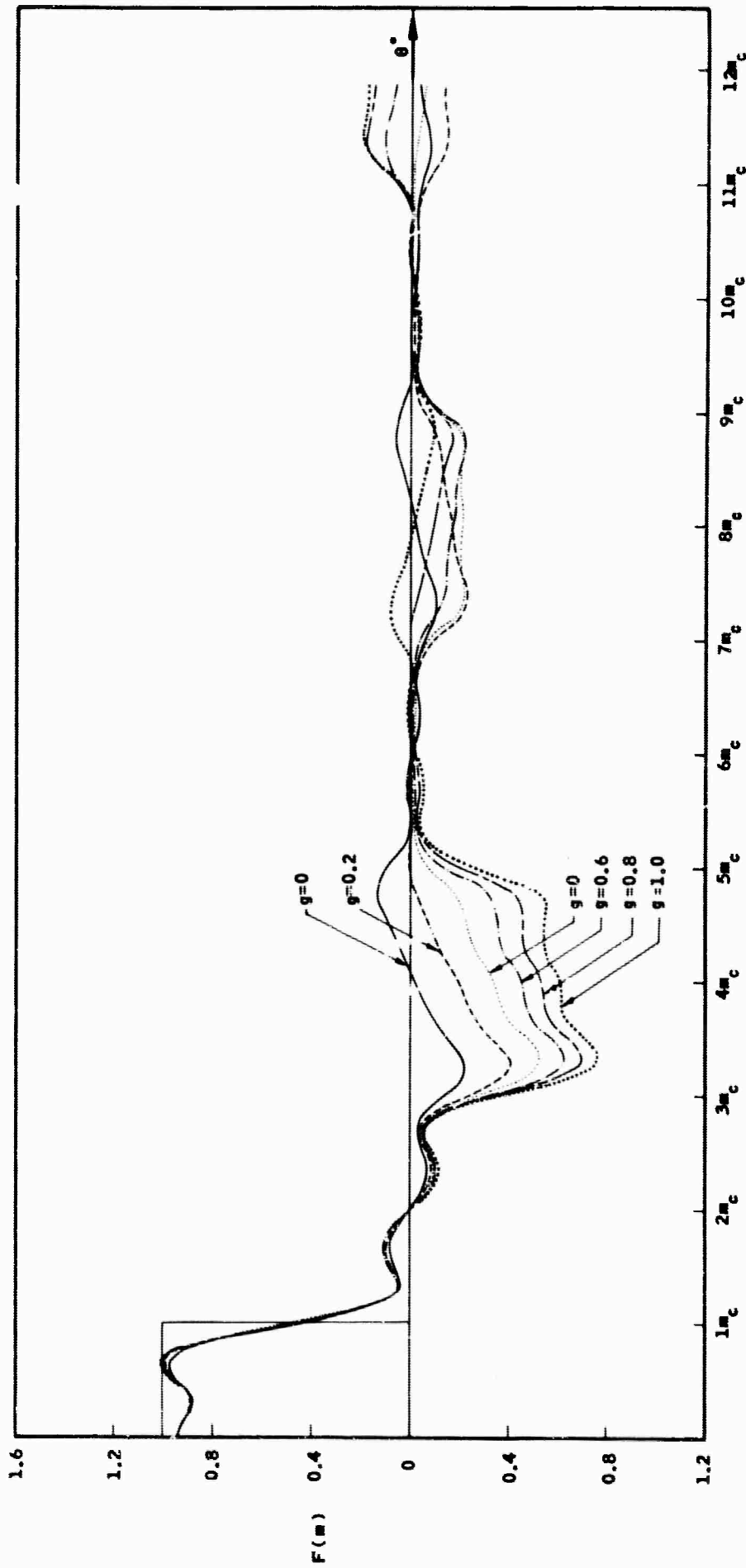
Figure 12

FREQUENCY RESPONSE OF A ONE-DIMENSIONAL SPATIAL FILTER AS A FUNCTION

OF DETECTOR GAP $X_T m_c - 1$

m   FREQUENCY, CYCLES/UNIT LENGTH

B3814:65-54

ASTRIONICS DIVISION

Figure 13

m = FREQUENCY, CYCLES/UNIT LENGTH

FREQUENCY RESPONSE OF A ONE-DIMENSIONAL SPATIAL FILTER FOR

VARIABLE DETECTOR GAP $X_T m_c - \frac{3}{4}$

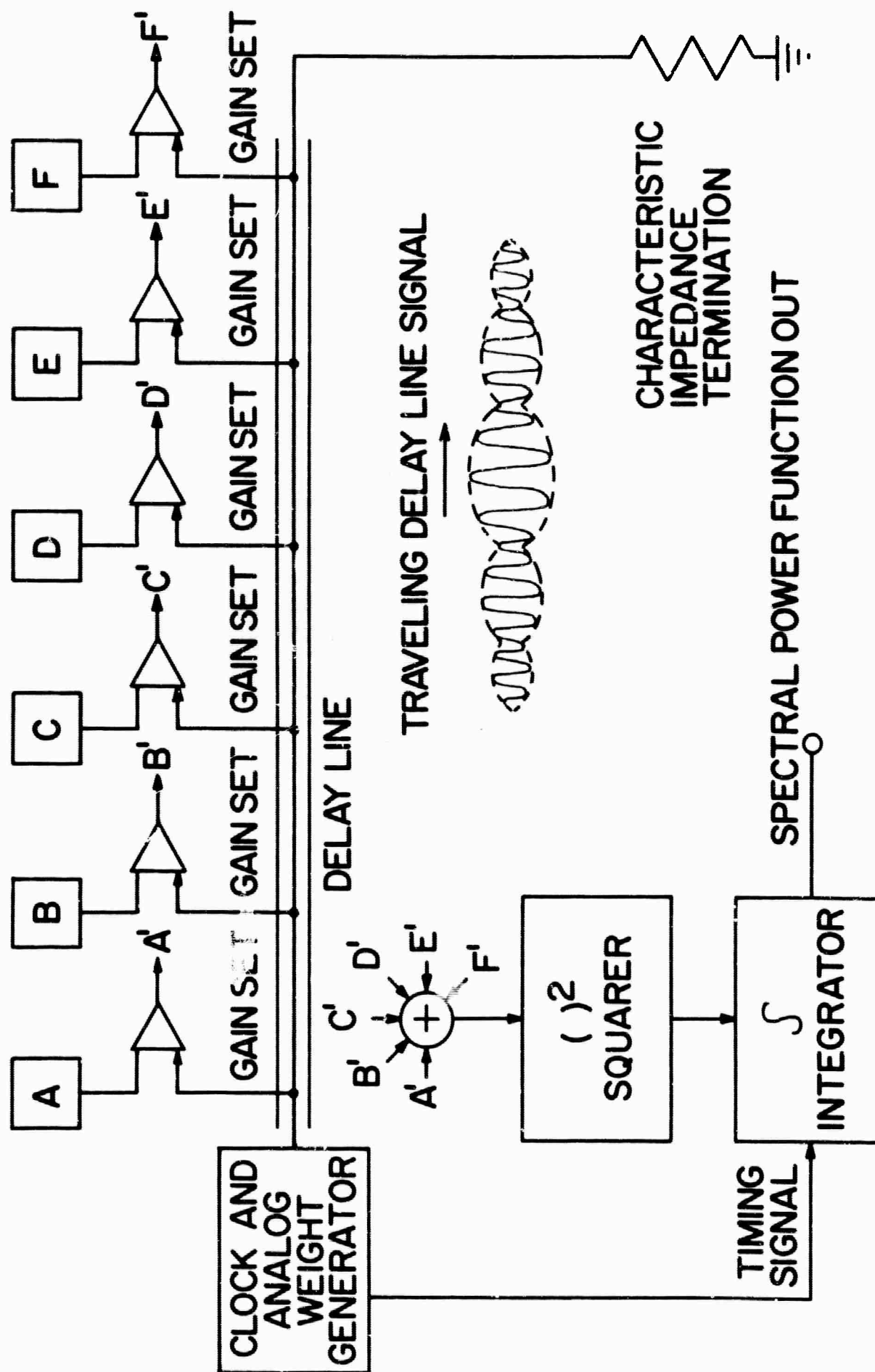Figure 14

SCHEMATIC DIAGRAM OF A SPATIAL FREQUENCY ANALYZER
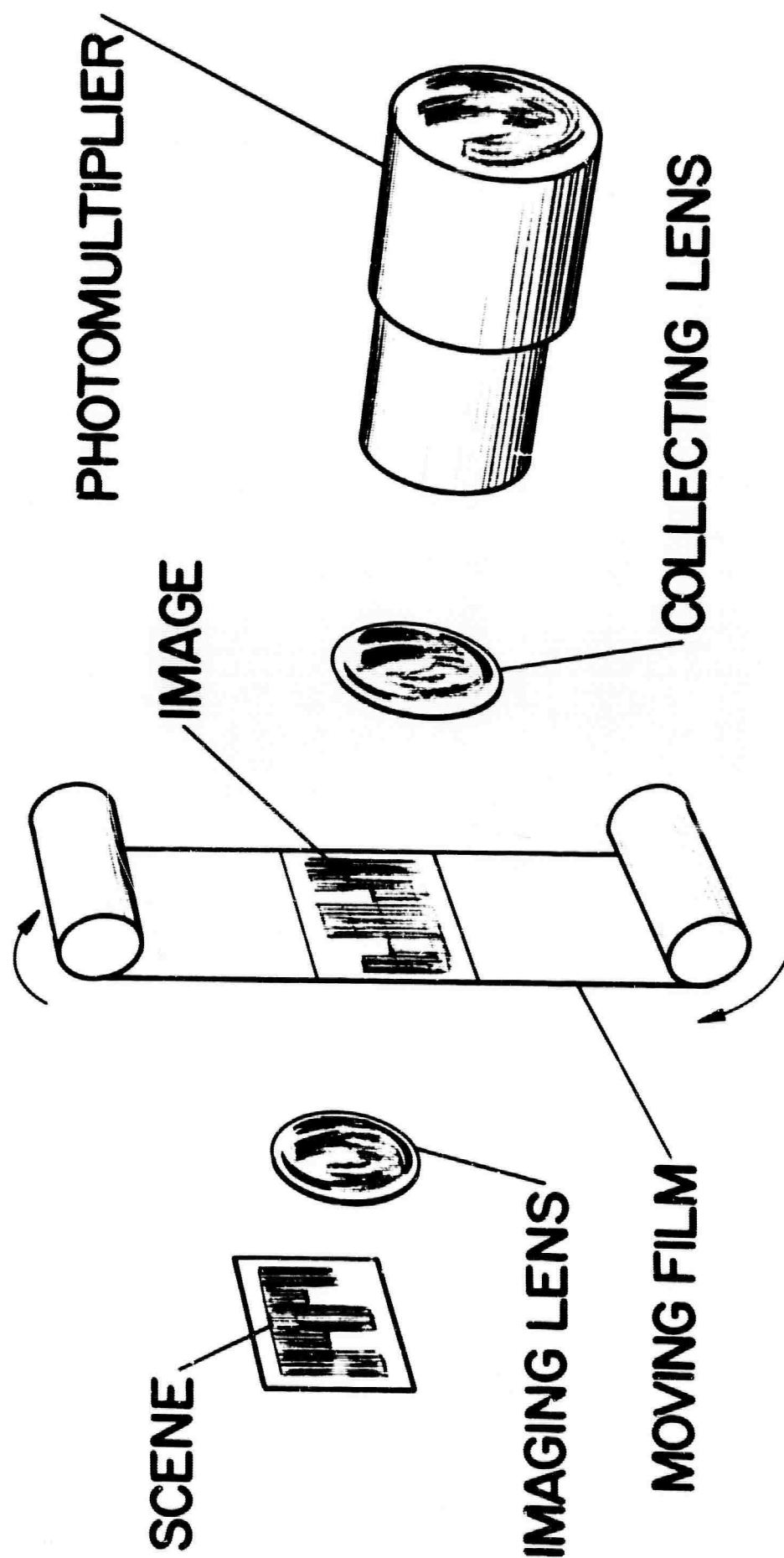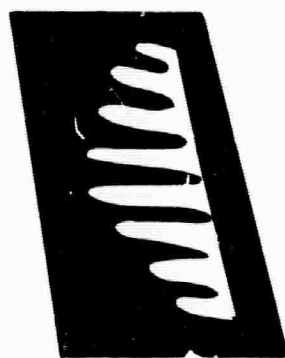
Figure 15

SCHEMATIC OF TRANSPARENCY ANALOG SYSTEM

PHOTOMULTIPLIER

IMAGE

COLLECTING LENS

SCENE

IMAGING LENS

MOVING FILM

Figure 16

1-DIMENSIONAL INTENSITY FUNCTION GENERATOR
USING A CYLINDRICAL LENS

1-DIMENSIONAL
INTENSITY DISTRIBUTION
AT IMAGE PLANE

VIEW
CAMERA

CYLINDRICAL
LENS

SPACE FUNCTION
SILHOUETTE

DIFFUSE
LIGHT SOURCE
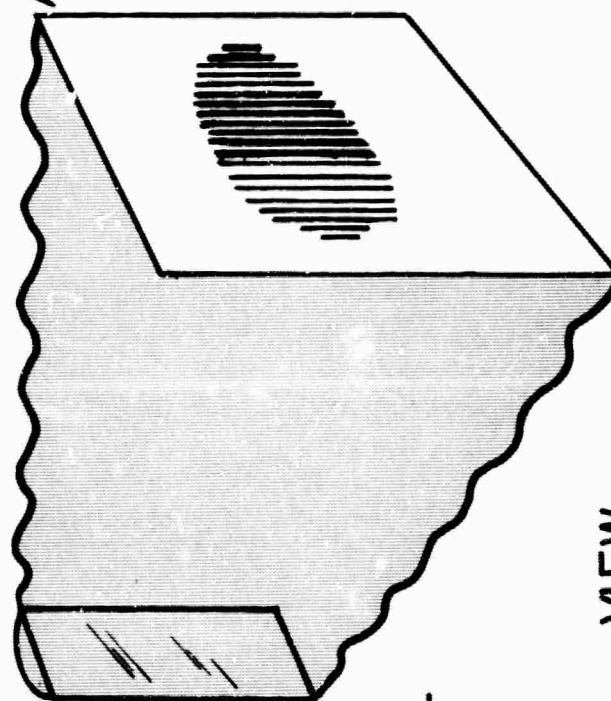
Figure 17

1-DIMENSIONAL BAND-PASS TRANSPARENCY

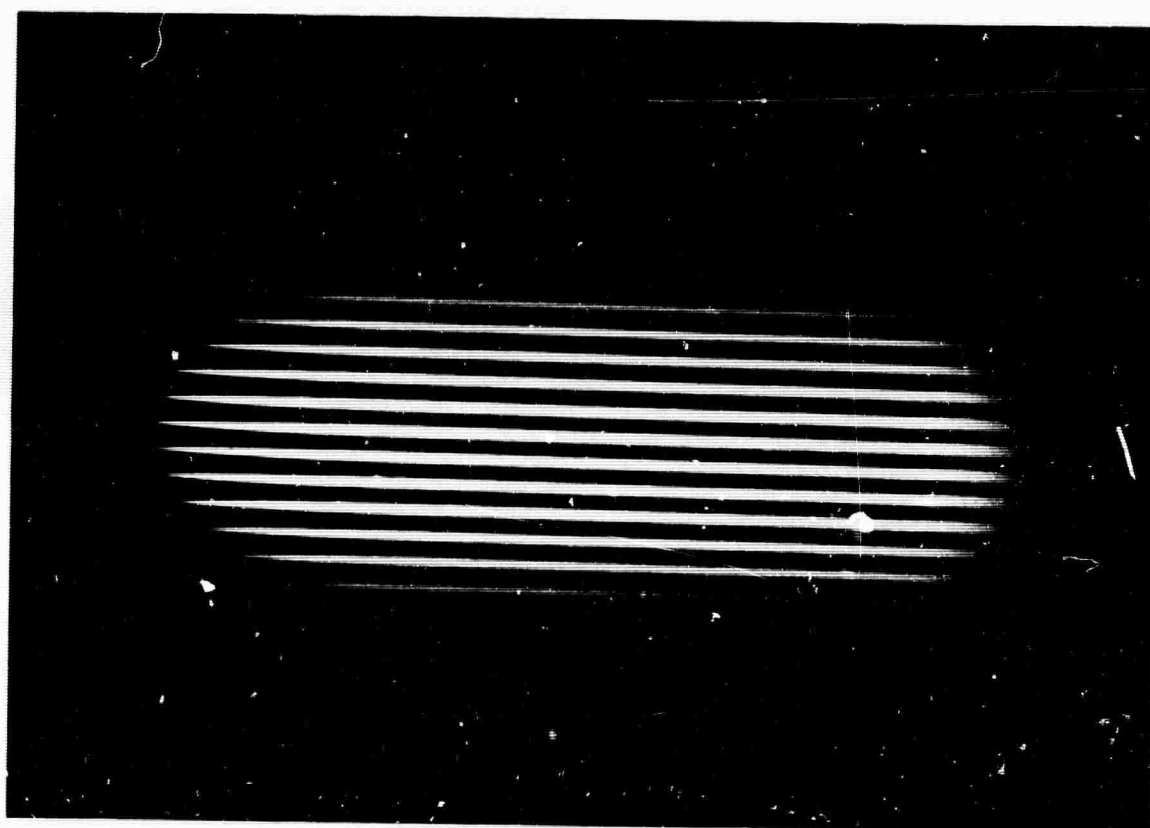Figure 18

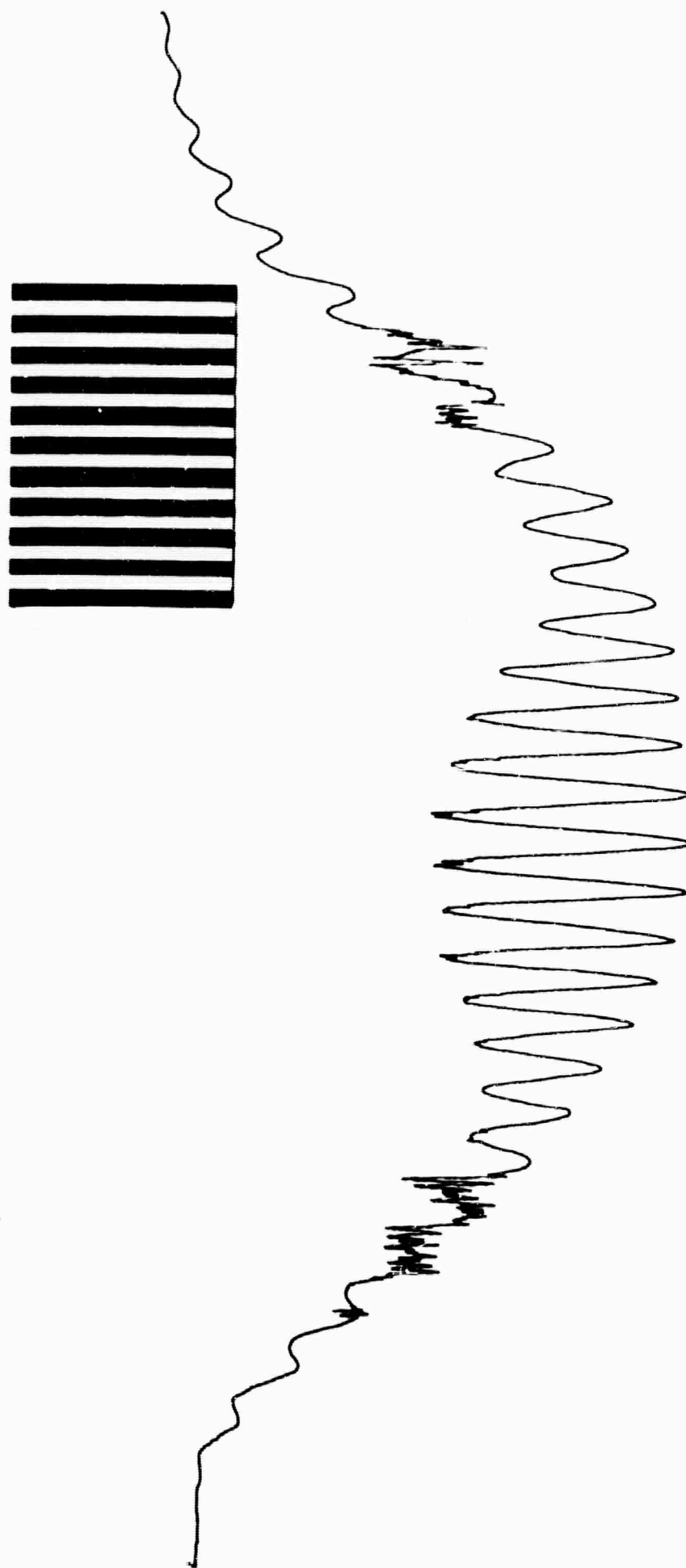**M_c PICKET-FENCE OBJECT AND FILTERED FUNCTION**

Figure 19

PICKET-FENCE OBJECT AND FILTERED FUNCTION

$\frac{M_c}{2}$
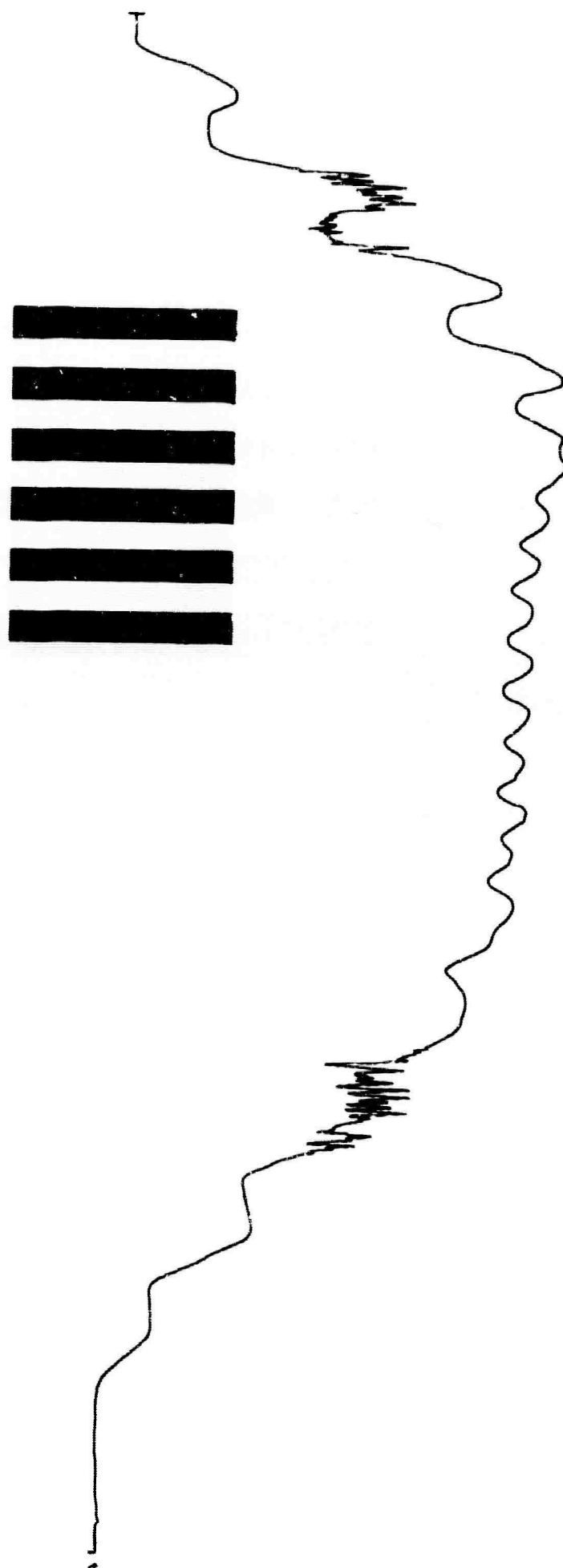
Figure 20

$$\frac{M_c}{3}$$ PICKET-FENCE OBJECT AND FILTERED FUNCTION
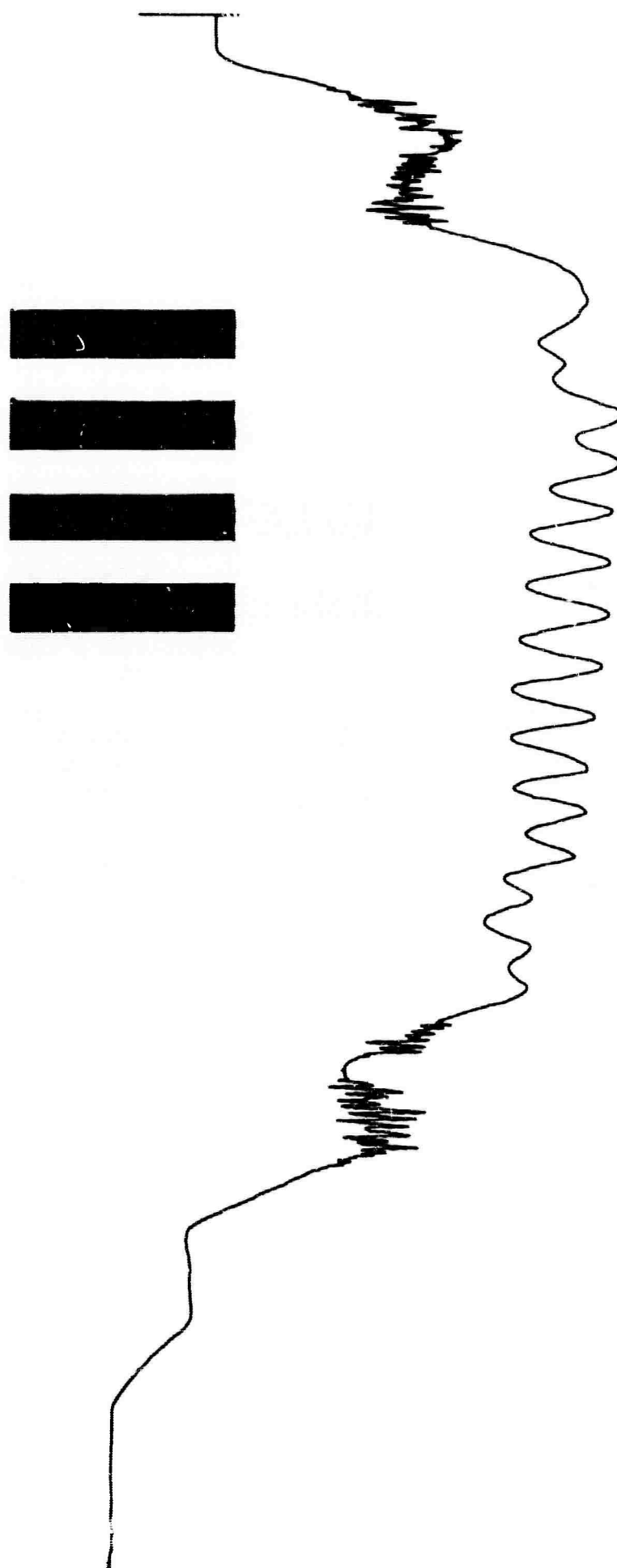
Figure 21

APPENDIX A

SPATIAL FILTER SYNTHESIS[*]

By K. Seyrafi and G. A. Davison

ABSTRACT

Design and synthesis of one-dimensional low-pass and band-pass spatial filters are developed by approximating the space domain transient response of the filters with rectangular detectors. The transforms of the approximating functions are derived analytically. Numerical solutions to the function are obtained through the use of a computer. The results indicate that for reasonable tolerances in the pass-band or stop-band, a small number of detectors is sufficient.

I. INTRODUCTION

Once it is given, the transfer function of an electrical network can generally be realized by a proper combination of lumped passive elements (resistors, capacitors, and inductors) and active elements such as vacuum tubes and transistors (References 1, 2 and 3). The exact configuration and number of necessary elements is determined by the required pass-band and stop-band characteristics (e.g., ripple and rate of attenuation). These requirements have led to systematic design procedures, such as Chebycheff (equal-ripple), and Butterworth (maximally flat) filters. There are also systematic procedures for realizing filter designs.

A similar design and synthesis has not yet been developed for space filtering, although the application of two-dimensional Fourier transforms to spatial filtering has been studied in some detail, and there has been empirical design in low- and band-pass spatial filters (Reference 4). There is no simple analogy between the concept of electrical filter elements and synthesis, and space filters, such that one is able to extend the well-systematized techniques of electrical-circuit synthesis to spatial-filter synthesis. However, one can apply the approximation techniques used to find the transfer function of an electrical filter when the impulse response is known. The time impulse response can be approximated by a series of triangular or rectangular pulses (References 5 and 6). The transfer function is found by summing the transfer functions of the elemental pulses, each with its corresponding delay.

The following discussion employs a suggestion of J. A. Jamieson to approximate the transfer function of a spatial filter using an ensemble of rectangular detectors, and it develops a method similar to the time-function approximation. A systematic scheme is thereby proposed for designing and synthesizing low-pass and band-pass spatial filters using a variable number of resolution elements or detectors. The outputs of the detectors are weighted according to their position in the

image plane, and are then summed. It is shown that by increasing the number of
detectors or resolution elements, one can approximate the desired transfer function
with arbitrary accuracy, which is analogous to increasing the number of elements
in an electrical filter.

II.   PRINCIPLE OF APPROACH

    A.   LOW PASS

        1.   Derivation

We begin by examining an ideal one-dimensional low-pass spatial
filter with a flat response of unity out to the frequency $m = m_c$ cycles/unit length
and thereafter a zero response, as shown in Figure 1A. The inverse Fourier trans-
form of this function, which is the spatial impulse response, has the characteris-
tic shown in Figure 1B.

The curve, $f(x)$, of Figure 1B can be approximated by an infinite
set of rectangular pulses with a uniform width, W. A summation of the transforms
of the rectangular pulses is an approximation to $F(jm)$ and in the limit as $W \rightarrow 0$,
is equal to it. The realization of each pulse is simply a detector of width W and
a sensitivity proportional to the pulse height (Figure 2).

The amplitude of the ith pulse, A_i (Figure 2), is:

$$A_i = \frac{1}{\pi} \frac{\sin(2i-1)\frac{W}{2}2\pi m_c}{(2i-1)\frac{W}{2}} \qquad \text{for i an integer} \qquad (1)$$

Therefore, the pulse can be represented in the space domain by
$f_i(x)$ where

$$f_i(x) = \frac{1}{\pi} \frac{\sin\frac{2i-1}{2}W2\pi m_c}{(2i-1)\frac{W}{2}} \qquad (i-1)\,W < x < iW \qquad (2)$$

$$= 0 \qquad x < (i-1)\,W$$

$$x > iW$$

The approximation of $f(x)$ will therefore be:

$$f(x) \cong \sum_{i=-\infty}^{i=\infty} f_i(x) \tag{3}$$

Practically, it is not possible to incorporate an infinite number of detectors. But because of the attenuating effect of the $\frac{\sin x}{x}$ factor for high values of x, the amplitude of the pulses becomes increasingly smaller and smaller, such that elimination of those detectors has slight effect on the transfer function. Therefore, if we truncate the approximation after n detectors and denote the truncation function by $f^*(x)$, we have:

$$f^*(x) = \sum_{i=1-n}^{i=+n} f_i(x) \tag{4}$$

The Fourier transform of $f^*(x)$, namely $F^*(jm)$ will be the sum of the individual transforms of $f_i(x)$:

$$F^*(jm) = \sum_{i=1-n}^{+n} \frac{1}{\pi} \frac{\sin\left[\frac{2i-1}{2} Wm_c 2\pi\right]}{(2i-1)\frac{W}{2}} \cdot W \frac{\sin 2\pi m \frac{W}{2}}{2\pi m \frac{W}{2}} e^{-\left[\left(\frac{2i-1}{2}\right)W \cdot j(2\pi m)\right]} \tag{5}$$

As $F^*(jm)$ is an even function of m, the exponential factor can be reduced to a cosine function.

$$F^*(jm) = \sum_{i=1}^{n} \frac{2}{\pi} \frac{\sin\left[\frac{2i-1}{2} Wm_c 2\pi\right]}{(2i-1) W} \frac{\sin 2\pi m \frac{W}{2}}{\pi m} \left[2 \cos \frac{2i-1}{2} W 2\pi m\right] \qquad (6)$$

By rearranging the terms of Equation (6), we can write

$$F^*(jm) = \frac{4}{\pi} \frac{\sin \pi m \, W}{\pi m W} \sum_{i=1}^{n} \frac{\sin\left[\left(\frac{2i-1}{2}\right)W \, 2\pi m_c\right] \cos\left[\left(\frac{2i-1}{2}\right) W \, 2\pi m\right]}{(2i-1)} \qquad (7)$$

since

$$\sin\left[\left(\frac{2i-1}{2}\right) W \, 2\pi m_c\right] \cos\left[\frac{2i-1}{2} W \, 2\pi m\right] = \frac{\sin\left[(2i-1)\pi W \, (m_c+m)\right] + \sin\left[(2i-1)\pi W \, (m_c-m)\right]}{2}$$

$$(8)$$

Equation (7) can also be written as

$$F^*(jm) = \frac{2}{\pi} \frac{\sin \pi m W}{\pi m W} \sum_{i=1}^{n} \frac{\sin\left[(2i-1) \, \pi W \, (m_c+m)\right] + \sin\left[(2i-1) \, \pi W \, (m_c-m)\right]}{(2i-1)} \qquad (9)$$

which is a parametric approximation to an ideal one-dimensional low-pass spatial filter.

2. Theoretical Discussion

The truncated, finite-detector, low-pass equation has several interesting properties that can be predicted analytically and are confirmed by the numerical results. In the limit as the truncation point moves out to infinity and as the detector size approaches zero, the space filter function approaches the ideal low-pass case.

The approximate filter function, Equation (7), can be separated into two factors,

$$\phi(m) = \frac{\sin \pi m W}{\pi m W} \text{ , which we call the envelope function, and}$$

$$\Psi(m) = \sum_{i=1}^{n} \frac{\sin (2i-1) \, W\pi m_c \, \cos (2i-1) \, W\pi m}{2i-1} \text{ , which we call the}$$

edge function.

It can be seen that the envelope function (Figure 3A) will cause the filter function to go to zero at every frequency $m = \frac{\alpha}{W}$ for which α is an integer. The edge function, $\Psi(m)$, which is a summation of odd cosines, is shown in Figure 3B. The edge function has a maximum at $m = \frac{\alpha}{W}$ for even values of α, and a minimum at $\frac{\alpha}{W}$ for odd values of α. The filter function, $F^*(jm) = \frac{2}{\pi} \, \phi(m) \, \Psi(m)$, will therefore have a maximum and minimum on either side of each $\frac{\alpha}{W}$. These harmonic maxima and minima can be seen later in the numerical curves. The effect of using increasingly smaller detectors (decreasing W) should therefore be to move the harmonic pairs of maxima and minima farther apart.

As n is increased and additional odd cosine functions are included in the edge function summation, the slope of the filter function will break more rapidly before and after each harmonic pair. Indeed, it is easily seen that the summation,

$$\frac{4}{\pi} \sum_{i=1}^{n} \sin (2i-1) \, W\pi m_c \, \frac{\cos(2i-1) \, W\pi m}{2i-1}$$

is very similar to the Fourier summation for a square wave having a period, $\frac{2}{W}$,

$$\frac{4}{\pi} \sum_{i=1}^{\infty} \frac{\sin (2i-1) \, \frac{\pi}{2} \, \cos (2i-1) \, W\pi m}{2i-1}$$

For those situations where $Wm_c = 0.5$, the curves are periodic square wave approximations modified by the $\frac{\sin \pi m W}{\pi m W}$ factor and limited by n terms. For the curves where $Wm_c < 0.5$, the coefficients are no longer exact. The effect of extending the truncation point should be therefore an increasingly sharper slope at the cutoff frequency, m_c, and also at the harmonic maxima-minima.

From Figure 1B it can be seen that the maximum usable detector width, W, would be $\frac{1}{2m_c}$. A larger detector width could not approximate the periodic nature of the $\frac{\sin 2\pi m_c x}{x}$ function.

B.   BAND PASS

1.   Derivation

The mathematics developed in the previous section was for a low-pass filter. A band-pass filter can be obtained from the difference of two low-pass filters.

For a band-pass filter with a center frequency, m_c, and bandwidth, Δm, we can assume that the filter is the subtraction of two low-pass filters - one with cutoff frequency of $m_c - \frac{\Delta m}{2}$ and the other with cutoff frequency of $m_c + \frac{\Delta m}{2}$. By the principle of superposition of a function and its transform, we can write the inverse transform of the band-pass filter as:

$$f(x) = \frac{1}{\pi}\left[\frac{\sin 2\pi(m_c + \frac{\Delta m}{2})\,x}{x} - \frac{\sin 2\pi(m_c - \frac{\Delta m}{2})\,x}{x}\right] = \frac{1}{\pi x}\left[2\,\cos 2\pi m_c x\, \sin \pi\Delta mx\right] \quad (10)$$

$$f(x) = \frac{2\,\sin \pi\Delta mx}{\pi x}\,\cos 2\pi m_c x = \frac{2\Delta m}{\pi}\,\frac{\sin \pi\Delta mx}{\Delta mx}\,\cos 2\pi m_c x \quad (11)$$

2.   Theoretical Discussion

Equation (11) reduces to a low-pass filter for a center frequency, $m_c = 0$, and will have $\frac{\sin \pi\Delta mx}{\Delta mx}$ characteristics. When $\frac{m_c}{\Delta m}$ is large compared to 1, $f(x)$ behaves like a cosine function ($\cos 2\pi m_c x$) damped by a modulating $\frac{\sin x}{x}$ function.

As the bandwidth of the filter decreases, $\frac{\sin \Delta mx}{\Delta mx}$, will have less damping effect. Therefore, terms for large values of x cannot be neglected. The detectors farther from the center will weigh more heavily, while the center detector weighting co-efficients or detector sensitivities will be smaller. On the other hand, if $\frac{m_c}{\Delta m}$ is small, the damping effect will dominate, and a few detectors near the center would be sufficient.

From Equation (11), it is seen that the inverse transform of the band-pass filter is a "carrier" of frequency $2\pi m_c$, amplitude-modulated by a "signal" of $\pi \Delta m$. The maximum detector width usable is determined by the center frequency, and is equal to $\frac{1}{4\ m_c}$. Larger width detectors would not fit between all the zeros of the filter function. Δm, the bandwidth, should determine the truncation point, since for smaller bandwidths, the cutoff rate becomes increasingly important.

III. NUMERICAL SOLUTION

Computing F^* (jm) by hand would have been very tedious. Therefore, an IBM 7094 was used to make a numerical computation. Since it seemed desirable to evaluate the effects of truncation and detector width separately, a doubly parametic series of curves was chosen. One parameter is the normalized detector width, Wm_c. The second parameter is the normalized truncation point, $x_T m_c$.

A. LOW PASS

Assuming a low-pass filter with a cutoff frequency, m_c, the zeros of $f(x)$ appear at $x = \frac{k}{2m_c}$, where k is an integer ranging from 1 to ∞. Normalized detector widths of Wm_c equal to 0.05, 0.1, 0.25, and 0.5 were chosen (see Figure 2), and also normalized truncation points $x_T m_c$ equal to 1.0, 2.0, and 4.0. The results are shown in Figures 4, 5, and 6.

1. Effect of Detector Width

For a given truncation point, for example, $x_T\ m_c$ = 1 (see Figure 4), the approximation is recognizable, but not good when only four detectors (2 each side, Wm_c = 0.5) are used. As the number of detectors is increased, the approximation is improved, particularly in the stop-band, because the harmonic maxima-minima are moved to larger values of m where they are attenuated. However, increasing

the number of detectors effects a diminishing gain in pass-band approximation ac-
curacy. Again, referring to Figure 4, the improvement is considerable when the
number is increased from 4 to 8, but barely discernible when increased from 20 to
40, and the small gain hardly justifies the numerical increase in detectors. This
effect is independent of truncation point as seen from Figures 5 and 6.

2.   Effect of Truncation Point

For a fixed detector width (e.g., $Wm_c = 0.5$), an increase in the
truncation point such as shown in Figures 4, 5, and 6, causes the slope at the cut-
off point to become sharper and sharper, and the number of ripples in the bass-band
to increase. For a truncation of $x_T m_c$ equal to only 1, the bass-band response is
relatively smooth.

3.   Practical Application of Results

In selecting the proper filter characteristics for a specific
application, both the pass-band and the stop-band requirements must be specified.
The detector size will result from the permissible behavior in both the pass-band
and the stop-band. If the first harmonic maxima-minima must be a given number of
octaves from m_c, the detector size is chosen accordingly. Pass-band ripple magni-
tude will also establish detector size. If a given cutoff rate is desired, the
truncation point is established.

B.   BAND PASS

Since the band-pass filter equation is derived from the difference of
two low-pass equations, the band-pass curves can be very nearly predicted from the
difference of two scaled low-pass filter curves. Four normalized detector widths
(0.25, 0.125, 0.05, and 0.025) were chosen for the numerical band-pass filter
characteristic. Two bandpasses - a narrow band $(\frac{\Delta m}{m_c} = 0.2)$ and a wide band $(\frac{\Delta m}{m_c} = 1.0)$ -
were investigated. Truncation points of 1, 2, and 4 were used for the wide band,
while values of 5, 10, and 20 were used for the narrow band.

1.   Effect of Detector Width

From Figures 7 through 12 it can be seen for both the wide and
the narrow bands that as the detector width **decreases**, the harmonic maxima and minima

spread and reduce in magnitude, in a fashion similar to that for the low-pass curves. The stop-band in the region through $8\ m_c$ (which is more than 2 octaves above the cutoff frequency) for the smaller detectors where Wm_c is equal to 0.05 and 0.025, is effectively zero. Above $8\ m_c$, however, there are periodic maxima and minima whose magnitudes are less than 0.2 and which become smaller with increasing m. When the lower resolution detectors are used (i.e., Wm_c = 0.25 and 0.125 unit lengths) the approximation is very sensitive to detector width. For the smaller detectors where Wm_c = 0.05 and 0.025, the approximation improvement - particularly in the pass band - becomes negligible. Figures 7 through 12 all illustrate the diminishing effect of decreasing detector width for fixed truncation.

2.   Effect of Truncation Point

Here also the results are what might be expected from extending the low-pass case. Increasing the truncation point sharpens the edges of the pass-band characteristics and also increases the number of ripples in the pass band. For the maximum detector width of Wm_c = 0.25 (see the wide-band filter, Figures 7, 8, and 9), the pass band exhibits an average decreasing magnitude for the larger truncations, though not for the minimum truncation of $x_T m_c$ = 1. This "slump" in the pass band is corrected by using smaller detector widths. Truncation and detector width therefore cannot be considered as having entirely independent effects.

3.   Practical Application of Results

Narrow-band spatial filters would be very useful in making spatial frequency measurements. An instrument could be constructed using variable weights for each detector channel, and could thereby be made to measure a set of frequency bands in turn. It is encouraging that even for minimum truncation, $x_T m_c$ = 5 (see Figure 10), a good narrow band pass can be obtained, even though it does not well approximate the square-sided ideal. For larger truncations and more detectors, the approximation is excellent.

IV.   CONCLUSION

The synthesis of two basic one-dimensional spatial filters, low-pass and band-pass, using an array of detectors has been demonstrated. The synthesis is truly spatial in that there is no functional dependence on time, and therefore the filter characteristic is independent of fluctuations in rate of scanning mechanisms.

The output signal of a spatial filter is proportional to the spectral power of the observed scene within the pass band of the filter.

Although only the two basic filters were discussed, finite size detectors make it possible for almost any finite bandwidth filter characteristic to be approximated and synthesized by this method. A specific application would involve design of a filter to best discriminate against its particular background distribution. Any such general filter approximation would be dependent on the individual detector field-of-view and also on the field-of-view of the array. A practical utilization of such a filter would amplify each output separately (because of signal-to-noise arguments), weight the outputs, and sum.

If, by scanning a detector, the spatial function is described as a parametric function of time, then the filtering can be theoretically accomplished with a set of parallel delay lines and associated gains whose outputs are summed. This method is completely equivalent to using the detector-array spatial-filter synthesis, and results from the same principle.

REFERENCES

1.   N. Balabanean, Network Synthesis, Prentice-Hall, Englewood Cliffs, N.J., 1958.

2.   M. E. Van Valkenburg, Introduction to Modern Network Synthesis, John Wiley
     & Sons Inc., New York, 1960.

3.   L. de Pian, Linear Active Network Theory, Prentice-Hall, Englewood Cliffs,
     N.J., 1962.

4.   Jamieson, McFee, Plass, Grube, Richards, Infrared Physics and Engineering,
     McGraw-Hill Book Co., 1963.

5.   E. A. Guilleman, Synthesis of Passive Networks, John Wiley & Sons Inc.,
     New York, 1957.

6.   J. G. Truxal, Automatic Feedback Control System Synthesis, McGraw-Hill
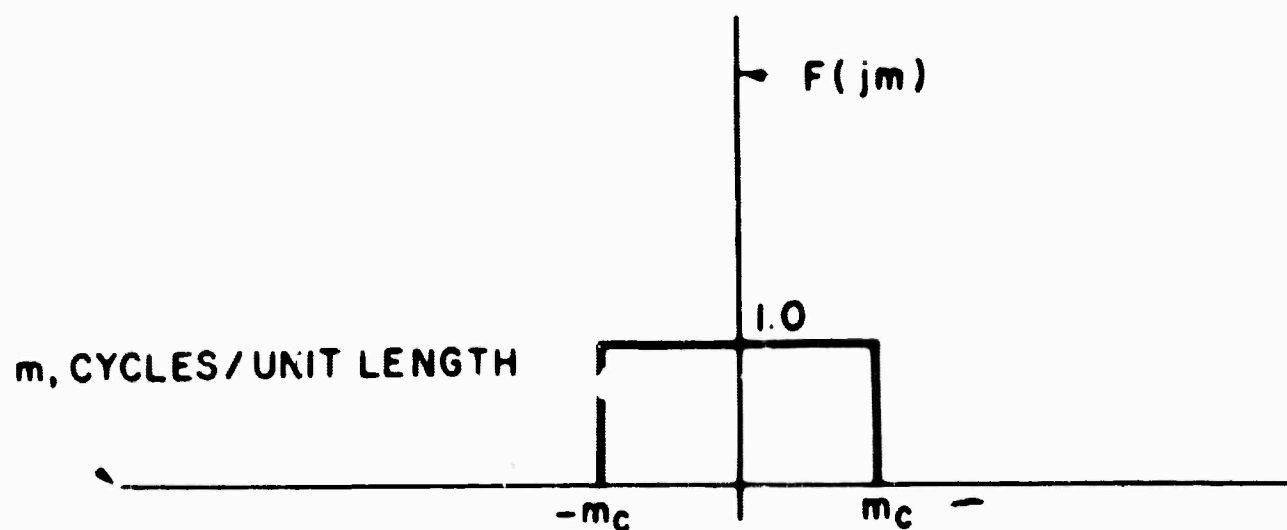   Book Co., New York, 1955.
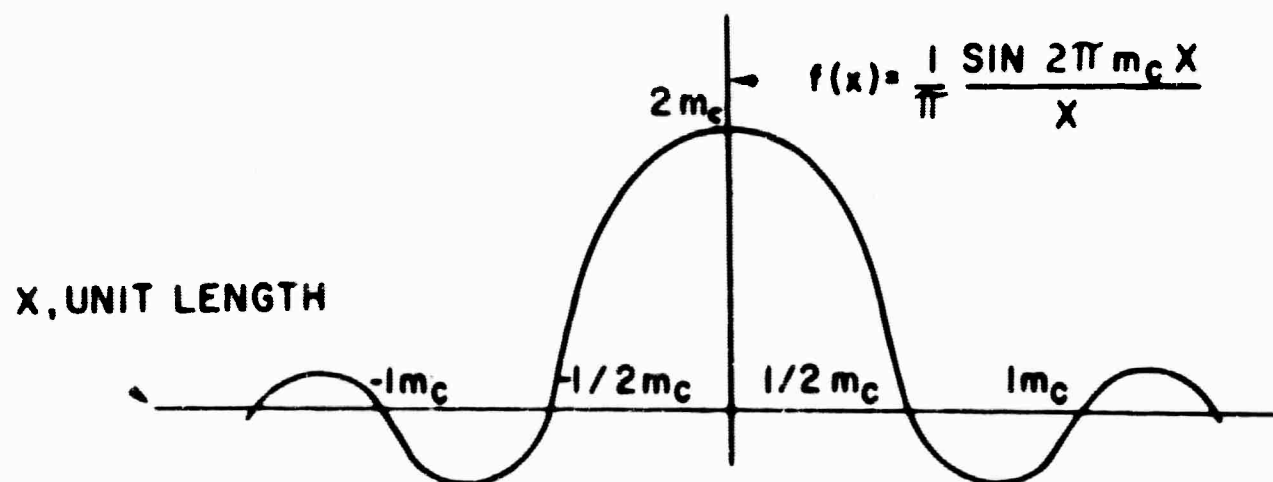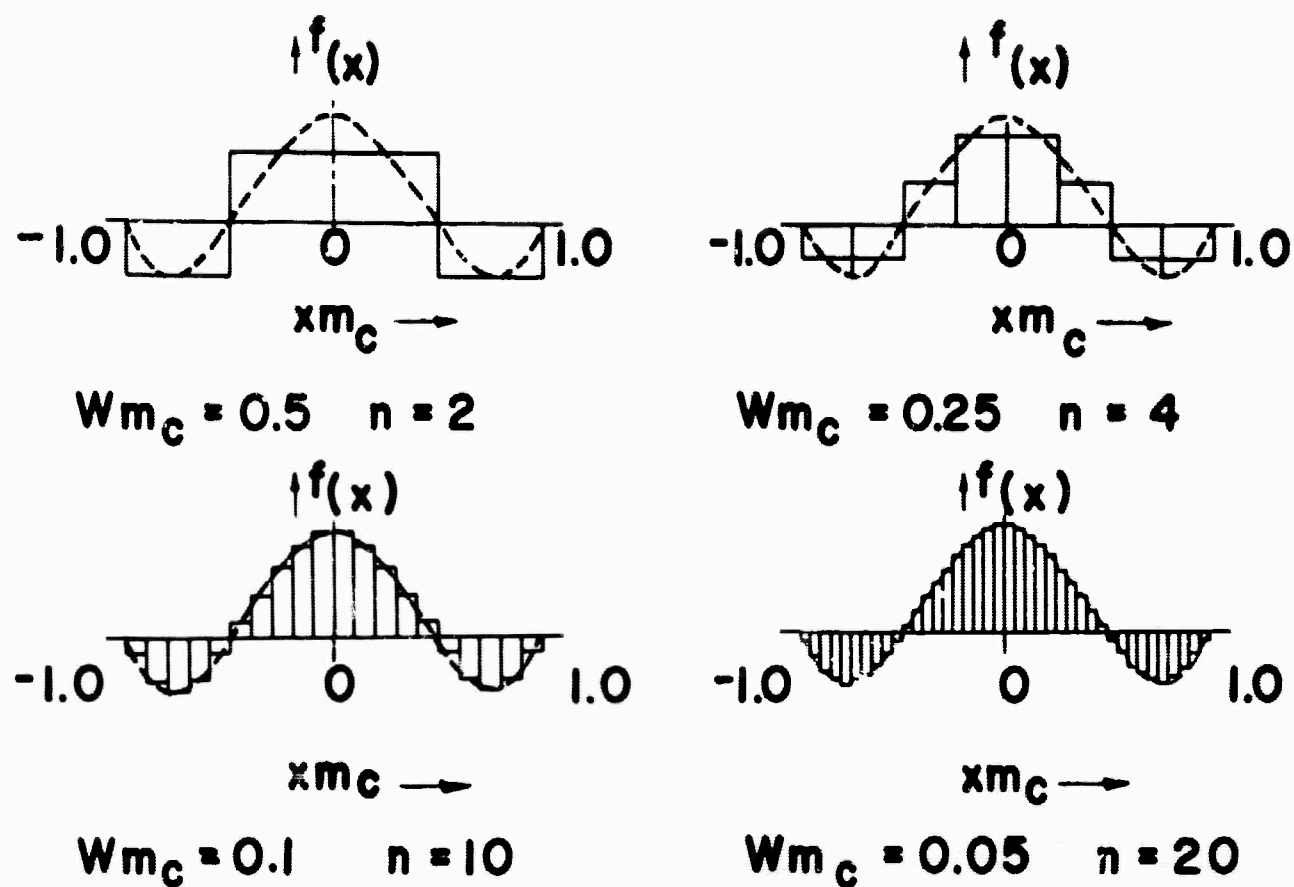
Fig. 1A Ideal Low-Pass Filter

$$f(x) = \frac{1}{\pi} \frac{SIN \ 2\pi m_c X}{X}$$

Fig. 1B Inverse Transform

A525:63-1671

Figures 1A and 1B
Appendix

$f(x)$

-1.0 0 1.0

$xm_c \longrightarrow$

$Wm_c = 0.5 \quad n = 2$

$f(x)$

-1.0 0 1.0

$xm_c \longrightarrow$

$Wm_c = 0.25 \quad n = 4$

$f(x)$

-1.0 0 1.0

$xm_c \longrightarrow$

$Wm_c = 0.1 \quad n = 10$

$f(x)$

-1.0 0 1.0

$xm_c \longrightarrow$

$Wm_c = 0.05 \quad n = 20$

FOUR EXAMPLES OF DETECTOR ARRAYS

$$X_T m_c = 1$$

A525:63-921A

Figure 2
Appendix
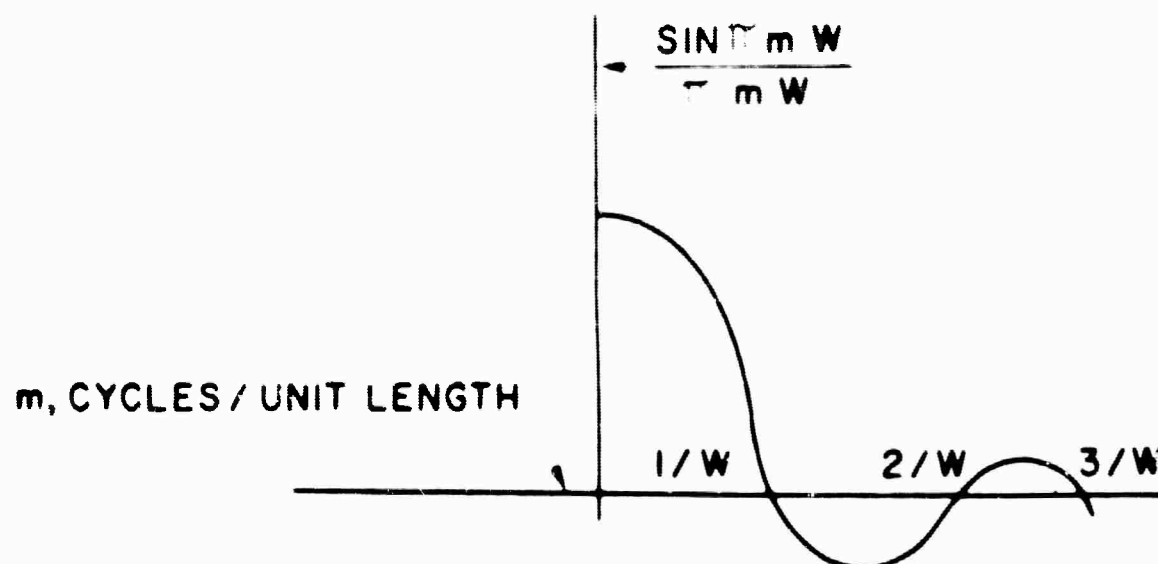
Fig. 3A Envelope Function
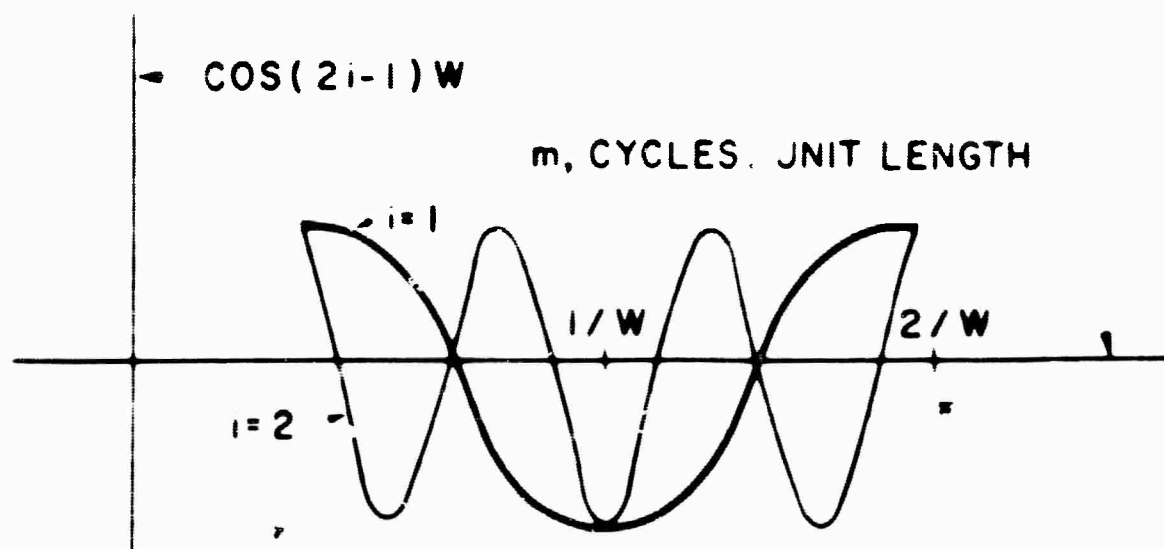
Fig. 3B Edge Function

Figures 3A and 3B
Appendix
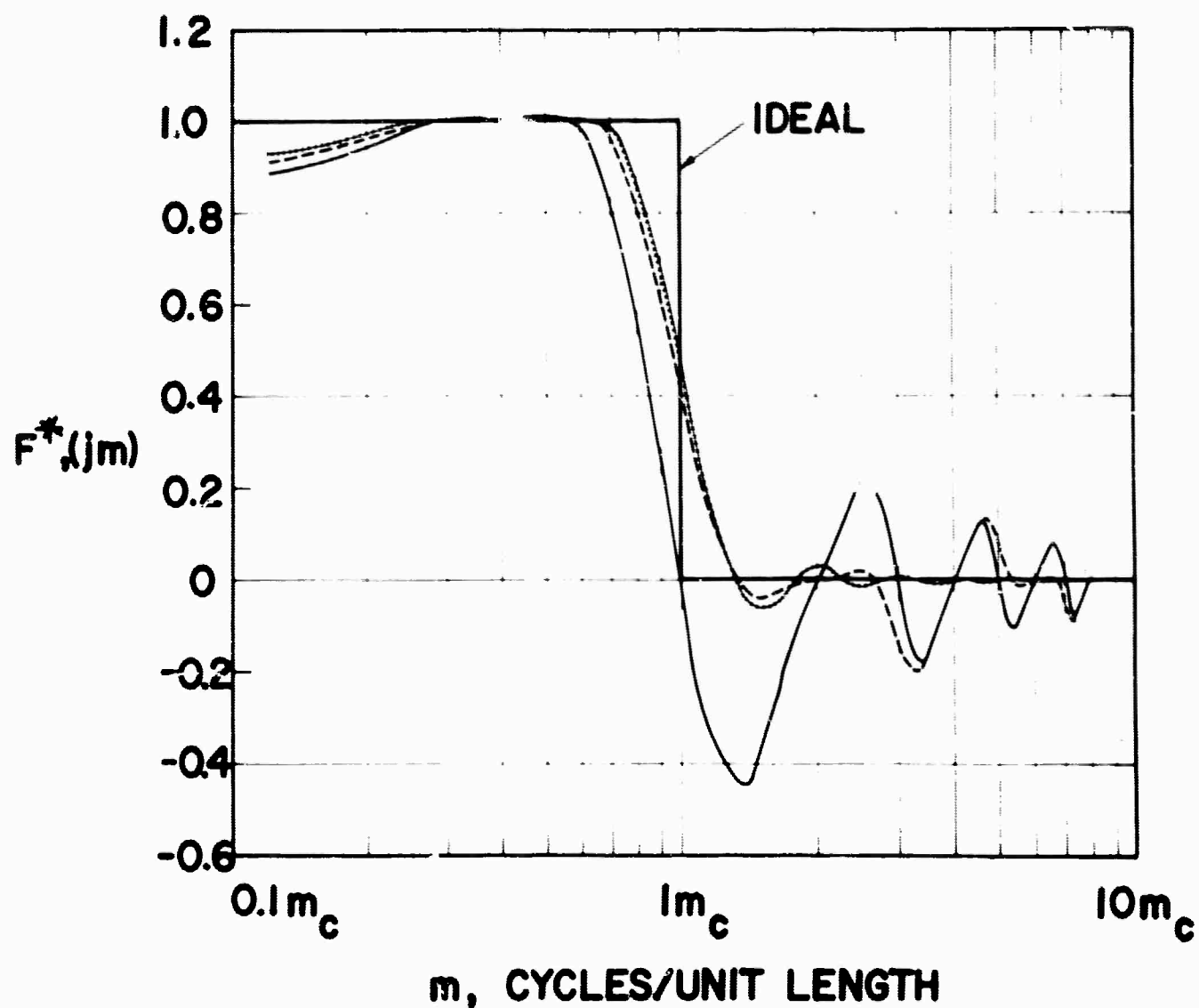
SPATIAL FILTER FREQUENCY RESPONSE
$$X_T m_c = 1$$

A525:63-950A

Figure 4
Appendix

$Wm_c = 0.5$ $n = 4$

$Wm_c = 0.25$ $n = 8$

$Wm_c = 0.1$ $n = 20$

$Wm_c = 0.05$ $n = 40$
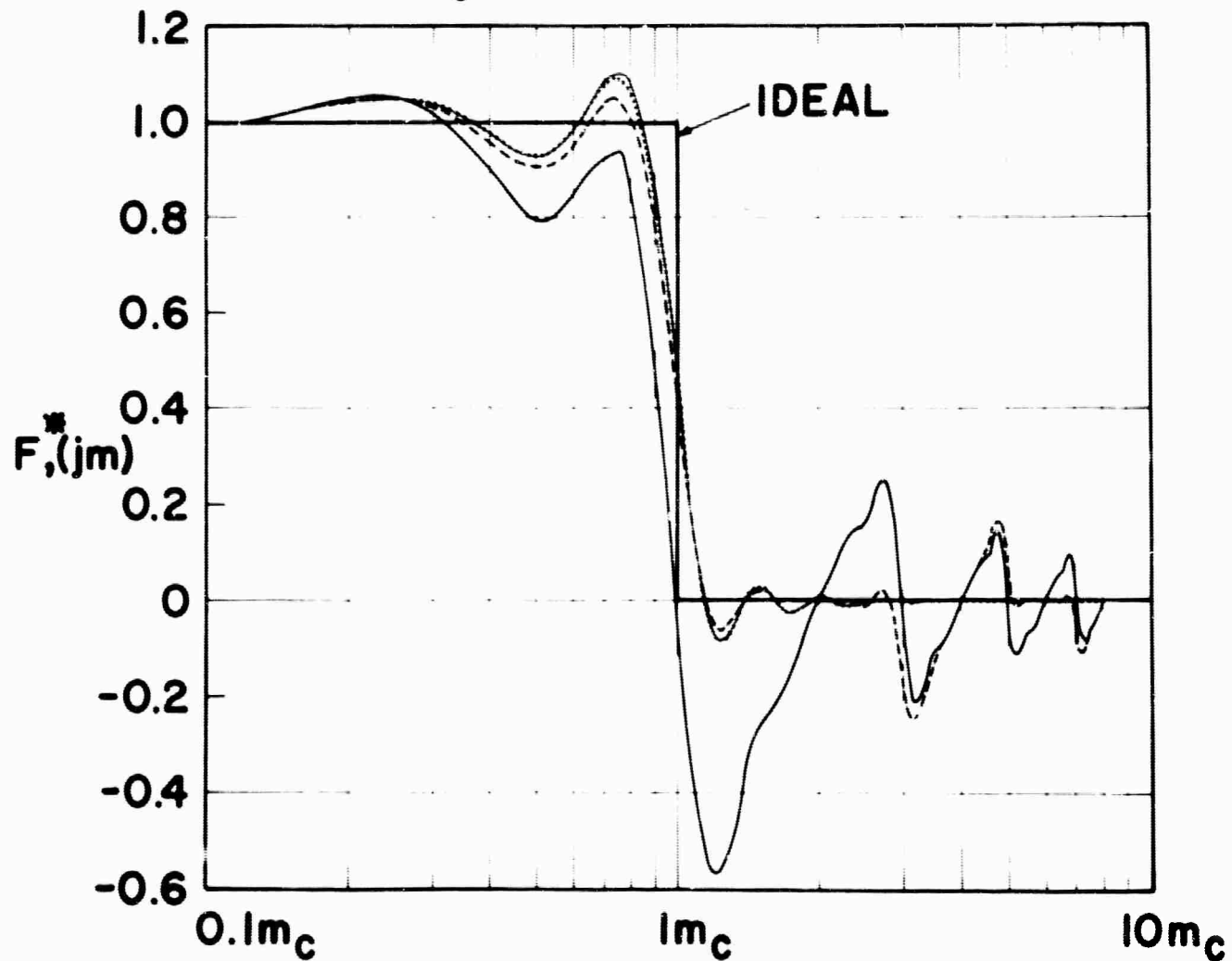
m, CYCLES/UNIT LENGTH

SPATIAL FILTER FREQUENCY RESPONSE

$$X_T m_c = 2$$

A525:63-951A

Figure 5
Appendix

363-687

CODE:

————	$Wm_c = 0.5$	$n = 8$
- - - - - -	$Wm_c = 0.25$	$n = 16$
··············	$Wm_c = 0.1$	$n = 40$
————	$Wm_c = 0.05$	$n = 80$
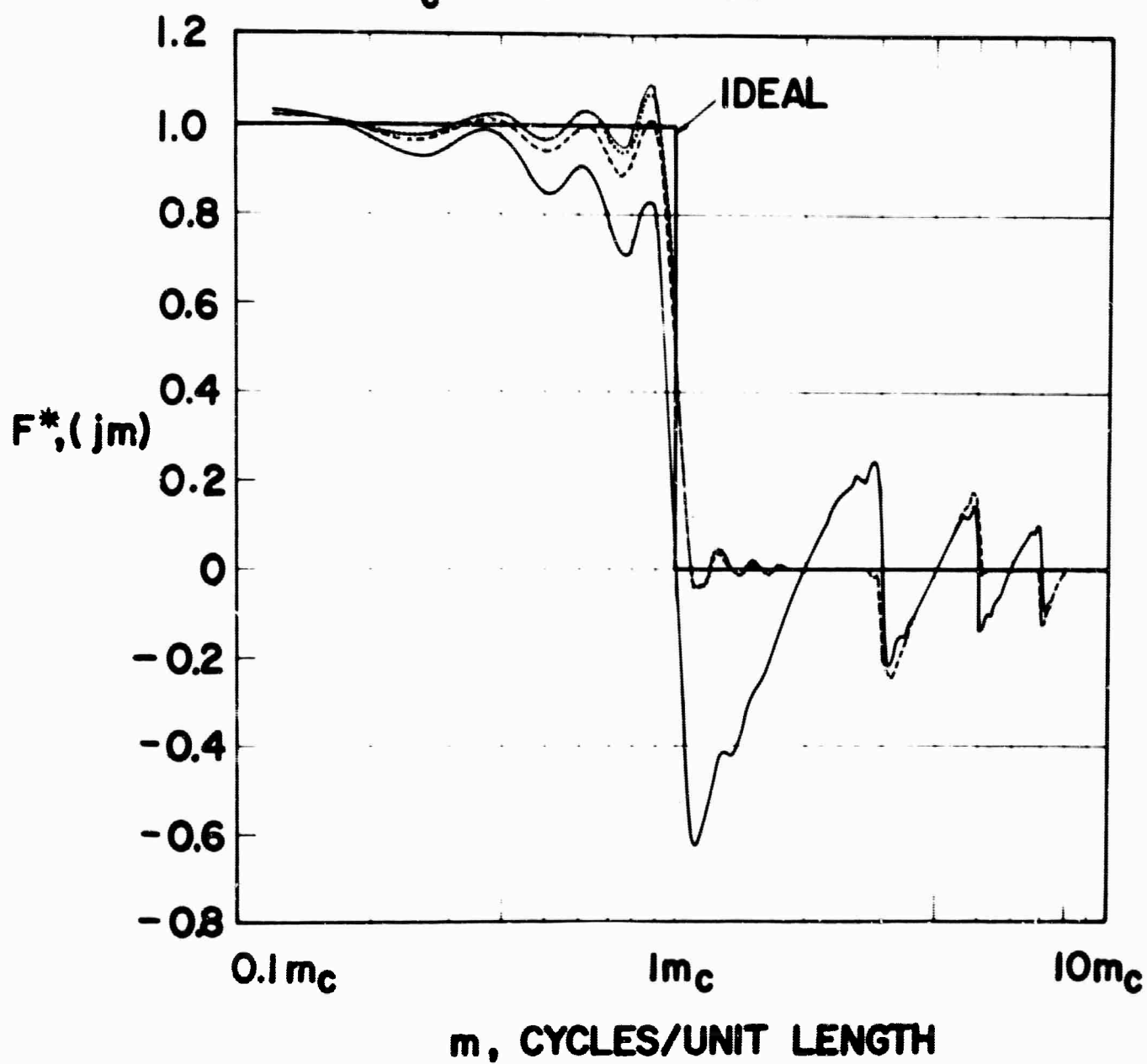
SPATIAL FILTER FREQUENCY RESPONSE
$$X_T m_c = 4$$

A525:63-949A

Figure 6
Appendix

CODE:

– – – –	$Wm_c = 0.25$	$n = 4$
············	$Wm_c = 0.125$	$n = 8$
————	$Wm_c = 0.05$	$n = 20$
–·–·–·–	$Wm_c = 0.025$	$n = 40$
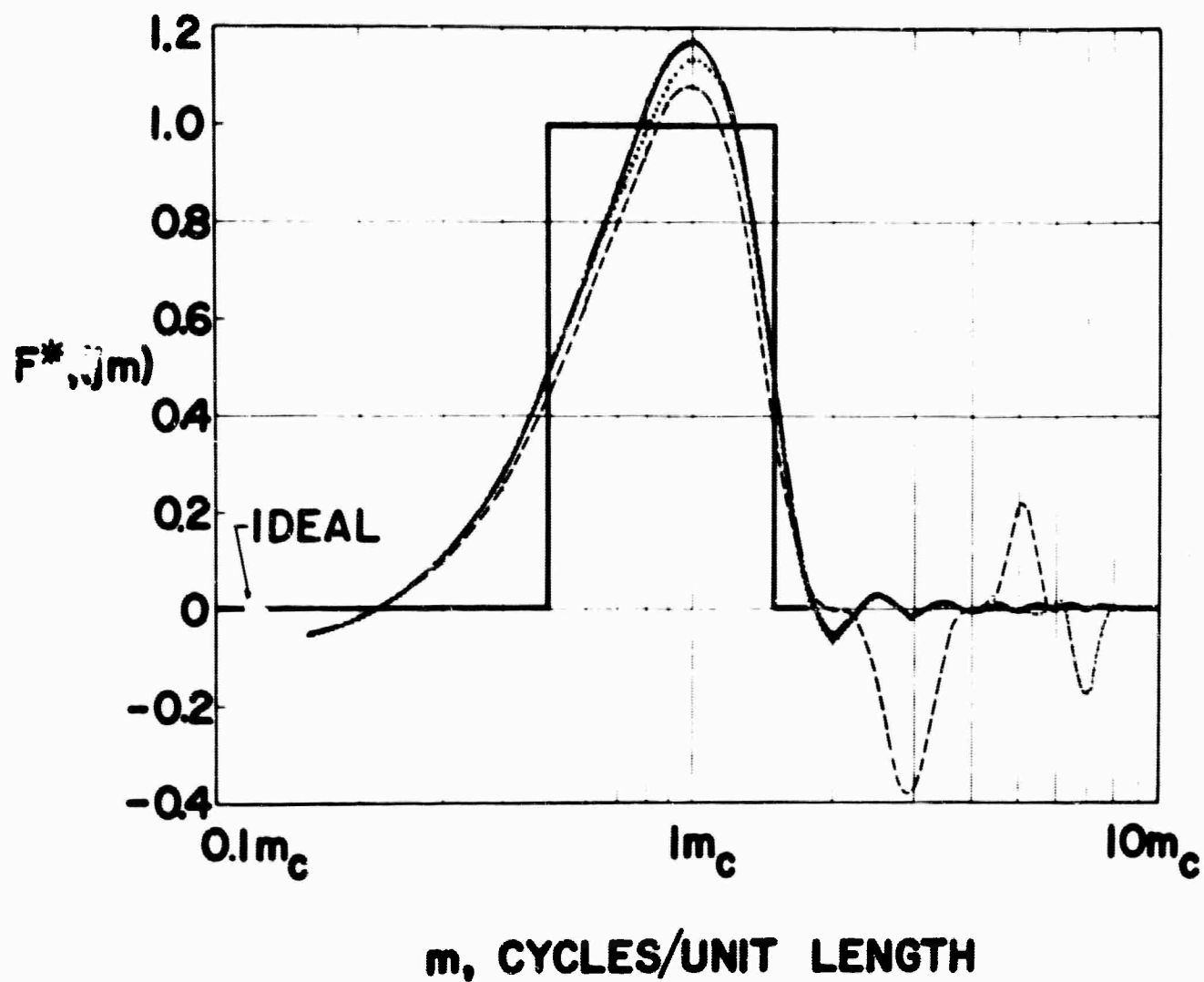
WIDE-BAND FREQUENCY RESPONSE

$$X_T m_c = 1$$

A525:63-1276

CODE:

------	$Wm_c = 0.25$	$n = 8$
....	$Wm_c = 0.125$	$n = 16$
———	$Wm_c = 0.05$	$n = 40$
—··—··—	$Wm_c = 0.025$	$n = 80$

$F_1^*(jm)$

IDEAL
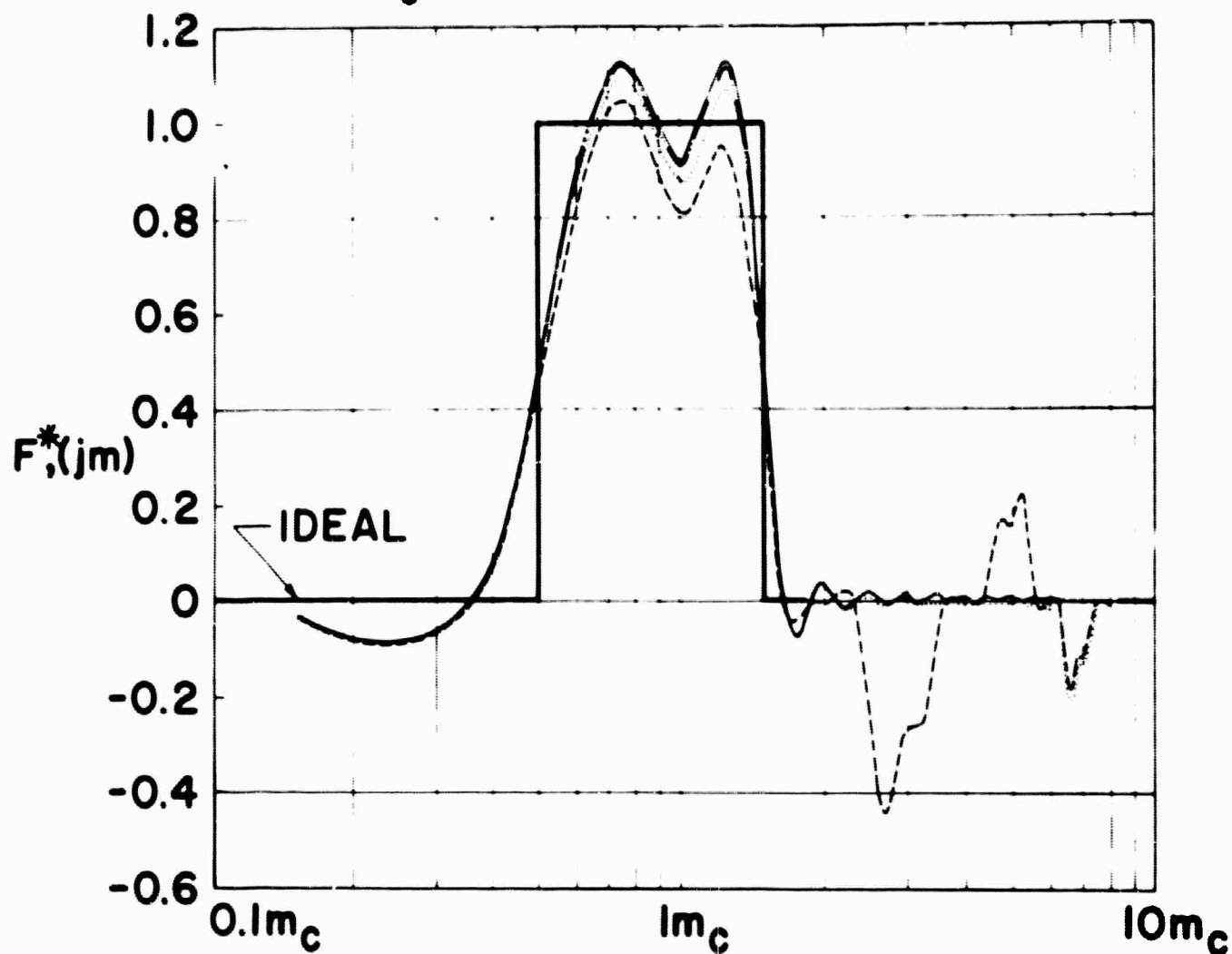
m, CYCLES/UNIT LENTH

WIDE - BAND FREQUENCY RESPONSE
$X_T m_c = 2$

A525:63-1270

Figure 8
Appendix

CODE:

------ Wm$_c$ = 0.25   n=14
.... Wm$_c$ = 0.125   n=32
——— Wm$_c$ = 0.05   n=80
—·—·— Wm$_c$ = 0.025   n=160
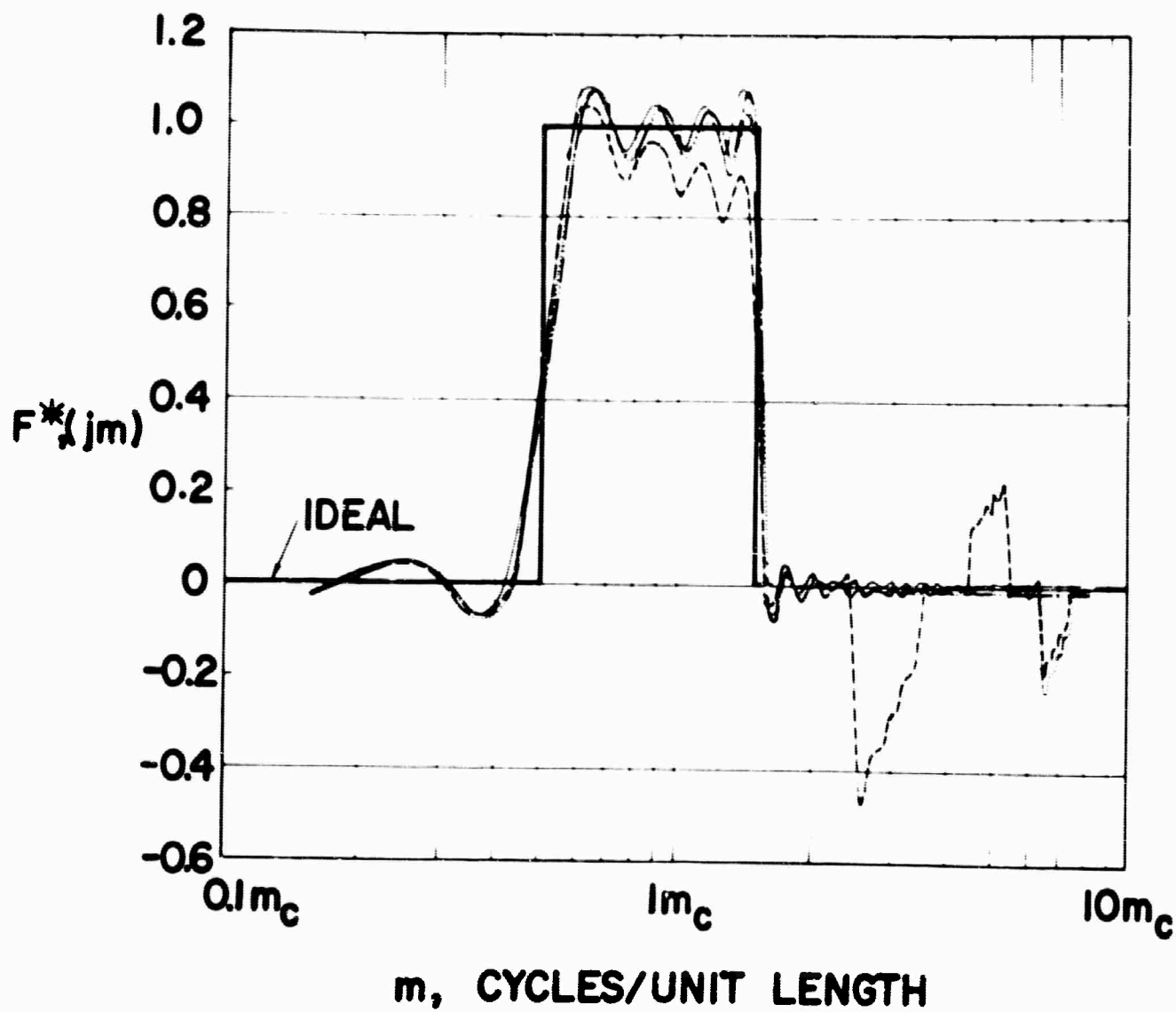
WIDE-BAND FREQUENCY RESPONSE
$X_T m_c = 4$

A525:63-1269

CODE:

-----	$Wm_c = 0.25$	$n = 20$
....	$Wm_c = 0.125$	$n = 40$
———	$Wm_c = 0.05$	$n = 100$
—·—·—	$Wm_c = 0.025$	$n = 200$
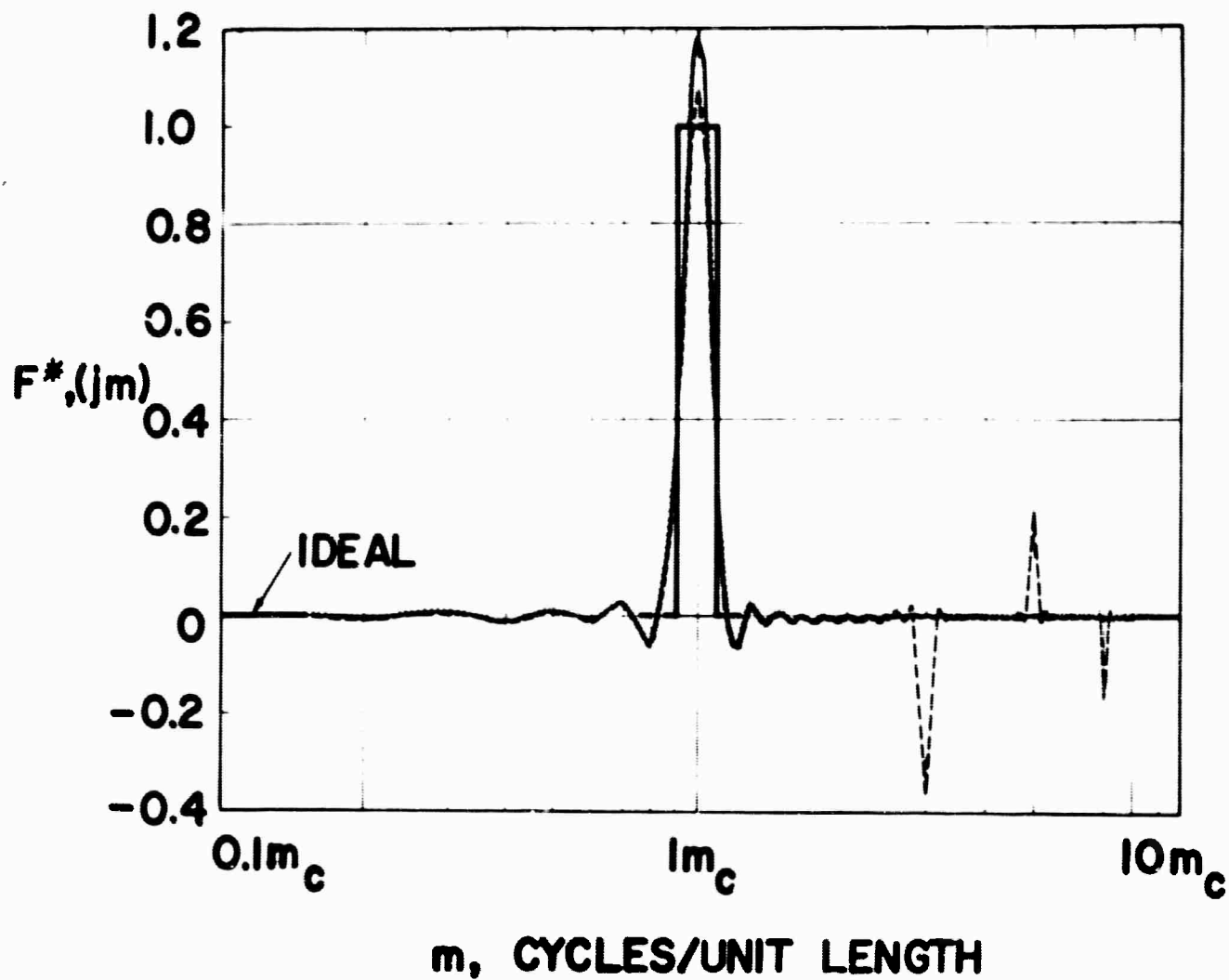
NARROW-BAND FREQUENCY RESPONSE

$$X_T m_c = 5$$

A525:63-1274

Figure 10
Appendix

CODE :
- - - - - $Wm_c = 0.25$ $n = 40$
.... $Wm_c = 0.125$ $n = 80$
———— $Wm_c = 0.05$ $n = 200$
—··— $Wm_c = 0.025$ $n = 400$

IDEAL

$F^*,(jm)$

m, CYCLES / UNIT LENGTH
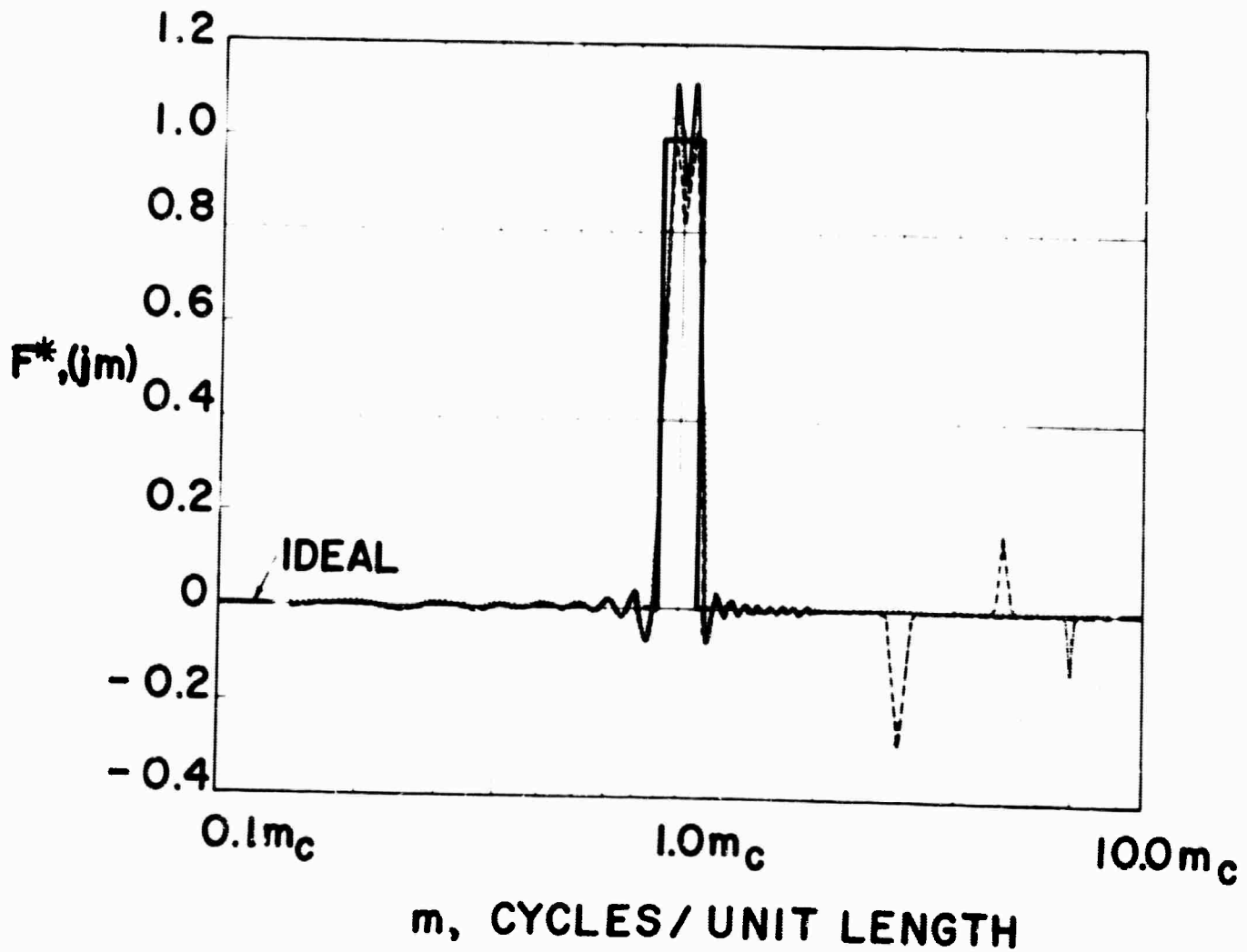
NARROW-BAND FREQUENCY RESPONSE
$X_T m_c = 10$

A525:63-1273

963-684

Figure 11
Appendix

CODE:

-----	$Wm_c = 0.25$	$n = 80$
....	$Wm_c = 0.125$	$n = 160$
———	$Wm_c = 0.05$	$n = 400$
—·—··—	$Wm_c = 0.025$	$n = 800$

NARROW-BAND FREQUENCY RESPONSE

$$X_T m_c = 20$$

A525:63-1271

Figure 12
Appendix

APPENDIX B

FILTERS WITH CIRCULAR SYMMETRY
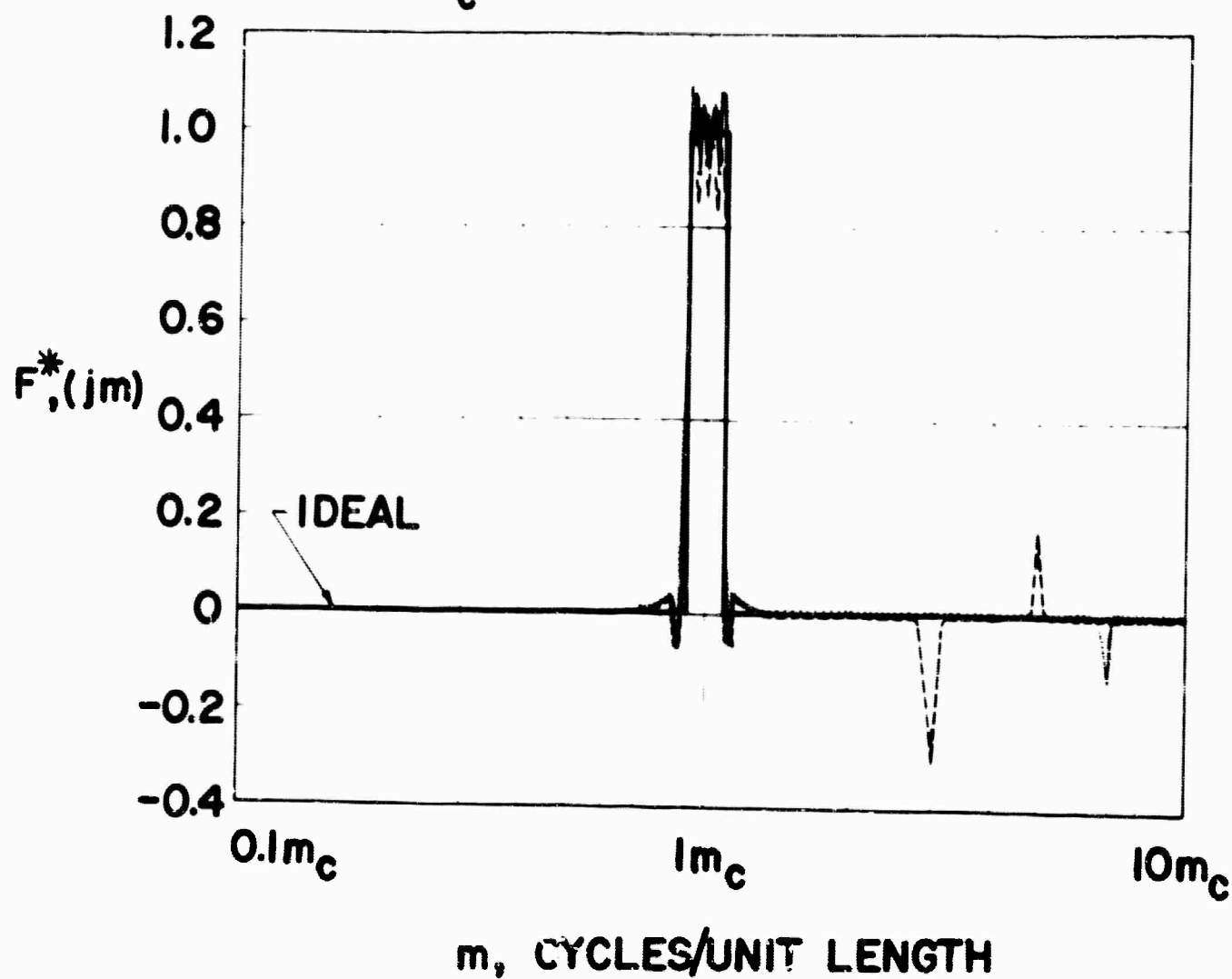
I. TWO-DIMENSIONAL CIRCULAR SYMMETRY LOW-PASS FILTER

The synthesis of a two-dimensional low-pass filter with a cutoff frequency, m_{c_1}, on the x axis and a cutoff frequency, m_{c_2}, on the y axis, was discussed in Section III. The cutoff frequency for any other axis is the intersection of that axis and the cube.

For a circularly symmetric low-pass characteristic, that is, one independent of the direction of scan, the response function is a cylinder in the frequency domain. The cylinder has a height, 1, for $\rho < \rho_c$ where ρ is the radial frequency in any direction and ρ_c is the cutoff frequency. See Figure 8.

The inverse transform of this function in polar form is $f(r, \theta)$ where

$$f(r, \theta) = \int_0^{\rho_c} \int_0^{2\pi} \rho \, e^{j2\pi\rho r \cos(\theta - \phi)} \, d\phi \, d\rho$$

$$= \int_0^{\rho_c} 2\pi \, \rho \, J_0 \, (2\pi \, \rho r) \, d\rho \tag{B-1}$$

$$= \frac{\rho_c}{r} \, J_1 \, (2\pi \, \rho_c \, r)$$

$f(r, \theta)$ is plotted in Figure 8.

Using annular detectors of width W and weight A_i, where the weight is taken from the value of $f(r, \theta)$ at $r = i\frac{W}{2}$,

$$A_i = \frac{2 \rho_c}{iW} J_1 (\pi \rho_c \, iW) \qquad (B-2)$$

The inverse transform of each annular detector is

$$F_i (\rho, \phi) = \int_{(i-1)W}^{W} \frac{2 \rho_c}{iW} J_1 (\pi \rho_c \, iW) \, 2\pi r \, J_0 (-2\pi \rho \, r) \, dr$$

$$= \frac{2 \rho_c}{\rho} J_1 (\pi \rho_c \, iW) \left\{ J_1 (2\pi \rho \, iW) - \left(\frac{i-1}{1}\right) J_1\left(2\pi \rho \, (i-1)W\right) \right\} \qquad (B-3)$$

and

$$F^* (\rho, \phi) = \sum_{i=1}^{n} \frac{2 \rho_c}{\rho} J_1 (\pi \rho_c \, iW) \left\{ J_1 (2\pi \rho \, iW) - \left(\frac{i-1}{i}\right) J_1\left(2\pi \rho \, (i-1)W\right) \right\} \qquad (B-4)$$

II.   TWO-DIMENSIONAL CIRCULAR SYMMETRY BAND-PASS FILTER

For an annular band-pass between $\rho_c - (\Delta\rho/2)$ and $\rho_c + (\Delta\rho/2)$ the inverse transform, $f(r, \theta)$, is

$$f(r, \theta) = \frac{\left(\rho_c + \frac{\Delta\rho}{2}\right)}{r} J_1 \left[2\pi \left(\rho_c + \frac{\Delta\rho}{2}\right)r\right] - \frac{\left(\rho_c - \frac{\Delta\rho}{2}\right)}{r} J_1 \left[2\pi \left(\rho_c - \frac{\Delta\rho}{2}\right)r\right] \qquad (B-5)$$

With annular detectors of width, W, the ith detector has a weight, A_i, of

$$A_i = \frac{2\left(\rho_c + \frac{\Delta\rho}{2}\right)}{iW} J_1 \left[2\pi\left(\rho_c + \frac{\Delta\rho}{2}\right) iW\right] - \frac{2\left(\rho_c - \frac{\Delta\rho}{2}\right)}{iW} J_1 \left[2\pi\left(\rho_c - \frac{\Delta\rho}{2}\right) iW\right] \qquad (B-6)$$

and therefore

$$F^* (\rho, \phi) = \sum_{i=1}^{n} \left\{ \left[\frac{2\left(\rho_c + \frac{\Delta\rho}{2}\right)}{iW} J_1\left[2\pi\left(\rho_c + \frac{\Delta\rho}{2}\right) iW\right] - \frac{2\left(\rho_c - \frac{\Delta\rho}{2}\right)}{iW} J_1\left[2\pi\left(\rho_c - \frac{\Delta\rho}{2}\right) iW\right] \right] \right.$$

$$\left. X \left\{ J_1\left[2\pi \rho\, iW\right] - \left(\frac{i-1}{i}\right) J_1\left[2\pi \rho\,(i-1)\,W\right] \right\} \right\} \tag{B-7}$$

III. TWO-DIMENSIONAL BAND-PASS WITH RECTANGULAR SYMMETRY

The two-dimensional band-pass space function is the difference of two low-pass space functions. That is

$$f(x,y) = \frac{1}{\pi^2} \left\{ \left[\frac{\sin 2\pi\left(m_{c_1} + \frac{\Delta m_1}{2}\right)x}{x} \cdot \frac{\sin 2\pi\left(m_{c_2} + \frac{\Delta m}{2}\right)y}{y} \right] \right.$$

$$\left. - \left[\frac{\sin 2\pi\left(m_{c_1} - \frac{\Delta m_1}{2}\right)x}{x} \cdot \frac{\sin 2\pi\left(m_{c_2} - \frac{\Delta m}{2}\right)y}{y} \right] \right\} \tag{B-8}$$

The weight for a detector whose center is located at x_i, y_k is

$$A_{ik} = \frac{1}{\pi^2} \left\{ \left[\frac{\sin 2\pi\left(m_{c_1} + \frac{\Delta m_1}{2}\right)(2i-1)\frac{W_1}{2}}{(2i-1)\,W_1/2} \cdot \frac{\sin 2\pi\left(m_c + \frac{\Delta m_2}{2}\right)(2k-1)\frac{W_2}{2}}{(2k-1)\,W_2/2} \right] \right.$$

$$\left. - \left[\frac{\sin 2\pi\left(m_{c_1} - \frac{\Delta m_1}{2}\right)(2i-1)\frac{W_1}{2}}{(2i-1)\,W_1/2} \cdot \frac{\sin 2\pi\left(m_{c_2} - \frac{\Delta m_2}{2}\right)(2k-1)\frac{W_2}{2}}{(2k-1)\,W_2/2} \right] \right\} \tag{B-9}$$

and the transform of the array, $F^*(m_1, m_2)$ is

$$F^*\ (m_1,\ m_2)\ =\ \frac{4}{\pi^2}\ \frac{\sin \pi\ m_1\ W_1}{\pi\ m_1\ W_1}\ \frac{\sin \pi\ m_2\ W_2}{\pi\ m_2\ W_2}\ \sum_{i=1}^{n}\ \sum_{k=1}^{p}$$

$$X\ \left\{ \left[\frac{\sin 2\pi \left(m_{c_1} + \frac{\Delta m_1}{2} \right)(2i-1)\frac{W_1}{2}\ \sin 2\pi \left(m_{c_2} + \frac{\Delta m_2}{2} \right)(2k-1)\frac{W_2}{2}}{(2i-1)} \cdot \frac{}{(2k-1)} \right] \right.$$

$$-\ \left[\frac{\sin 2\pi \left(m_{c_1} - \frac{\Delta m_1}{2} \right)(2i-1)\frac{W_1}{2}\ \sin 2\pi \left(m_{c_2} + \frac{\Delta m_2}{2} \right)(2k-1)\frac{W_2}{2}}{(2k-1)} \cdot \frac{}{(2k-1)} \right] \left. \right\}$$

$$X\quad \cos (2i-1)\ W_1\ \pi m_1\ \cos (2k-1)\ W_2\ \pi m_2 \qquad\qquad\qquad (B-10)$$

APPENDIX C

RELATION BETWEEN MAXIMUM SLOPE OF SPATIAL
FREQUENCY FUNCTIONS AND MAXIMUM SCANNING DETECTOR DIMENSIONS

We already know that the spatial frequency response functions of scanning array detectors do not exactly reproduce the desired functions. A useful parameter for characterizing quality of those spatial frequency functions that are designed to have band- or low-pass characteristics is the slope of $F(\omega)$, that is $\frac{dF(\omega)}{d\omega}$.

When $F(\omega)$ represents the Fourier transform of an arbitrary space-limited function, $f(x)$, an interesting relationship, known as Bernstein's theorem, gives the maximum slope of $F(\omega)$ in terms of the width of $f(x)$. Here we apply this theorem to one- and two-dimensional rectangular coordinate Fourier transforms, and to the polar coordinate Fourier-Bessel transform (Hankel Transform). Its derivation is given by Arsac,[*] who follows the work of Boas.[**]

For a one-dimensional Fourier transform the relationship is

$$\left| \frac{d\,F(\omega)}{d\,\omega} \right| \leq L\,B(F) \tag{C-1}$$

where L represents the half-width of a function $f(x)$ that extends from -L to +L, and $B(F)$ represents the maximum value of $|F(\omega)|$.

---

[*] J. Arsac, _Transformation de Fourier et Theorie des Distributions_ (Paris, Dunod, 1961), pp. 234-239.

[**] R. P. Boas, _Entire Functions_ (New York, Academic Press, 1954), pp. 210, 211.

In two-dimensional rectangular coordinates

$$\left| \frac{\partial F (\omega_x, \omega_y)}{\partial \omega_x \, \partial \omega_y} \right| \leq L_x L_y \, B (F) \tag{C-2}$$

where L_x and L_y represent maximum dimensions in x and y directions.

For a circular function of bounded domain, that is, a filter function confined to the circle $x^2 + y^2 \leq R^2$

$$\left| \frac{\partial F (\omega_r)}{\partial \omega_r} \right| \leq \sqrt{2} \, R \, B (F) \tag{C-3}$$

Although the slopes of the $F (\omega)$ functions that result from the scanning weighted detector arrays will be less than the maxima given here, the bounds can be useful in guiding preliminary design.

APPENDIX D

COMPARISON OF TRANSPARENCIES WITH ELECTRICALLY WEIGHTED DETECTOR ARRAYS

Since most of this report uses the ideal low-pass spatial frequency filter as an example for specific discussion, we shall use it here also. Thus, consider the function $f(x) = (1/\pi)(\sin x/x)$; that is, the inverse Fourier transform of an ideal low-pass filter, shown in Figure A-1B. As described in Appendix A and shown in Figure A-2, an array of electrically weighted detectors approximates $f(x) = (1/\pi)(\sin x/x)$ by a number of rectangles, each representing one detector. The height of a rectangle corresponds to the electrical weighting of its detector and can be positive or negative, the negative weighting realizable by electrical inversion.

Instead of an array of detectors forming $f(x) = (1/\pi)(\sin x/x)$, why not cover a single detector with a screen of prescribed, variable transmission, $T(x) = (\sin x/x)$? The obvious objection is, of course, the fact that $T(x)$ can have only positive transmission; that is, $0 \leq T(x) \leq 1$. As we show here, there are ways to get around this difficulty, but first let us point out the limitation that a positive function imposes on its Fourier transform

This limitation is clearly seen by examining the Fourier transform. Assume that $f(x)$ has been normalized so that

$$\int_{-\infty}^{+\infty} f(x)\ dx = 1 \tag{D-1}$$

Then from

$$F(\omega) = \int_{-\infty}^{+\infty} f(x) \, \epsilon^{-i\omega x} \, dx \qquad (D-2)$$

we see at once that $F(0) = 1$. Next,

$$\left| F(\omega) \right| \le \int_{-\infty}^{+\infty} \left| f(x) \, \epsilon^{-i\omega x} \right| dx \le \int_{-\infty}^{+\infty} f(x) \left| \epsilon^{-i\omega x} \right| dx \le \int_{-\infty}^{+\infty} f(x) \, dx = 1 \quad (D-3)$$

using the fact that $f(x)$ is real and positive. Thus, $\left| F(\omega) \right| \le F(0)$; this means that, in a strict sense, $F(\omega)$ cannot form a high-pass filter function. The qualification is needed because $F(\omega)$ can have a greater magnitude at a higher frequency that at some lower one. A noteworthy case in which $F(\omega)$ acts as a band-pass filter, though it is the Fourier transform of a positive function, arises when

$$f(x) \; = \; \left\{ \begin{array}{ll} 1 + \cos \omega_0 x & \quad -L \le x \le L \\ 0 & \quad x \quad L \end{array} \right. \qquad (D-\;)$$

Its transform

$$F(\omega) = 2L \left\{ \frac{\sin \omega L}{\omega L} + \frac{1}{2} \left(\frac{\sin (\omega - \omega_0)L}{(\omega - \omega_0)L} + \frac{\sin (\omega + \omega_0)L}{(\omega + \omega_0)L} \right) \right\} \qquad (D-5)$$

amounts to a pair of $(\sin x/x)$ functions centered at ω_0 and $-\omega_0$, and a larger $(\sin x/x)$ centered at $\omega = 0$ with twice the amplitude of the pair at ω_0 and $-\omega_0$. Thus, $F(\omega)$ can be considered as a band-pass function; but the large amplitude pass-band at $\omega = 0$ distinguishes $F(\omega)$ from what an electrical engineer might conventionally consider as a band-pass filter.

While the foregoing example does indeed show how a positive function can, in a restricted sense, act as a band-pass filter, it is in fact an exceptional case. Consequently, we return to the discussion of how to realize negative transmission.

Recent work[*,**] has shown some practical schemes that provide negative transmission in image processing experiments. But this work is concerned with processing in which the negative transmittance effect precedes photographic recording of the processed image. Our need for negative transmission is easier to satisfy because the electrical outputs of separate detectors can be subtracted just as easily as added, whereas in the work referenced above, subtraction uses either the Herschel effect in which long wavelength light erases an image that has previously been formed with shorter wavelength light[**]; or, a fluorescent screen which brightens under ultraviolet radiation and darkens under infrared.

With two electrical detectors, negative transmission can be achieved in the following way. From $t(x,y)$, the desired transmission function, form the two positive functions $t_+(x,y)$ and $t_-(x,y)$, where $t(x,y) = t_+(x,y) - t_-(x,y)$, defined as

$$t_+(x,y) = \begin{cases} t(x,y) & \text{where} \quad t(x,y) > 0 \\ 0 & \text{elsewhere} \end{cases} \tag{d-6}$$

$$t_-(x,y) = \begin{cases} |t(x,y)| & \text{where} \quad t(x,y) < 0 \\ 0 & \text{elsewhere} \end{cases} \tag{D-7}$$

Next, construct transparencies representing these functions. Then simply split the image illumination into two identical beams; send one beam through $t_+(x,y)$ onto a detector whose output has the electrical weight of plus one; send the other beam through $t_-(x,y)$ onto a detector whose output has the electrical weight of minus one; and, finally, sum the two detector outputs. This process can be described in terms of the Fourier transforms of the image and the transparencies as follows.

---

[*] E. A. Trabka and P. G. Roetling, J. Opt. Soc. Am., 54, 1242 (1964).

[**] D. H. Kelly, J. Opt. Soc. Am., 51, 1095 (1961).

Let $I(\omega_x, \omega_y)$ represent the Fourier transform of the image intensity. Let $T(\omega_x, \omega_y)$ represent the Fourier transform of the transmission function, where

$$T(\omega_x, \omega_y) = T_+(\omega_x, \omega_y) - T_-(\omega_x, \omega_y) \tag{D-8}$$

corresponding to $t(x, y) = t_+(x, y) - t_-(x, y)$. With $O(\omega_x, \omega_y)$ the processed transform, we find

$$O(\omega_x, \omega_y) = T(\omega_x, \omega_y) \, I(\omega_x, \omega_y) = T_+ I - T_- I \tag{D-9}$$

This equation summarizes the negative transmission process.

Having described one way of realizing negative transmission, we now discuss some practical differences between such schemes and the electrically weighted detector array. First of all, the two-transparency filter reduces detector illumination, whereas electrical weighting allows each detector to receive full illumination. In those applications in which detector and preamplifier (amplification prior to summation of detector signals) noise is significant, the reduced detector signal of the two-transparency filter presents a disadvantage in comparison with the electrically weighted detector array. (We assume equal detector area in the two schemes, but factors which have been overlooked here may make this an unreasonable basis for comparison.)

Electrically weighted detector arrays offer the advantage of flexibility in that their weighting can be varied to give different spatial frequency filter functions. It is conceivable that such filter function control could help to correct optical non-isoplanaticism. That is, if a filter had been designed to, in some prescribed manner, operate on an optical point spread function, and the spread function varied from place to place across the image, then an electrically controllable filter function could compensate such variations.

Another advantage of electrically weighted detector arrays might arise if detectors had non-uniform gain. Thus, electrical weighting could compensate gain variations from detector to detector while simultaneously providing the weighting demanded by the transmission function.

Finally, electrically weighted detector arrays may some day serve in image processing systems that require filters with transmission functions that can be altered in response to changes in input images. The disadvantage in the inflexibility of the two-transparency filter is evident here, as well as in the two preceding applications.